Antiviral intervention strategies against RNA viruses: Roles of Paliperidone and RIG–I

Inaugural Dissertation

submitted to the

Faculty of Medicine

in partial fulfillment of the requirements

for the PhD-Degree

of the Faculties of Veterinary Medicine and Medicine

of the Justus Liebig University Giessen

by

Panagiotidis Georgios – Dimitrios

of

Thessaloniki

Gießen 2022

From the Institute for Virology

Director / Chairman: Prof. Dr. Friedemann Weber

of the Faculty of Veterinary Medicine or Medicine of the Justus Liebig University Giessen

First Supervisor and Committee Member: Prof. Dr. Friedemann Weber

Second Supervisor and Committee Member: Prof. Dr. Stefan Bauer

Committee Members: Prof Dr. Lienhard Schmitz, Prof Dr. Stefan Finke

Date of Doctoral Defense: 01.03.23

Declaration:

"I declare that I have completed this dissertation single–handedly without the unauthorized help of a second party and only with the assistance acknowledged therein. I have appropriately acknowledged and referenced all text passages that are derived literally from or are based on the content of published or unpublished work of others, and all information that relates to verbal communications. I have abided by the principles of good scientific conduct laid down in the charter of the Justus Liebig University of Giessen in carrying out the investigations described in the dissertation."

Panagiotidis Georgios – Dimitrios

Table of Contents

1 Summary

Human viral respiratory pathogens influenza A virus (FLUAV) and Severe Acute Respiratory Syndrome Coronavirus 2 (SARS–CoV–2) are a significant burden on human health. Even though antivirals are available, the infection numbers still remain significant. Recent *in silico* data provided insight on potential inhibitors against these viruses. One of the top hits was the schizophrenia drug Paliperidone which was predicted to disrupt the interaction of FLUAV polymerase subunit PB2 with the nucleoprotein NP and to inhibit SARS–CoV–2 protease 3CLpro. In this work the effect and mechanism of action of Paliperidone against FLUAV and effect on SARS–CoV–2 were to be determined. Paliperidone exhibited early inhibitory effect against A/PR/8/34 in RNA, protein and titer levels with the latter observed, in human airway bronchial cell system. Furthermore, Paliperidone exhibited mild inhibitory effect against other H1N1 strains in RNA, protein and viral polymerase levels, failing to affect strain A/WSN/33 PB2 627E (avian) whatsoever. In this study, was, also, *in vitro* proved, that Paliperidone disrupts the interaction of PB2 and NP of A/PR/8/34. Paliperidone was also found, here, to inhibit SARS–CoV–2 only on RNA levels. All these indicate that Paliperidone might represent a compound of interest for further development of FLUAV and SARS–CoV–2 antivirals.

RIG–I is an innate immune cytosolic pattern recognition receptor inducing type 1 interferon response and senses RNA of FLUAV and SARS–CoV–2. RIG–I domains CARDs and helicase are indispensable for interferon response. Studies with signalling deficient RIG–I, indicated that it has direct antiviral effect against FLUAV. Thus, in this study, a set of mutations on RIG–I that affect signalling were inhibitory against A/PR/8/34 in RNA levels in kidney cells. Furthermore, in adenocarcinoma alveolar cells, the signalling deficient RIG–I DC (ΔCARD) exhibited inhibitory effect against only strain A/PR/8/34 on RNA levels, failing to affect strain A/WSN/33 PB2 627E (avian) and SARS–CoV–2. These indicate that, signalling deficient RIG–I is of interest to study for its direct antiviral activity against FLUAV.

2 Zusammenfassung

Humane virale Influenza–A–Virus (FLUAV) und schweres akutes respiratorisches Syndrom Coronavirus 2 (SARS–CoV–2) sind eine erhebliche Belastung für die menschliche Gesundheit. Obwohl Virostatika verfügbar sind, bleiben die Infektionszahlen signifikant. *In silico* Daten lieferten Einblicke in potenzielle Inhibitoren gegen diese Viren. Ein Top–Hit war das Schizophrenie–Medikament Paliperidon, von dem vorhergesagt wurde, dass es die Wechselwirkung der FLUAV–Polymerase–Untereinheit PB2 mit dem Nukleoprotein NP stört und die SARS–CoV–2–Protease 3CLpro hemmt. In dieser Arbeit werden Wirkung und Wirkmechanismus von Paliperidon gegen FLUAV und Wirkung auf SARS–CoV–2 ermittelt. Paliperidon zeigte eine frühe inhibitorische Wirkung gegen A/PR/8/34 in RNA, Protein und Titerspiegeln, wobei letztere im Primärzellen der menschlichen Atemwege beobachtet wurden. Außerdem zeigte Paliperidon eine leichte Hemmwirkung gegen anderen H1N1 Stämmen in RNA, Protein und viralen Polymerase–Spiegeln, mit Ausnahme des A/WSN/33 PB2 627E (Vogel) zu beeinflussen. In dieser Studie wurde *in vitro* bewiesen, dass Paliperidon die Interaktion von PB2 und NP von A/PR/8/34 und SARS–CoV–2 nur auf RNA–Ebene hemmt. All dies deutet, dass Paliperidon eine interessante Verbindung für weitere Entwicklung von antiviralen Medikamenten gegen FLUAV und SARS–CoV–2 darstellen könnte.

RIG–I ist ein angeborener zytosolischer Mustererkennungsrezeptor des Immunsystems, der eine Typ–1–Interferonantwort induziert und die RNA von FLUAV und SARS–CoV–2 wahrnimmt. RIG–I–Domänen CARDs und Helikase sind für die Interferonantwort unverzichtbar. Studien mit signaldefizitärem RIG–I zeigten, dass es eine direkte antivirale Wirkung gegen FLUAV hat. Daher war in dieser Studie eine Reihe von Mutationen auf RIG–I, die die Signalübertragung beeinflussen, inhibitorisch gegen A/PR/8/34 in RNA–Spiegeln in Nierenzellen. Darüber hinaus zeigten in Adenokarzinom–Alveolarzellen die signaldefizitären RIG–I DC (ΔCARD) eine inhibitorische Wirkung nur gegen den Stamm A/PR/8/34 auf RNA–Ebene, ohne den Stamm A/WSN/33 PB2 627E (Vogel) und SARS zu beeinflussen –CoV–2. Diese weisen darauf hin, dass es von Interesse ist, das signalisierende defiziente RIG–I auf seine direkte antivirale Aktivität gegen FLUAV zu untersuchen.

3 Introduction

3.1 Human viral pathogens

3.1.1 Influenza A virus

Influenza A viruses (FLUAVs) and their continuous emergence are an important cause of global concern, morbidity and mortality, clinical, and economical burden in humans. The frequent mutations and recombination of the influenza A virus create the possible threat of antigenically novel strains/subtypes that might rise with unpredictable pathogenicity and ultimately fear of it evolving into a pandemic strain (Yu Hsu 2018). There have been many influenza pandemics, since the beginning of the twentieth century. The 1918 pandemic was the most severe, killing more than 20 million people worldwide (Patterson and Pyle 1991). The knowledge on mechanisms of FLUAV infection, host immune responses, and how viruses evade from such defensive responses at the molecular and structural levels have been consistently kept updated in the past years. This has helped our understanding of virus–host interactions and human immunology, and has led to the development of several antiviral drugs. Unfortunately, these drugs have minimal impact on the clinical outcomes of infection (Yu Hsu 2018). This is due to antigenic drift and shift. Due to the lack of a proofreading function of the viral polymerase, every cycle of influenza viral replication tends to produce different point mutations (Aggarwal et al., 2010, Nobusawa et al., 2006, Parvin et al., 1986, Hu et al., 2017). This is the antigenic drift. From the other side, the genome of the influenza virus is composed by eight individual segments. Different influenza strains can swap their genomes if they infect the same host, which normally happens in swine species. Under these circumstances, novel strains of influenza viruses will be produced. This is the antigenic shift (Zambon 1999). The constant use of the antiviral drugs has also imposed selective pressure on FLUAV to evolve and develop resistance mechanisms (Hurt et al., 2011). Vaccination remains the major countermeasure of public health effort against influenza, however, sufficient mass–production of vaccines is unlikely to occur immediately after the beginning of a pandemic. This, consequently, requires novel therapeutic strategies against this continually, threatening, emerging virus with higher specificity and reactivity against multiple strains/subtypes of FLUAVs (Yu Hsu 2018).

3.1.1.1 FLUAV composition and the function of the viral proteins

FLUAV belongs to the *Orthomyxoviridae* family and is classified as type A, B, C, or D (Hause et al., 2104). It is a negative sense, single–stranded RNA virus (~80–120 nm in diameter) (Lamb and Choppin., 1983). The viral envelope is composed of two surface glycoproteins, hemagglutinin (HA) and neuraminidase (NA) (Palese and Shaw 2007). A small number of M2, which is an ion channel is also embedded in the viral envelope (Zebedde and Lamb 1988). Within the virion, there are eight segments of influenza RNA, which are coated with nucleoprotein (NP) and the polymerase complex (Braudin et al., 1994, Compans et al., 1972, Murti et al., 1988) forming the viral nucleoprotein (vRNP) complex (Resa–Infante et al., 2011). The vRNP is presented in structural models as an anti–parallel double helix of NP–coated vRNA containing the polymerase (Moeller et al., 2012). This forms the so–called dsRNA panhandle (Schlee et al., 2009). The RNA–dependent RNA polymerase is composed of three subunits, polymerase basic 1 (PB1), PB2, and polymerase acidic (PA) (Lamb and Choppin 1983). Segments 1, 2, 3, 4, 5, and 6 encode for PB2, PB1, PA, HA, NP, and NA, respectively (fig. 1). Segment 7 encodes for matrix 1 (M1) protein and M2 ion channel through alternative splicing. Segment 8 encodes for non–structural protein (NS1) and nuclear export protein (NEP) (Hu Ysu 2018).

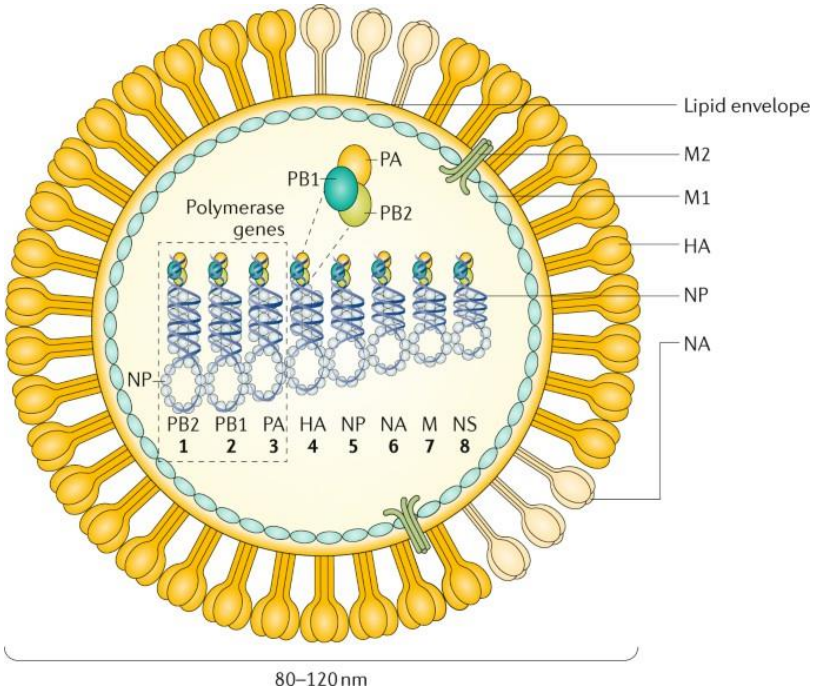

Figure 1: Graphical representation of Influenza A virion and nucleocapsid.

The virion is composed by the proteins (HA, NA, M2, M1) and the eight segments encoding for the viral proteins. Each segment (numbered) represented is double stranded RNA in a form of a panhandle structure, coated with NP protein and complexed with the trimeric polymerase. (figure from Krammer et al., 2018)

Regarding the function of the mentioned proteins, HA is responsible for the entry of the virus into the host cells by binding to host cell surface glycoproteins. These proteins are terminated with sialic acid residues at specific linkages. For example, human FLUAVs preferentially bind to glycoproteins containing the terminal SAα2,6Gal linkage, which are predominately found in human upper airway epithelium (Ito et al., 1997, Ito et al., 2000, Ryan–Poirier et al., 1998). Upon this, the virus is internalized into endosomes into the host epithelial cells. The low endosomal pH environment in connection with the proteins HA, M2 and M1 (Pinto et al., 1992, Pinto and Lamb 2006) lead to a subsequent release of viral RNP into the host cellular cytoplasm (Whittaker and Helenius 1998, Zhirnov 1992, Bui et al., 1996, Martin and Helenius 1991). The secondary surface glycoprotein, NA, is an enzyme that cleaves the bond between the sialic acid and galactose units (Hamming 2020.) It is believed that the role of NA is to prevent aggregation of the virus and enable release of progeny viruses from the surface of host cells (de Graaf and Fouchier 2014). NS1 is a multi–functional protein, with an RNA–binding domain at its N–terminus (residue 1–73) which recognizes double–stranded RNA (dsRNA) sequences and blocks the host RNA detection system. From the other side, the effector domain (residue 74–230) at the carboxyl–terminus of NS1 can stabilize the RNA–binding domain, but its major function is to interact with host cellular proteins and interfere with host messenger RNA (mRNA) processing as well as host innate immune responses (Hu Ysu 2018). Thus, HA, NA, M2, NS1 proteins function in order to either release the virions in the cytoplasm or protect the vRNPs to reach the host cell nucleus, where replication occurs (Samji 2009).

The viral proteins that make up the vRNP are NP, PA, PB1, and PB2. All of these proteins contain known nuclear localization signals (NLSs) that can bind to the cellular nuclear import machinery and, thus, enter the nucleus and replicate (Boulo et al., 2007). Replication is carried out by the viral RNA dependent RNA polymerase (RdRp). Since the viral genome is negative sense, in order to be transcribed, it first has

to be converted into a positive sense RNA that serves as a template for the production of viral RNAs (Fodor et al., 1994).

The trimeric polymerase of FLUAV is composed by PB1, PB2 and PA proteins. Accordingly, PB1 interacts with the cap–binding subunit PB2 and the endonuclease subunit PA (González et al., 1996). PB2 is highly conserved (Patel and Kukol 2017) and consists of several domains. The N–and C–terminal of PB2 can bind either PB1 or NP, but not both simultaneously. More specifically as previously described (Poole et al., 2004) it was suggested that PB2 contains independent N– and C–terminal regions capable of binding NP, located between residues 1–269 and 580–683, respectively. Furthermore, PB2 is mainly responsible for generating, from capped host mRNA, the cap structure for viral mRNA to initiate transcription. The PB2 residues responsible for "cap snatching" reside between positions 318–482, which bind to the host cell RNA (Patel and Kukol 2017). PB2 also consists of the mid–domain, the cap–binding domain, the cap–627 linker, the so called 627–domain, which is named after amino acid residue 627, a host range determinant of influenza viruses (Subbarao et al., 1993), and the C–terminal NLS domain (teVelthuis and Fodor 2016). The characteristic PB2 host–determining residue at position 627 is prevalent in mammalian strains lysine (K) and glutamic acid (E) in avian strains (Subbarao et al., 1993). The 535–684 residues have also been shown to have RNA binding activity (Kuzuhara et al., 2009) (fig. 2).

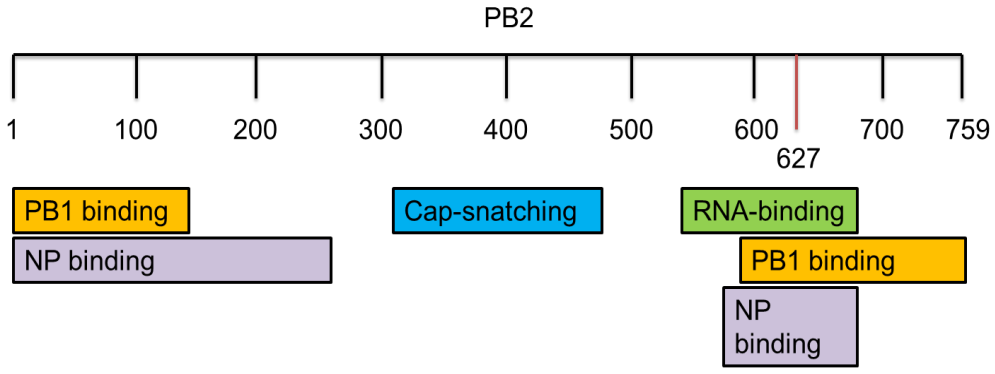

Figure 2: Graphical representation of PB2 protein and domains.

PB2 functional domains, protein interacting domains and 627 host range determinant residue are shown.

NP protein is moderately conserved among influenza A virus strains from different species (Hu et al., 2017). It primarily has a structural role in maintaining the structure of the RNP, but is also an essential cofactor and possible regulator of genome replication (Portela and Dingard 2002). A protein–protein interaction between the influenza virus NP and PB2 has been identified (Biswas et al., 1998). The functional significance of this interaction is suggested to be important in the transcription–replication process. Multiple regions of NP interact with PB2. The C–terminus (amino acid (aa) (340 to 498) of NP contains a PB2 binding site as well as a sequence regulating the NP–PB2 interaction in the last 33 aa of NP. It was shown that the sequences at the C–terminus of NP regulate the strength and stability of NP–PB2 interaction since the deletion of 33 aa at the C–terminus increases the amount of NP–PB2 complex formation. NP I (1–161), III (255–341), IV (340–498) and V (340–465) domains contain PB2 binding sites (Biswas et al., 1998). NP II is the only domain (aa 161 to 256) that does not bind to PB2, while an RNA binding region of NP has been identified within N–terminal aa 1 to 180 (Albo et al., 1995), which overlaps with the NP I region consisted by aa 1 to 161 (Biswas et al., 1998). (fig. 3).

Figure 3: Graphical representation of NP protein and domains.

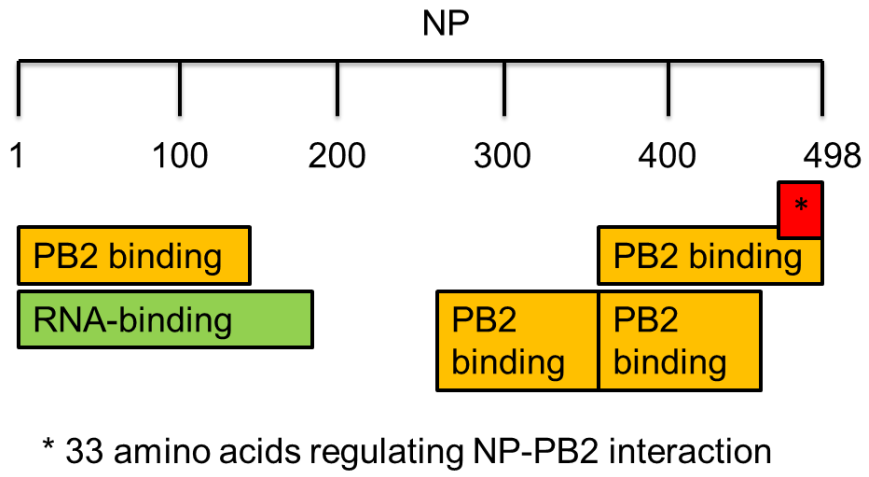

NP functional domains, protein interacting domains and residues affecting the interaction are shown.

Consequently, since both NP and PB2 proteins are, in different levels, conserved among the different subtypes and have many functions which are indispensable for the viral replication, compounds that would interrupt their interaction might have a broad range antiviral activity.

3.1.2 Severe Acute Respiratory Syndrome Coronavirus

Another major virus is the severe acute respiratory syndrome coronavirus 2 (SARS–CoV–2), causing coronavirus disease 19 (COVID–19) (V'kovski et al., 2021). SARS–CoV–2 has rapidly spread throughout the world by infecting more than 169 million people and causing more than 6.5 million deaths worldwide by 10th August 2022, confirmed by the World Health Organization (WHO Coronavirus (COVID–19) Dashboard). The primary organ affected in patients with COVID–19 is the lung, where the main cause of mortality is hypoxic respiratory failure, arising from acute respiratory distress syndrome (ARDS), with severe hypoxemia, often requiring assisted ventilation (Siddiqi et al., 2020). Antiviral drugs and vaccines are two common strategies to combat viral diseases. The WHO had listed more than 200 COVID–19 vaccines to be under development as of August 9, 2022 (Draft landscape and tracker of COVID–19 candidate vaccines (WHO)). The list of antivirals throughout the years of the pandemic has increased exponentially ranging from monoclonal antibodies to Molnupiravir and Paxlovid reducing viral loads, hospitalizations and deaths (Drożdżal et al., 2021). On the other hand, taking account the high infectivity and the fact that SARS–CoV–2 is still a global concern, there is an urgent need to identify new compounds with potent anti–SARS–CoV–2 activity (Xu et al., 2021).

3.1.2.1 SARS–CoV–2 composition and the function of the viral proteins

SARS–CoV–2 is enveloped, single–stranded, positive–sense RNA virus, classified in the *Coronaviridae* family, Betacoronavirus genus. The genome size of SARS–CoV–2 is approximately 29.9 kb having 14 open reading frames (orfs), which encode 27 proteins (Lu et al., 2020). These include four structural (nucleocapsid (N), envelope (E), membrane (M) and S (spike)), as well as nine accessory (ORF3a–ORF10) and 16 non–structural (nsp1–16) proteins (Rastogi et al., 2020, Gordon et al.,2020) (fig. 4).

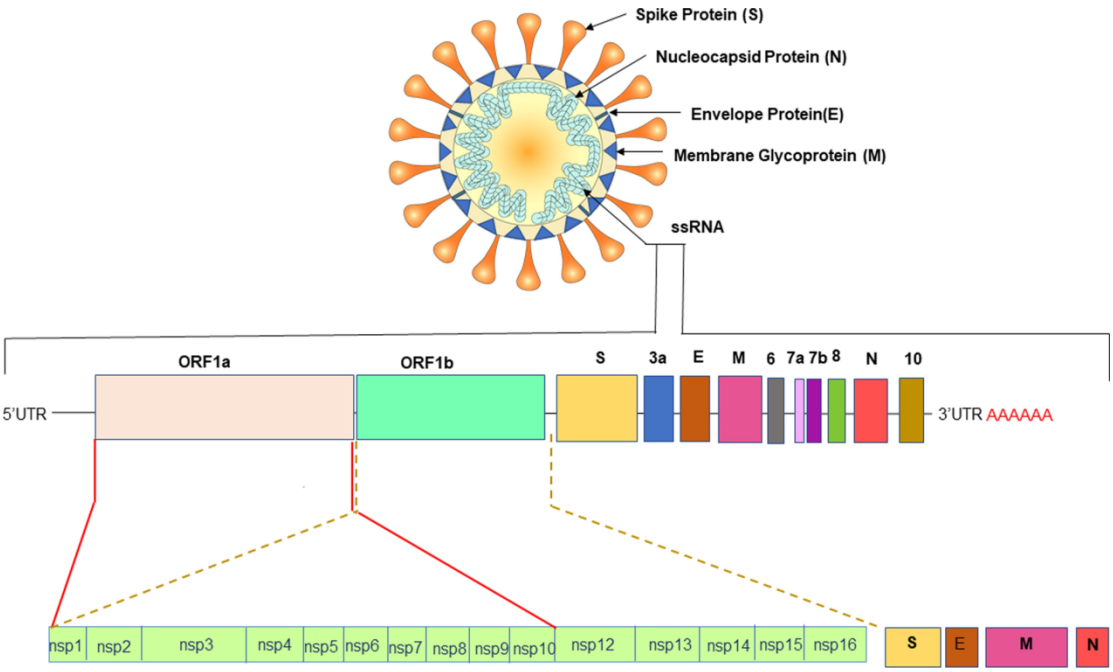

Figure 4: Graphical representation of SARS–CoV–2 virion and genome.

The virion (upper image) is composed of a lipid envelope covered with Spike protein. The genome (lower image) is coated with nucleoprotein and encodes for the viral proteins (picture from Rastogi et al., 2020).

The structural proteins encoded by the SARS–CoV–2 genome have essential roles in virus replication and packaging. The S protein interacts with the host cell receptors and is required for virus entry into host cells (Rastogi et al., 2020). The S1 subunit recognizes the cellular receptor, angiotensin–converting enzyme 2 (ACE2) on the host cell, which ultimately leads to entering of SARS–CoV–2 into the target cell. Furthermore, upon entry, the E and M proteins participate in virion assembly and release (De Maio et al., 2020). The M protein binds to the N and accessory proteins 3a and 7a to enable the budding of viral particles (Tang et al., 2020). The N protein is a multifunctional protein, which encapsidates the viral genome into vRNPs and recruits them for virion formation by interacting with the M protein (Wang et al., 2022, Scherer et al., 2022). Also, N protein hijacks innate immune interferon signalling by inhibition of IFN–β (Li J.–Y. et al., 2020). These four structural proteins are encoded at the 3'–end of the viral genome (Paules et al., 2020).

Besides the expression of the four structural proteins, the 3'–end also encodes nine accessory proteins (Orf3a, Orf3b, Orf6, Orf7a, Orf7b, Orf8, Orf9b, Orf9c, and Orf10) (Gordon et al., 2020) with their role being not fully clear (Wu A. et al., 2020).

Orf3a is a multifunctional ion channel protein, mediating apoptosis (Ren et al., 2020). SARS–CoV, causing the 2002–2004 outbreak (de Wit et al., 2016), is a predecessor of SARS–CoV–2 and shares high resemblance with its successor (Hu et al., 2021). Evidence from SARS–CoV indicate that Orf3a supports virus budding by interacting with the structural proteins N, M and S (Tan, 2005). Orf3b shows antagonistic function against the human innate immune system's type I interferon (IFN) signalling (Konno et al., 2020). Another IFN antagonist is Orf6 (Lei et al., 2020). Evidence from SARS–CoV, suggest that Orf7a might play a role in virus budding and release (Taylor et al., 2015). The function of Orf7b is still unclear, but due to the high sequence conservation with SARS–CoV, it is predicted to have a pro–apoptotic function (Schaecher et al., 2007). Another IFN antagonistic factors are Orf8 and ORf9b (Li J.–Y. et al., 2020, Zhang et al., 2020, Han et al., 2021). More specifically, ORf9b interacts with innate immune proteins retinoic–acid inducible gene (RIG–I) and Mitochondrial antiviral–signalling protein (MAVS) and inhibits downstream interferon signalling (Han et al., 2021). Evidence from SARS–CoV (Gordon et al., 2020), suggest that Orf9c and Orf10 are inhibitors of the antiviral host response.

At the 5′ end of the genome, the virus encodes two polypeptides, due to the transcription and translation of a frameshift of two Orfs. The Orfs, Orf1a and Orf1b encode for two polypeptides pp1a and pp1ab. These polypeptides are cleaved by viral proteases producing the 16 non–structural proteins (Mousavizadeh and Ghasemi 2020).

The 16 non–structural proteins show a wide variance of functions. The nsp1 is known to be a translation inhibitor, by binding and reducing the available number of ribosomes that can carry out the translation (Schubert et al., 2020). The nsp2 is an interferon inhibitor by repressing the translation of Interferon β (Xu et al. 2022). The nsp3 encoding shows proteolytic cleavage function (Mariano et al., 2020). The nsp4 induces changes to the endoplasmic reticulum structure (Hackstadtet al., 2021) which is connected with the replication of coronaviruses (Hagemeijer et al., 2012). The nsp5, encoding for 3CLpro, is the main protease and, together with the nsp3, is responsible of cleavage and release of the mature nsps (Mousavizadeh and Ghasemi, 2020). The nsp7, nsp8 are cofactors to the core RNA–dependent RNA polymerase nsp12 (Gao et al., 2020). The nsp9's role is still unclear but it seems to play a role together with nsp15, to the RNA processing and production (Mariano et al., 2020). The nsp10 forms a complex with nsp14 which has ribonuclease activity (Baddock et al., 2022). The nsp10,

also, forms a complex with nsp16 (Lin et al., 2020) which was suggested in the relevant SARS–CoV, to improve translation efficiency and immune evasion (Chen et al., 2011). The nsp13 protein is a helicase, which is also part of the replication transcription complex with nsp7, nsp8 and nsp12 (Chen et al., 2020). The nsp15 is an RNA uridylate–specific endoribonuclease (Frazier et al., 2021).

These mentioned viruses, are detected by the innate immune system.

3.2 Immunity against FLUAV and SARS–CoV–2

Human infection by influenza viruses starts out in the respiratory tract and in most cases, infection is contained within this organ. The first anatomic barrier of the respiratory epithelium against influenza viruses that enter the host through the oral or nasal cavities is the mucus. If the virus manages to successfully overcome the mucous layer, it next attaches to and invades the respiratory epithelial cells. Upon this, the virus can spread to both non–immune and immune cells in the respiratory tract (Manicassamy, et al. 2010, Perrone et al 2008). In the case of SARS–CoV–2, cells that are targeted depend on the expression of the target ACE2 receptor (Zhou et al., 2020). Thus, the host cells are alveolar, ciliated and goblet cells in the respiratory system, intestinal epithelium cells, vascular endothelia and cardiac cells (Hamming et al., 2004, Sims et al., 2005, Sungnak et al., 2020, Xu et al., 2020).

The defence mechanisms by the innate immune system are a formidable barrier to influenza and SARS–CoV–2 viruses. A specialized immune system exists at distinct mucosal surfaces to counteract invasion by pathogens. The viral RNA that is present within infected cells is recognized as foreign by various pattern recognition receptors (PRRs), which leads to the production and release of type I interferons (IFNs), pro–inflammatory cytokines, and chemokines. Type I IFNs which are produced by several types of cells stimulate the expression of hundreds of genes, known as IFN–stimulated genes (ISGs) in self and neighbouring cells, which induce an antiviral state (Kallfass et al., 2013, Jewell et al., 2007, Lazear et al., 2019).

Despite that, as previously mentioned the defence mechanisms by the innate immune system are a formidable barrier to influenza and SARS–CoV–2 viruses.

3.2.1 Innate recognition of Influenza and SARS–CoV–2 virus infection

The innate immune system detects viral infections through the recognition of pathogen–associated molecular patterns (PAMPs) by pattern recognition receptors (PRRs). PAMPs are infectious agent products, and more specifically protein, protein/lipid complexes, and viral nucleic acid, which are specific to the infectious agent or, on the other hand, atypically located within the cell and accumulate during infection. During virus infection PAMPs accumulate at different compartments within the infected cell, including at the cell surface, inside endosome or free in the cell cytosol (Janeway 1989, Kell et al., 2015). The major sensor for Influenza infection is the RIG–I like receptor (RLR), retinoic acid–inducible gene I (RIG–I) recognizing 5′–triphosphate dsRNA (5´ppp–dsRNA) panhandle (Kato et al., 2006). RIG–I detects virus that is present within the cytosol of infected cells (cell–intrinsic recognition). RIG–I is indispensable for FLUAV recognition and clearance since, high or lethal doses of influenza A virus in mice that are deficient in RIG–I have revealed, delayed recovery and lower survival compared to the wild type mice (Kandasamy et al., 2016). On the other hand, SARS–CoV–2 virus is sensed by the RLRs RIG–I and melanoma differentiation–associated protein 5 (MDA5) (Bortolotti et al., 2021, Yang et al., 2021). Also, *in–vitro* studies show that both MDA5 and RIG–I detect SARS–CoV–2 infection and are upregulated due to the infection (Thorne et al., 2021, Yamada et al., 2021).

3.2.1.1 RIG–I like receptors

The human genome encodes three RLRs, RIG–I, melanoma differentiation associated gene 5 (MDA5), and laboratory of genetics and physiology 2 (LGP2). These are DExD/H box–containing RNA helicases and ubiquitously expressed in the cytoplasm (Yoneyama et al., 2005). These RLRs commonly have a central helicase domain with ATP–ase function and a C–terminal domain (CTD) critical for RNA recognition. RIG–I and MDA5 also contain a tandem caspase recruitment domain (CARD) in their N–terminal region, which is required for associating with the adapter molecule mitochondrial antiviral–signalling protein (MAVS, also known as IPS–1, VISA, and Cardif), which also contains a single CARD at its N–terminus. The interaction between the CARDs of RIG–I/MDA5 and MAVS leads to the recruitment of downstream signalling proteins, to activate transcription factors Interferon

Regulatory Factor (IRF–3/7) (Yoneyama et al., 2015, Rehwinkel and Gack., 2020, Paz et al., 2006).

More specifically, IRF3 and IRF7 are potent transcription factors that upon signal transduction are phosphorylated and activated. Phosphorylated IRF3 and IRF7 form homo– and heterodimers that accumulate in the nucleus, where they attach to target sequences to initiate gene transcription. Activated IRF3 and/or IRF7 direct IFN–β transcription (Panne 2008). In most cell types, IRF3 is constitutively expressed while IRF7 expression remains low until induced by IFN in a positive feedback loop (Sato et al. 1998). All these ultimately lead to the transcriptional activation of IFN and interferon stimulated genes (ISGs) (Rehwinkel and Gack., 2020). An example of RIG–I recognition of FLUAV and downstream interferon signalling is shown (fig. 6).

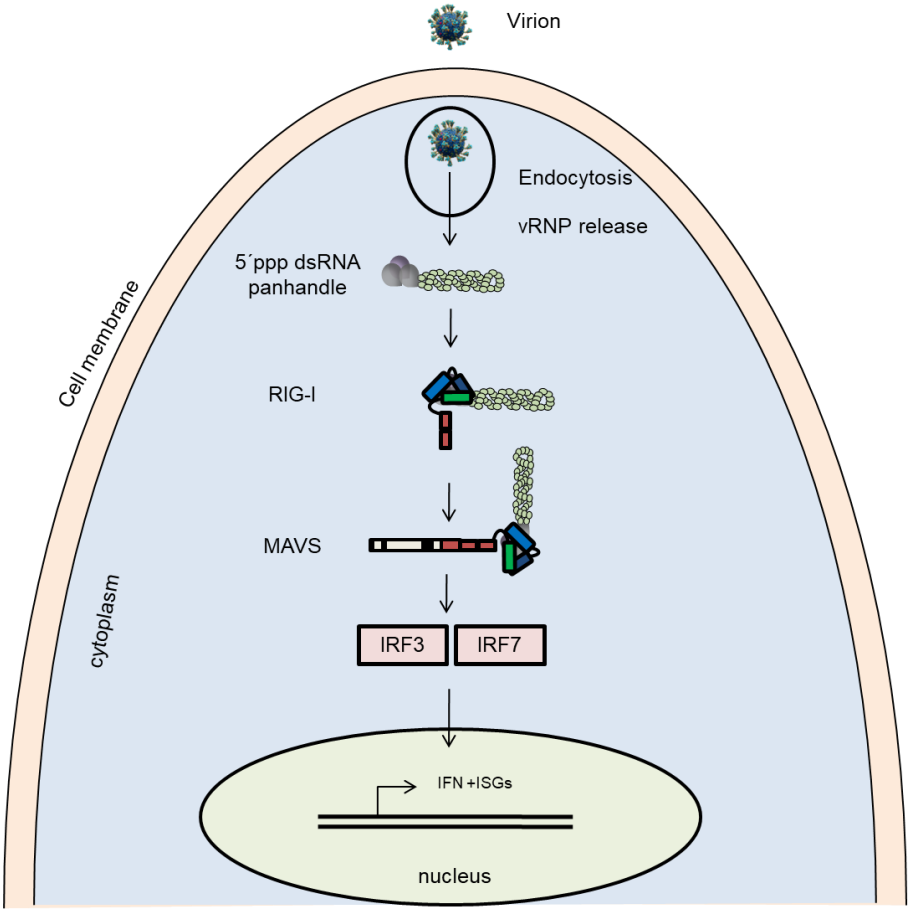

Figure 5: Influenza virus infection is detected by RIG–I host sensor that recognize unique features associated with the infection.

Within infected cells, vRNPs in the cytosol are recognized by RIG–I (Kato et al., 2006), which, through the activation of MAVS and downstream IRF3, leads to the induction of type I IFN and ISGs (Panne 2008, Sato et al. 1998, Paz et al., 2006).

IFN–β that is produced and secreted as a result of the RLR cascade, binds to the membrane interferon–α/β receptor (IFNAR) in an autocrine or paracrine (nearby cells) manner to initiate Janus kinase/signal transducer and activator of transcription (JAK–STAT) signalling and also the interferon–stimulated gene factor 3 (ISGF3)–dependent expression of interferon stimulated genes (ISGs). The JAK family, which are tyrosine kinase non–receptor proteins, phosphorylate STAT proteins to induce downstream IRF signalling inducing inflammation and immune fitness (Hu et al., 2021). In addition, interaction of phosphorylated STAT1 and STAT2 with IRF9, forming ISGF3, activates the transcription of over 300 antiviral ISGs (Michalska et al., 2018). This signalling serves to amplify the IFN response by increasing the expression of IFN in a positive feedback loop. ISGs include those encoding proteins with antiviral activity such as the ISG56, PAMP receptors including all three RLRs and transcription factors such as IRF7 (Loo et al. 2008, Poeck et al. 2010). The result of ISG expression is the induction of cellular conditions and immune regulation that cooperate to control infection and the establishment of an antiviral state.

Since RIG–I acts as a major host sensor for virus infections in the cytoplasm (Yoo et al., 2014), its structure and function has been studied extensively.

3.2.1.1.1 RIG–I structure and function

RIG–I protein is composed of three major domains: the C–terminal domain (CTD), the ATP–helicase domain and the two CARD domains, which compose the N terminus (fig. 6A) (Louber et al., 2015). Several studies have shown that when not bound to its ligand *i.e.* its inactive state, RIG–I exists in a closed conformation, such that the helicase domain segregates the CARD domains. Upon recognition of the proper ligand, RIG–I hydrolyzes ATP and undergoes a series of allosteric changes that eventually release the CARD domains free (Wang et al., 2010, Jiang et al., 2011, Civril et al., 2011, Kowalinski et al., 2011, Beckham 2013). The list of RIG–I–activating ligands becomes bigger through the recent years and includes 5–ppp single–stranded RNA, 5–ppp RNA in a panhandle structure (fig. 6B), 5–pp(diphosphate) dsRNA viral genome. In addition, internal RNA sequences, such as poly–U/A–rich areas, blunt–

ended 5–p dsRNA or 5–OH (no phosphate) and 3–OH, various 3–ppp RNAs, both single and double stranded, and occasionally 5–capped mRNAs are recognized. Moreover, RIG–I was shown to prefer RNAs with length that are less than 300 base pairs, although this also seems to be variable, perhaps depending on other structural features of the RNA (Kato et al., 2006, Pichlmair et al., 2006, Goldeck et al., 2006, Kato et al., 2008, Schmidt et al., 2009, Baum et al., 2010).

On the other side, towards the N–terminus of RIG–I, the pincer motif (also called the bridging domain or regulatory element) is also regulating RIG–I activation (Kowalinski et al., 2011). The pincer motif interacts with both Hel1 and Hel2 domains and connects the CTD domain to the helicase (Leung and Amarasinghe 2012).

At the N–terminal domain, the CARD domains, are indispensable for the signalling capacity of RIG–I (Kowalinski et al., 2011). Evidence show that the CARD domain has auto–inhibitory function forming an interaction with the helicase domain. Interestingly, the C–terminus of CARD2 makes contacts with Hel2i, suggesting that the aforementioned interaction contributes to the formation of a rigid inactive conformation (Kowalinski et al., 2011). These CARD–helicase interactions may also prevent access to MAVS directly or by blocking RIG–I for posttranslational modifications (Gack et al., 2007, Zeng et al., 2010), which are important for downstream signalling. Contrary to that, when RIG–I is in active state, the CARDs form a 2CARD tetramer to induce filament formation with MAVS CARD and downstream signalling activation (Wu and Hur 2015).

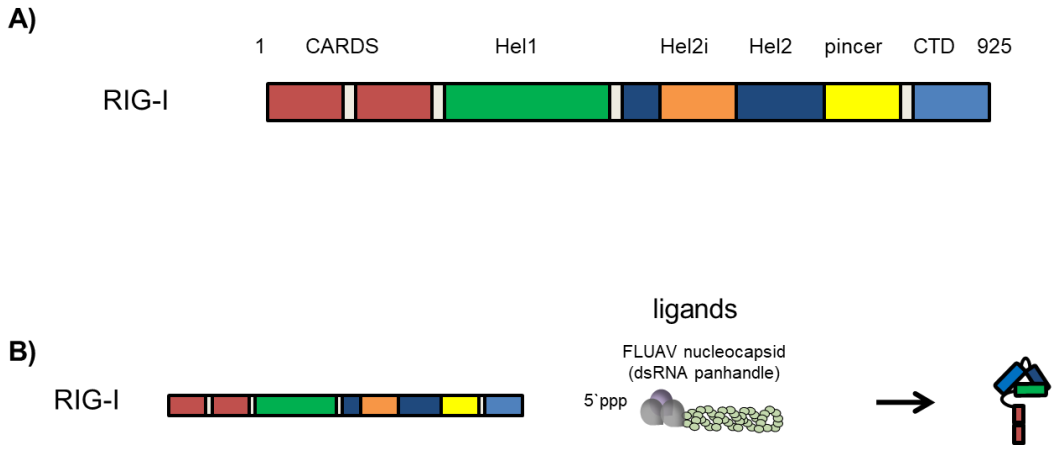

Figure 6: RIG–I and the associated activation machinery.

Primary structure of RIG–I. RIG–I contains repeated caspase recruitment domains (CARDs), a DExD/H box–containing RNA helicase domain composed of helicase Hel1, Hel2i, Hel2, and pincer domains and the C–terminal domain (CTD). RIG–I recognizes 5′–triphosphate (ppp)–containing panhandle double–stranded RNA (Kato et al., 2006). Recognition of substrate RNAs induces ATP–dependent conformational changes of RIG–I (Kowalinski et al., 2011).

RIG–I´s helicase domain consists of the RecA–like Hel1 and Hel2 domains belonging to the SF2 helicase family, with helicases presenting a structural similar catalytic core and playing central role in the DNA and RNA metabolism (Fairman–Williams et al., 2010). The helicase domain consists of an ATP binding and hydrolyzing domain, an insertion domain Hel2i and the pincer (Wu and Hur 2015). Unlike other DExD/H box helicases where RNA binding catalyzes the ATP binding site to obtain the active conformation, the ATP binding site in RIG–I remains open and structurally dynamic following RNA binding. This is possible by the ATP binding site being formed by the two Hel domains, which are relatively far apart (Rawling and Pyle 2014, Fairman–Williams et al., 2010). ATPase binding and hydrolysis is required for full activation of RIG–I and expression of IFNβ (Anchisi et al., 2015).

ATP binding of RIG–I is adequate for interaction with dsRNA (Devarkar et al., 2018). Upon successful interaction with PAMPs, the helical arm relocates and the two helicase domains are brought together to form an active ATPase site (Civril et al., 2011). RIG–I then catalyzes ATP to break the 5′ppp dsRNA interactions. ATP is then hydrolyzed to forward translocation of RIG–I to the opposite dsRNA end, after which the RIG–I is oligomerized (Devarkar et al., 2018). On the other hand, ATP hydrolysis drives rapid disassociation of RIG–I from host RNA features. Even though ATPase activity primarily acts on the translocation upon interaction with PAMP (dsRNA), it may be directed towards rapid disassociation from host dsRNA and degradation of RNA–DNA hybrids (Brisse and Ly 2019).

Mutations in the helicase domain, indicate its central role in signalling.

3.2.1.1.1.1 RIG–I mutants

As previously described, besides the CARDs domains which are dispensable for signalling (Kowalinski et al., 2011), the ATP–ase and ATP–binding activity of RIG–I are essential for its signalling function. A widely used and studied RIG–I mutant, K270A, which shows reduced ATP binding activity (Rawling et al., 2015), is deficient

on inducing immune response (Lassig et al., 2015, Yoneyama et al., 2005). RIG–I ATPase activity is inhibited in the absence of PAMP (dsRNA). The importance of this is apparent when a defect in ATP breakdown may result in constitutive signal transduction and autoimmune diseases. The ATP–hydrolysis–deficient RIG–I, E373Q, is retained in an ATP–bound state, which senses self–RNAs. More specifically, this E373Q mutant senses and is activated by 28s rRNA (Lassig et al., 2015). On the other hand, in another study, the IFN–promoter activation capacity of another RIG–I helicase mutant, T409A/S411A was tested. The authors found out that, this mutant resulted in a limited response to promoter activation upon challenge with RIG–I ligands (Louber et al., 2015). On the other side, the signalling capability of mutants K270A and T409A/S411A are highly dependent on the nature of ligand upon challenge, with single stranded RNA being inhibitory and double stranded RNA inducing signalling (Kumar et al., 2009).

Despite the fact that the innate immune system is complex and upon activation induce the expression of several antiviral factors and antivirals exist, the number of Influenza and SARS–CoV–2 still remains a burden. Thus, studies have focused on finding potential novel antivirals against these viruses.

3.3 Compound prediction disrupting PB2–NP interaction of FLUAV

Influenza NP and PB2 proteins are, in different levels, conserved among the different subtypes and both have many functions which are indispensable for the viral replication (Patel and Kukol 2017, Subbarao et al., 1993, Portela and Dingard 2002, Hu et al., 2017, Biswas et al., 1998). Thus, compounds that would interrupt PB2–NP interactions might have a broad range antiviral activity. An *in silico* screening of potential compounds that fit in PB2, disrupting the FLUAV polymerase function or interaction with other proteins was done (Patel and Kukol 2017). Fifteen ligand–binding potential targets, which represent favorable binding protein regions with small organic molecules were predicted, many of which were located in highly conserved areas of PB2. The binding affinities of 1738 Food and Drug Administration (FDA)–approved small molecule drugs were screened against the PB2 target site surrounding a region of highly conserved amino acids. The top hit drug was Paliperidone, with the chemical structure and docking models showing that the nitrogen atom of the central pyridine ring of Paliperidone is able to form a hydrogen bond with the oxygen atom of

Glu241 of PB2 protein, and the drug–protein complex is maintained via hydrophobic interaction with sixteen surrounding residues of the target site (Patel and Kukol 2017) (fig. 7A). This site of PB2 was predicted to be interacting with NP protein (Poole et al., 2004).

3.4 Compound prediction disrupting SARS–CoV–2 3CLpro

Regarding SARS–CoV–2, a screening of potential inhibitors against 3CLpro protein was carried out, due to its essential role as the major processor of viral RNA (Mousavizadeh and Ghasemi 2020). Docking models revealed a high affinity of Paliperidone binding to 3CLpro *in silico*. According to this study, interacting residues of 3CLpro with Paliperidone were Thr25, Ser46, Leu141, Gly143, Glu166, Gln189, and the catalytic dyad residues composing the active site of the protease His41, Cys145 (fig. 7B). With this *in silico* analysis, the authors suggested Paliperidone as one of many potential inhibitor candidates against SARS–CoV–2 through interaction with 3CLpro protein (Gul et al., 2020).

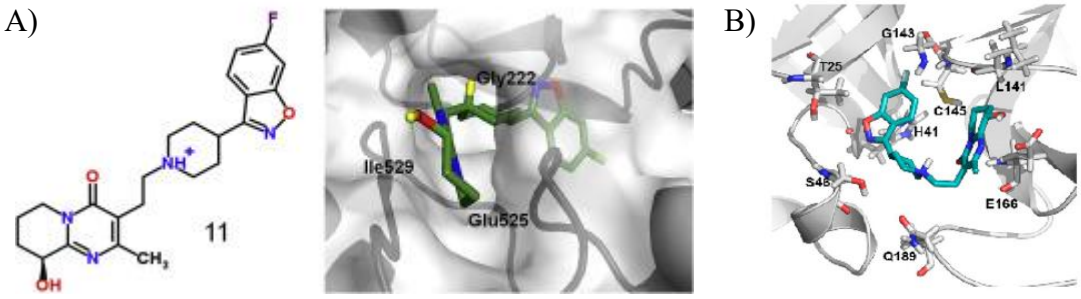

Figure 7: Predicted binding of Paliperidone to Influenza PB2–NP binding domain and SARS–CoV–2 3CLpro.

A) Docking models of one of top hit compounds targeting the PB2 protein: Paliperidone identified by virtual screening. Interacting PB2 residues are color–labelled (Modified from Patel and Kukol 2017). B) Docking models of one of top hit compounds targeting the SARS–CoV–2 3CLpro. Interacting residues are labelled (Modified from Gul et al., 2020).

3.5 Paliperidone

Paliperidone (fig. 8) (R076477, Invega; Johnson & Johnson Pharmaceuticals, L.L.C., Titusville, NJ) is an atypical antipsychotic FDA–approved drug. The molecular formula is C23H27FN4O3 and the molecular weight is 426.49. Its chemical name is

(±)–3–[2–[4–(6–fluoro–1, 2–benzisoxazol–3–yl)–1–piperidinyl] ethyl]–6, 7, 8, 9–tetrahydro–9–hydroxy–2–methyl–4Hpyrido [1, 2–a] pyrimidin–4–one. Paliperidone (or 9–hydroxyrisperidone) is the major and active metabolite of risperidone (Risperdal; Johnson & Johnson Pharmaceuticals, L.L.C.) (Mannens et al., 1993, Megens and Awouters 1994). Paliperidone is a centrally active dopamine D2 and serotonin 5–HT2A antagonist, as demonstrated in both *in vitro* and *in vivo* animal and human studies (Karlsson et al., 2005). Paliperidone is also active as an antagonist at α1– and α2–adrenergic receptors and H1 histamine receptors. Paliperidone has no affinity for cholinergic muscarinic or α1– and α2–adrenergic receptors (Megens and Awouters 1994, Schotte et al., 1996, Karlsson et al., 2005).

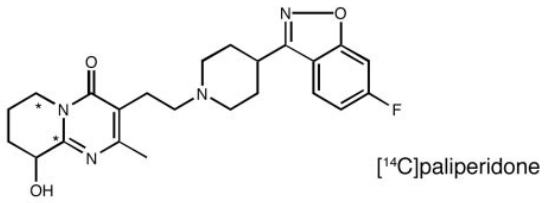

Figure 8: Chemical representation of Paliperidone

Paliperidone metabolism is limited *in vitro*. Paliperidone was metabolized to a very limited extent in humans, rabbits, dogs and mice liver matrices, whereas it was extensively metabolized in Wistar rat liver matrices and Sprague–Dawley rat hepatocyte suspensions. The major compound observed in primary hepatocyte cultures was Paliperidone (20–90%) (Invega, INN–paliperidone EMEA 2007).

Regarding toxicity, single doses of Paliperidone have been investigated in mice and rats via oral and intravenous routes of administration. Sedation and ptosis were consistently noted across rodent species. On the other hand, side effects after repeated dose used in humans against schizophrenia are described as mild, rare and are, enhanced prolactin release, associated with changes in the following tissues: pituitary gland, mammary gland, endocrine pancreas, female genital tract, male accessory sex organs and adrenal glands. This was also found in repeat dose toxicity and carcinogenicity studies in mice rats and dogs. In dietary carcinogenicity studies, in mice, predominantly at the highest dose level, non–neoplastic histopathological changes were observed in the pituitary gland, female genital tract, and female mammary glands, male endocrine pancreas and male accessory sex organs. In rats, non–neoplastic changes were found in

the pituitary gland, male and female mammary glands, and male and female genital tract were seen at all dose levels. As for immunotoxicity, there were no adverse effects indicating the safety of the drug (Invega, INN–paliperidone EMEA 2007).

4 Objective of this work

Human viral respiratory pathogens FLUAV and SARS–CoV–2 are a significant burden on human health. Their pathogenicity is a result of both virus–mediated cell death and excessive reaction of the IFN response. Both pathogens are sensed by the innate immune sensor RIG–I which shows both direct and signalling antiviral activity. Even though antivirals are available, infection number remain still a burden. Thus, the search for new antivirals was the objective of this work. Those can be of a chemical nature or even be the sensor RIG–I itself, but optimized in order not to lead to excessive IFN response.

Thus Paliperidone, an FDA approved drug against schizophrenia, which was predicted *in silico* to disrupt NP–PB2 binding of FLUAV on one side and disrupt the enzyme function of 3CLpro of SARS–CoV–2 on the other side, was evaluated against these viruses. Furthermore, a set of RIG–I mutants were tested initially for their capability of signalling and the RIG–I ΔCARD, being signalling deficient, was evaluated against FLUAV and SARS–CoV–2 for its antiviral activity in two different *in vitro* systems. Gaining insights into the mechanism of action and antiviral effect of both Paliperidone and RIG–I ΔCARD is of interest for further development of antivirals against these pathogens.

5 Materials and methods

5.1 Materials

5.1.1 Viruses

Table 1: Viruses

Abbreviation	Virus	Description	Origin
A/PR/8/34	Influenza virus	Influenza virus, isolate from Puerto Rico	Pichlmair et al., 2006
A/WSN/33 PB2 627E	Influenza virus	Influenza virus, isolate from United Kingdom, encoding glutamic acid in position 627 of PB2 protein (avian adapted)	Weber et al., 2015
A/WSN/33 PB2 627K	Influenza virus	Influenza virus, isolate from United Kingdom, encoding lysine in position 627 of PB2 protein (mammalian adapted)	Weber et al., 2015
A/HAM/2009	Influenza virus	Influenza virus, isolate from Hamburg, Germany	Weber et al., 2015
SARS–CoV–2	Severe acute respiratory syndrome coronavirus 2	SARS–CoV–2 patient isolate 984, BetaCoV/Munich/BavPat1/2020, from Christian Drosten, Charité Berlin	EPI_ISL_406862

5.1.2 Eukaryotic cell lines

Table 2: Eukaryotic cell lines

Name	Organism	Type and Origin	Reference
A549	Homo sapiens, human	lung, adenocarcinomic alveolar basal epithelial cell line	Wuerth et al., 2020

A549 CTRL KO	Homo sapiens, human	lung, adenocarcinomic alveolar basal epithelial cell line, lenticrispr non–targeting control knockout	Willemsen et al., 2017
A549 RIG–I KO	Homo sapiens, human	lung, adenocarcinomic alveolar basal epithelial cell line, lenticrispr RIG–I knockout	Willemsen et al., 2017
A549 MDA5 KO	Homo sapiens, human	lung, adenocarcinomic alveolar basal epithelial cell line,lenticrispr MDA5 knockout	Willemsen et al., 2017
A549 MAVS KO	Homo sapiens, human	lung, adenocarcinomic alveolar basal epithelial cell line, lenticrispr MAVS knockout	Willemsen et al., 2017
HEK293	Homo sapiens, human	kidney, embryonic cell line	Wuerth et al., 2020
HEK293 RIG–I KO	Homo sapiens, human	kidney, embryonic cell line, zinc finger nuclease editing targeting RIG–I	Weber et al., 2015

Huh7	Homo sapiens, human	liver, hepatocyte–derived carcinoma cell line	Schoen et al. 2020
A549 CTRL KO	Homo sapiens, human	lung, adenocarcinomic alveolar basal epithelial cell line, lenticrispr non–targeting control knockout	Schilling et al., 2020
A549 RIG–I KO	Homo sapiens, human	lung, adenocarcinomic alveolar basal epithelial cell line, lenticrispr RIG–I knockout	Schilling et al., 2020
MDCK	Canis familiaris, dog	Kidney, epithelial cell line	Weber et al., 2015
Primary human airway bronchial cells	Homo sapiens, human	Lung, differentiated bronchial cells isolated from non–smoking donors (see section 5.2.1)	Mueller et al., 2020

5.1.3 Prokaryotic cells

Table 3: Prokaryotic cells

Name	**Organism**	**Genotype**	**Origin**
DH10B	Escherichia coli, bacterium	F– mcrA Δ(mrr–hsdRMS–mcrBC) φ80lacZΔM15	Thermo Fisher Scientific, Schwerte

		ΔlacX74 recA1 endA1 araD139 Δ (ara–leu)7697 galU galK λ– rpsL(StrR) nupG	
TOP10	Escherichia coli, bacterium	F– mcrA (mrr–hsdRMS–mcrBC) 80lacZM15 lacX74 recA1 ara139 (ara–leu)7697 galUgalKrpsL (StrR) endA1 nupG>	Thermo Fisher Scientific, Schwerte

5.1.4 Cell culture and transfection reagents

Table 4: Eukaryotic cell culture reagents

Name	**Supplier**
CCM34	Viro Vet Diagnostik GmbH, Giessen Dulbecco's modified Eagle's medium (D MEM) + 17.8 mg/l L–alanine + 0.7 g/l glycine + 75 mg/l L–glutamic acid +25 mg/l L–proline + 0.1 mg/l biotin + 25 mg/l hypoxanthine + 3.7 g/l sodiumbicarbonate
Cell culture medium (CCM34+10% FBS+1X P/S/Q)	CCM34 + 10% FBS + 1% penicillin–streptomycin (P/S) + 1% L–glutamine (Q)
DMEM (Dulbeccos's modified Eagle medium)	Gibco, Thermo Fisher Scientific, Schwerte

FBS (Fetal Bovine Serum)	BioChrom GmbH, Berlin
2X MEM (Temin's modification), no phenol red	Gibco, Thermo Fisher Scientific, Schwerte
OptiMEM	Gibco, Thermo Fisher Scientific, Schwerte
Penicillin–Streptomycin–Glutamine (P/S/Q; 100X)	Gibco, Thermo Fisher Scientific, Schwerte
Puromycin	Sigma–Aldrich, Steinheim
2X Trypan blue (0.4% Trypan blue in H_2O, sterile filtered)	Merck, Darmstadt
0.05% Trypsin–EDTA (1X), phenol red	Gibco, Thermo Fisher Scientific, Schwerte
Trypsin–EDTA–Solution, pH 7.4	ViroVet Diagnostik GmbH, Giessen

Table 5: Transfection reagents

Name	**Supplier**
EndoFectin™ Max	Genecopoeia, Rockville, MD, U.S.A.
TransIT®–LT1	Mirus Bio LLC, Madison, WI, U.S.A.

Table 6: Prokaryotic cell culture reagents

Name	**Composition**	**Supplier**
Infectious medium	CCM34 medium + 5% Penicillin–Streptomycin–Glutamine + 0.2 % BSA + 1 µg/ml L–1–tosylamido–2–phenylethyl chloromethyl ketone (TPCK)–treated trypsin	Vet Viro diagnostic GmbH, Giessen Gibco, Thermo Fisher Scientific, Schwerte Sigma–Aldrich, Steinheim Sigma–Aldrich, Steinheim
LB agar	1.5% agar in LB medium	Roth, Karlsruhe
LB medium	10% tryptone/peptone 5% yeast extract 0.5% NaCl, pH 7.0	Roth, Karlsruhe Roth, Karlsruhe

	in ddH2O	Sigma–Aldrich, Steinheim
SOC medium	0.5% yeast extract 2% tryptone/peptone 10 mM NaCl 2.5 mM KCl 10 mM MgCl2 10 mM MgSO4 20 mM glucose in ddH2O	Roth, Karlsruhe Roth, Karlsruhe Sigma–Aldrich, Steinheim Roth, Karlsruhe Fluka, Seelze Fluka, Seelze Fluka, Seelze

5.1.5 Buffers and solutions

Table 7: Buffers for Western blotting

Name	**Composition**	**Supplier**
10% APS	10% APS in H2O	Sigma–Aldrich, Steinheim
10% SDS	10% SDS in H2O	Roth, Karlsruhe
10X Tris buffered saline (TBS)	200 mM Tris, pH 7.6 1.37 M NaCl in ddH2O	Roth, Karlsruhe Sigma–Aldrich, Steinheim
4X SDS sample buffer	114 mM tris–HCl, pH 6.8 4.6% SDS 23% glycerol 20% β–mercaptoethanol 3.4 mM bromophenol blue in ddH2O	Roth, Karlsruhe Roth, Karlsruhe Roth, Karlsruhe Sigma–Aldrich, Steinheim Sigma–Aldrich, Steinheim
Blocking buffer (BSA)	5% bovine serum albumin (BSA) in 1X TBS–T	Sigma–Aldrich, Steinheim
Blocking buffer (milk)	10% milk powder in 1X TBS	dm Drogeriemarkt, Giessen
Color Prestained Protein Standard, Broad Range (11–245 kDa)	n.a.	Cell Signalling Technology, Frankfurt a.M.
Mild stripping buffer	200 mM glycine	Roth, Karlsruhe

	0.1% SDS 1% Tween20 in ddH2O, pH 2.2	Roth, Karlsruhe Serva Electrophoresis GmbH, Heidelberg
RIPA	50 Mm Tris–HCl pH 7.5, 0.15 M NaCl, 1% NP40	Roth, Karlsruhe Sigma–Aldrich, Steinheim Thermo Fisher
Rotiphorese® PAGE Matrixpuffer plus	n.a.	Roth, Karlsruhe
SDS running buffer	25 mM tris 192 mM glycine 0.1% SDS in ddH2O	Roth, Karlsruhe Roth, Karlsruhe Roth, Karlsruhe
Transfer buffer (for semidry blotting)	48 mM tris 39 mM glycine 1.3 mM SDS 20% methanol in ddH2O	Roth, Karlsruhe Roth, Karlsruhe Roth, Karlsruhe Roth, Karlsruhe
Wash buffer (TBS–T)	0.1% Tween20 in 1X TBS	Serva Electrophoresis GmbH, Heidelberg

Table 8: Buffers for Immunostainings

Name	**Composition**	**Supplier**
IF blocking buffer	2% BSA 5% glycerol 0.2% Tween20 in 1X PBS	Sigma–Aldrich, Steinheim Roth, Karlsruhe Serva Electrophoresis GmbH, Heidelberg
IF fixation solution	4% PFA in 1X PBS	Roth, Karlsruhe
IF permeabilization buffer	0.5% Triton–X 100 in 1X PBS	Sigma–Aldrich, Steinheim
IF wash buffer	0.05% Tween–20 in 1X PBS	Sigma–Aldrich, Steinheim

Table 9: Other buffers

Name	**Composition**	**Supplier**

Crystal violet staining solution	0.75% crystal violet 3.75% formaldehyde 20% ethanol, absolute 1% methanol in ddH2O	Sigma–Aldrich, Steinheim Roth, Karlsruhe Roth, Karlsruhe Roth, Karlsruhe
1X Phosphate buffered saline PBS	137 mM NaCl 2,7 mM KCl 10 mM NaHPO4 1,76 mM KH2PO4 in ddH2O, pH 7.4	Sigma–Aldrich, Steinheim Roth, Karlsruhe Merck, Darmstadt Merck, Darmstadt

5.1.6 PCR reagents

Table 10: Polymerases

Name	**Supplier**
JumpStart™ Taq DNA Polymerase with MgCl2	Sigma–Aldrich, Steinheim
KOD Hot Start DNA Polymerase	Merck, Darmstadt
Phusion® High–Fidelity DNA Polymerase	New England Biolabs, Frankfurt a.M

Table 11: Restriction enzymes

Name	**Supplier**
BamHI–HF	New England Biolabs, Frankfurt a.M
DpnI	New England Biolabs, Frankfurt a.M
KpnI–HF	New England Biolabs, Frankfurt a.M
XhoI	New England Biolabs, Frankfurt a.M

Table 12: Other PCR reagents

Name	**Supplier**
Deoxynucleotide (dNTP) Solution Mix, 10mM each	New England Biolabs, Frankfurt a.M
CutSmart Buffer	New England Biolabs, Frankfurt a.M

5.1.7 qPCR primers

Table 13: qPCR primers

Gene Symbol	Alias	Assay Name/Sequence	Cat No.
SARS–COV–2 E gene_F	qPCR SARS–CoV(–2) E gene	ACAGGTACGTTAATAGTTAATAGCGT	Corman et al., 2020
SARS–COV–2 E gene_ P	qPCR SARS–CoV(–2) E gene probe	FAM–ACACTAGCCATCCTTACTGCGCTTCG–BBQ	Corman et al., 2020
SARS–COV–2 E gene_R	qPCR SARS–CoV(–2) E gene reverse primer	ATATTGCAGCAGTACGCACACA	Corman et al., 2020
GAPDH	glyceraldehyde–3–phosphate dehydrogenase	Hs_GAPDH_2_SG	QT01192646
IFIT1	ISG56	Hs_IFIT1_1_SG	QT00201012
IRF3		Hs_IFIT1_1_SG	QT00201012
IRF7		Hs_IRF7_1_SG	QT00210595
QPCR FluA/PR8_ M For	FLUAV M segment forward	GGACTGCAGCGTAGACGCTT	
QPCR FluA/PR8_ M Rev	FLU M segment reverse	CATCCTGTTGTATATGAGGCCCAT	
RRN18S	Ribosomal 18s RNA	Hs_RR18s	QT00199367

5.1.8 Antibodies

Table 14: Antibodies

Target	Species	Mono/Polyclonal	Company/source	Product number
AKT–pan (40D4)	Mouse	monoclonal	Cell–signalling	2920
Alexa Fluor 488 Donkey anti–mouse IgG	Donkey	polyclonal	Invitrogen/Molecular Probes	A21202
Beta–tubulin	Rabbit	polyclonal	abcam	ab6046
Flag M2	Mouse	monoclonal	Sigma	F3165
Influenza A Virus Nucleoprotein [9G8]	Mouse	monoclonal	abcam	ab43821
Mouse IgG HRP conjugated (Mouse TrueBlot® ULTRA), clone eB144	Rat	monoclonal	BioMol	18–8817–33
p53 (Ab–6) (Pantropic) (DO–1)	Mouse	monoclonal	Calbiochem	OP43
Rabbit IgG HRP conjugated (Rabbit TrueBlot®), clone eB182	Mouse	monoclonal	BioMol	18–8816–33
RIG–I (Alme–1)	Mouse	monoclonal	AdipoGen	ag–20b–0009

SARS–CoV Nucleocapsid (N) Protein	Rabbit	Polyclonal	biomol	200–401–A50
Caspase–3	Rabbit	polyclonal	Cell Signalling	Cat#9662
GAPDH	Mouse	monoclonal	abcam	ab8245
Influenza A virus NP (nucleoprotein)	Rabbit	polyclonal	Genetex via BIOZOL	GTX125989
Influenza A virus PB2 antibody, IgG, Unconjugated	Rabbit	polyclonal	Genetex via BIOZOL	GTX125926–25
IRF3	Mouse	monoclonal	Biolegend	655701
p21 (187)	Mouse	monoclonal	Santa Cruz	sc–817
Peroxidase–conjugated Goat anti–Mouse IgG	Goat	polyclonal	Thermo Fisher	"0031430 1892913 new ref : 31430"
Peroxidase–conjugated Goat anti–Rabbit IgG	Goat	polyclonal	Thermo Fisher	"0031460 1892914 NCI1460 new ref : 31460"
Phospho–AKT (ser473)	Rabbit	polyclonal	Cell–signalling	9271

5.1.9 Primers

Table 15: Primers

Name	Description	Sequence
3_RIG_DC_FusRev	Binds to 3′ of ΔCARD–RIG–I to	CCGCTTTACTTGTACACTCGAGTCATTTGGACATTTCTGCTGG

	clone into pE GIP (pL 646)	
3'_RIG_FusRev–AK	Binds to 3′ of WT–RIG–I to clone into pE GIP (pL 646)	CCGCTTTACTTGTACACTCGAGTCATTTGGACATTTCTGCAGG
FLAG–DC–RIG–I–F	Binds to 5′ Flag tagged of ΔCARD–RIG–I to clone into pE GIP (pL 646)	GCAGCCCGGGGGATCCACCGGTCGCCACCATGGATTATAAGGATGATGATGATAAAGGTGATTATAAGG
FLAG–Rev	For amplification of the vector backbonepE GIP (pL646) with FLAG tag	AGATGAAGAACCGCCACCTTTATCATCATCATCCTTATAATC
GST–Fwrd_fus	For cloning GST into the vector pE GIP (pL 646) with FLAG tag	GGCGGTTCTTCATCTTCCCCTATACTAGGTTATTGGAAAATTAAGGGC
GST–Rev–Fus	For cloning GST into the vector pE	ACTTGTACACTCGAGTTATTTTGGAGGATGGTCGCCACCACC

	GIP (pL 646) with FLAG tag	
huRIG–I seq primer (1938–1957) fwd	intern seq Primer for huRig–I (nt 1938–1957)	GATTGAAGGAAATCCTAAAC
huRIG–I seq primer (911–935) fwd	intern seq Primer for huRig–I (nt 911–935) fwd	AACAGCAGAAATCTGTATTCTCAAA
huRIG–I seq primer (911–935) rev	intern seq Primer for huRig–I (nt 911–935) rev	TTTGAGAATACAGATTTCTGCTGTT
pEF–BOS for primer	for sequencing pEF–BOS vector	GGGATTTCTTGTCTCCCACG
pEF–BOS rev primer	for sequencing pEF–BOS vector	GGAGAGCGGGCGGGT
pEGIP_Fwrd	For amplification of the vector backbone pEGIP (pL 646) with FLAG tag	CTCGAGTGTACAAGTAAAGCGGCCGCG

wt_RIG_FLAG_F_AK	Binds to 5′ Flag tagged of WT–RIG–I to clone into pE GIP (pL 646)	GCAGCCCGGGGGATCCACCGGTCGCCACCATGGACTACAAAGACCATGACGGTG

5.1.10 Plasmids

Table 16: Plasmids

Name	System	Description	Source
pE 2xFLAG GST	Cell	AmpR, template pE DC RIG–I amplification of the vector containing the FLAG tag fused with amplified GST from pVax GST Strep.	This work
pE DC RIG–I	Cell	AmpR, Template pEF–BOS–2×Flag–RIG–I DeltaCARD cloned into pE GFP backbone after restriction removal of GFP with BamH1 Bsrg1	This work
pE GIP (pL 646)	Lentiviral system	PuroR, Lentiviral vector for stable integration of GFP expression cassette with puromycin selection.Addgene	Zou et al., 2009
pE WT RIG–I	Cell	Template pI.18 3×Flag huRIG–I cloned into pE GFP backbone after restriction removal of GFP with BamH1 Bsrg1	This work
pEF–BOS RIG–I K270A–Flag	cell	AmpR, pEF–Bos vector, cDNA was inserted into XbaI–Cla1 restricted sites, Flag tagged	Kageyama et al., 2011
pEF–BOS RIG–I wt–Flag	cell	AmpR, pEF–Bos vector, RIG–I cDNA was inserted into XbaI–Cla1 restricted sites, Flag tagged	Kageyama et al., 2011

pEF–BOS–2×Flag–RIG–I DeltaCARD	cell	AmpR. pEF–BPS containing human RIG–I delta CARD mutant synthesized by BIOCAT	This work
pEF–BOS–2×Flag–RIG–I K270A/E373Q	cell	AmpR. pEF–BPS containing human RIG–I double mutant K27A/E373Q. Synthesized by BIOCAT	This work
pEF–BOS–2×Flag–RIG–I T409A/S411A	cell	AmpR. pEF–BPS containing human RIG–I double mutant . T409A/S411A synthesized by BIOCAT	This work
pEGFP–N1	REP	KanR, EGFP fusion vector, Clontech	
pI.18 3×Flag huRIG–I	cell	AmpR, contains human RIG–I, 5' 3×Flag. Cloned by PCR amplification of plasmid pEF–BOS RIG–I wt–Flag and cloned into BamHI/XhoI digested pI.18 by In–Fusion cloning.	
pLP1HIV	Lentiviral system	Modified from ViraPowerTM Kit	Thermo Fischer
pLP2REV	Lentiviral system	Modified from ViraPowerTM Kit	Thermo Fischer
pLP3 VSV	Lentiviral system	Modified from ViraPowerTM Kit	Thermo Fischer
pRRL–SIN–CMV GFP	Lentiviral system	AmpR, Control plasmid for lentiviral system	Zufferey et al., 1998

pVax GST Strep	GST Strep ctrl	Provided by Gleyder Roman Sosa and Andreas Schoen	

5.1.11 Commercial reagents

Table 17: Commercial reagents

Name	**Supplier**
4′,6–diamidino–2–phenylindole (DAPI)	Sigma–Aldrich, Steinheim
Acrylamid/Bis (Rotiphorese® Gel 30 (37.5:1))	Roth, Karlsruhe
Agar	Merck, Darmstadt
Agarose	SERVA, Heidelberg
Ammonium persulfate (APS)	Sigma–Aldrich, Steinheim
Ampicillin sodium salt (50 mg/ml)	Sigma–Aldrich, Steinheim
Avicel	FMC BioPolymer, Philadelphia, PA, U.S.A.
Complete Protease Inhibitor Cocktail Tablets	Roche/Merck, Darmstadt
Crystal violet	Sigma–Aldrich, Steinheim
Dimethylsulfoxide (DMSO)	Sigma–Aldrich, Steinheim
Dynabeads™ Protein G for Immunoprecipitation	Thermo Fisher Scientific, Schwerte
Ethanol, absolute	Roth, Karlsruhe
Ethanol, denatured	Roth, Karlsruhe
Ethidium bromide	Promega, Walldorf
Ethylenediaminetetraacetic acid (EDTA)	Roth, Karlsruhe
FluorSave Reagent	Merck, Darmstadt
Formaldehyde (37%)	Roth, Karlsruhe
Glycerol	Roth, Karlsruhe
Glycine	Roth, Karlsruhe
Hydrochoric acid (HCl)	Roth, Karlsruhe
Immobilon® ECL Ultra Western HRP Substrate	Merck, Darmstadt
Isopropanol	Sigma–Aldrich, Steinheim
L–1–tosylamido–2–phenylethyl chloromethyl ketone (TPCK)–treated trypsin	Sigma–Aldrich, Steinheim

Methanol	Roth, Karlsruhe
Milk powder	dm Drogeriemarkt, Giessen
N,N,N',N'–tetramethylethylenediamine (TEMED)	Sigma–Aldrich, Steinheim
NaOH	Sigma–Aldrich, Steinheim
Neutral Red	Merck, Darmstadt
NP–40 (Igepal®)	Sigma–Aldrich, Steinheim
Paliperidone	Sigma–Aldrich, Steinheim
Paraformaldehyde	Roth, Karlsruhe
Retinoic acid	Sigma–Aldrich, Steinheim
Sodium bicarbonate (7.5%)	Sigma–Aldrich, Steinheim
Sodium chloride (NaCl)	Sigma–Aldrich, Steinheim
Sodium dodecyl sulfate (SDS)	Merck, Darmstadt
SuperSignal™ West Femto Maximum Sensitivity Substrate	Thermo Fisher Scientific, Schwerte
Triton X–100	Sigma–Aldrich, Steinheim
TrueBlue™ Peroxidase Substrate	SeraCare, Milford USA
Tween–20	Sigma–Aldrich, Steinheim
Yeast extract	Merck, Darmstadt
β–Mercaptoethanol	Sigma–Aldrich, Steinheim

5.1.12 Kits

Table 18: Commercial kits

Name	**Supplier**
Dual Luciferase Reporter Assay system	Promega, Walldorf
Dynabeads® Antibody Coupling Kit	Thermo Fisher Scientific, Schwerte
E.Z.N.A.® Gel Extraction Kit	Omega bio–tek, Norcross, GA, U.S.A.
E.Z.N.A.® Plasmid DNA Midi Kit	Omega bio–tek, Norcross, GA, U.S.A.
Premix Ex Taq™ (probe qRT–PCR)	Takara, Saint–Germain–en–Laye, France

PrimeScript™ RT reagent Kit with gDNA Eraser	Takara, Saint–Germain–en–Laye, France
QIAamp® Viral RNA Mini Kit	Qiagen, Hilden
Rapid DNA Ligation Kit	Thermo Fisher Scientific, Schwerte
RNeasy® Mini Kit	Qiagen, Hilden
TB Green™ Premix Ex Taq™ II (Tli RNase H Plus)	Takara, Saint–Germain–en–Laye, France
ViraPowerTM Kit	Thermo Fisher Scientific, Schwerte
ZymoPure™ Plasmid Midiprep Kit	Zymo Research, Freiburg

5.1.13 Consumables and other materials

Table 19: Plasticware

Name	**Supplier**
Biosafety container (Biotainer 1.8 l)	E3 Cortex, Mitry–Mory, France
Cell culture flasks, 25 – 175 cm2	Greiner Bio–One, Frickenhausen
Cell culture plates, 6–, 12–, 24–, and 96–well	Greiner Bio–One, Frickenhausen
Collagen IV–coated trans well plates CLS3470–48EA	Corning Costar, Wiesbaden
Cryotubes	Sarstedt, Nuembrecht
Dispensertips PD–Tips, BIO–CERT®	Brand, Wertheim Bestenheid
Graduated TipOne® Filter Tip (sterile), 0.1 – 1000 µl	Starlab, Hamburg
MicroAmp™ Fast Optical 96–Well Reaction Plate, 0.1 ml	Thermo Fisher Scientific, Schwerte
MicroAmp™ Optical Adhesive Film	Thermo Fisher Scientific, Schwerte
Microscope slide	Roth, Karlsruhe
Parafilm	Kobe, Marburg
PCR tubes, 0.2 ml	Biozym, Hessisch Oldendorf
Petri dishes	Sarstedt, Nuembrecht
Pipet tips, Tip–One, 0.1 – 1000 µl	Starlab, Hamburg
Polypropylen tubes (Falcon), 15 – 50 ml	Sarstedt, Nuembrecht

PVDF Membrane: Immobilon®–P Transfer Membrane	Millipore, Schwalbach
Reaction tubes, 1.5 ml	Sarstedt, Nuembrecht
Reaction tubes, 2 m	Eppendorf, Wesseling–Berzdorf
Screw cap tubes, 1.5 ml	Sarstedt, Nuembrecht

5.1.14 Instruments

Table 20: Instruments

Name	**Supplier**
(Wide) Mini–Sub® Cell GT agarose gel chamber	Bio–Rad, Feldkirchen
2720 Thermal Cycler	Applied Biosystems, Thermo Fisher Scientific,Schwerte
Allegra® X–15R Centrifuge	Beckman Coulter, Krefeld
Allegra® X–30R Centrifuge	Beckman Coulter, Krefeld
ChemiDoc XRS+	Bio–Rad, Feldkirchen
Color Sprout Plus Mini Centrifuge	Biozym, HessischOldendorf
DNA gel chamber	Bio–Rad, Feldkirchen
DS–11+ Spectrophotometer	DeNovix, Wilmington, DE, U.S.A
EVOS® XL Core Imaging System	Thermo Fisher Scientific, Schwerte
Handy Step electronic	Brand, Wertheim Bestenheid
Heat block	Steute, Loehne
IKAMAG REO S6 Magnetic Stirrer	Ika, Staufen
INCU–Line bacterial incubator	VWR, Darmstadt,
Labotect Incubator C200	Labotect, Goettingen
Leica DFC3000 G fluorescence camera	Leica, Wetzlar
Microfuge® 20R Centrifuge	Beckman Coulter, Krefeld
Mini–PROTEAN® Tetra System	Bio–Rad, Feldkirchen
MSC–Advantage biological safety cabinet	Thermo Fisher Scientific, Schwerte
Olympus IX70 Inverted Fluorescence Phase Contrast Microscope	Olympus, Tokyo, Japan
PowerPac™ basic	Bio–Rad, Feldkirchen

Precision scale	Sartorius, Goettingen
REAX top vortex mixer	Heidolph, Schwabach
Scale PB602	Mettler–Toledo, Giessen
SimpliAmp™ Thermal Cycler	Life Technologies, Thermo Fisher Scientific, Schwerte
StepOnePlus Real–Time PCR System	Applied Biosystems, Thermo Fisher Scientific, Schwerte
T100™ Thermal Cycler	Bio–Rad, Feldkirchen
ThermoMixer F1.5	Eppendorf, Wesseling–Berzdorf
Trans–Blot® Turbo Transfer System	Bio–Rad, Feldkirchen
TriStar2 Multimode Reader LB 942	Berthold, Bad Wildbad
Vacuum system Integra Vacusafe	Integra, Biebertal
Waterbath	Memmert, Schwabach

5.1.15 Software

Table 21: Software

Name	**Supplier**
BlastN	NCBI
BlastP	NCBI
Clustal Omega	EMBL
GraphPad PRISM 8.0.2	GraphPad Software, LLC
GraphPad PRISM 9.0.2	GraphPad Software, LLC
Image Lab 5.2.1	Bio–Rad
Instrument Control and Evaluation (ICE) software	Berthold
Ligation Calculator	http://www.insilico.uni–duesseldorf.de/Lig_Input.html
Microsoft Office Word, Excel, PowerPoint 2016	Microsoft
SnapGene viewer	GSL Biotech LLC
StepOne software v2.3	Life Technologies Corporation

5.2 Methods

5.2.1 Cells

Human A549 WT and CRISPR/Cas9–mutated knockout cells A549 CTRL KO, A549 RIG–I KO, A549 MDA5 KO, A549 MAVS KO (puromycin sensitive) (Willemsen et al., 2017), A549 WT, A549 RIG–I KO (puromycin resistant) (Schilling et al., 2020), and HEK 293T, HEK 293T RIG–I KO as well as canine MDCK and human HuH7 cells were cultivated as described (Weber et al., 2015). Cells were cultivated in sterile plastic flasks or plates at 37°C in a 5% CO_2 atmosphere and passaged in cell culture medium CCM34 with 10% fetal bovine serum (FBS) and 1X penicillin–streptomycin–glutamine (P/S/Q). The set of cells A549 WT, A549 RIG–I KO (Schilling et al., 2020) stable transfected with glutathione–s–transferase (GST), RIG–I WT or RIG–I DC were cultivated in cell culture medium with 0.5 µg/ml puromycin. When 90–100% confluency was reached, cells were passaged as follows: cells were washed once with PBS, to remove FBS which inactivates trypsin activity, and incubated with trypsin–EDTA solution. Upon detachment, cells were resuspended in cell culture medium and either passaged or seeded for further use. When passaged, for 1:10 dilution, cells were resuspended in total volume of 10 ml, 9 ml were discarded and 1 ml was resuspended in fresh cell culture medium. For seeding, cells were pelleted by centrifugation at 800×g for 5 min, and the supernatant were discarded. Afterwards, cells were resuspended with cell culture medium, counted in Neubauer chamber, and seeded for the desired cell number.

Primary human airway epithelial cells, prepared from cryo–preserved normal human bronchial epithelial cells of non–smoking donors, were obtained from Lonza (CC–2540). The undifferentiated cells were seeded on collagen IV–coated trans well plates (Corning Costar) and grown in a mixture of DMEM (Thermo Fisher) and BEGM (CC–3170, Lonza) supplemented with retinoic acid (75 nM, Sigma Aldrich) with medium exchange every second day. After reaching confluence, the cells were cultivated under air–liquid interface conditions for at least four additional weeks for full differentiation into pseudostratified human airway epithelia. Medium from the basolateral compartment was renewed every second day and the apical surface was washed weekly with PBS.

5.2.2 Infections

Before infection, the cells were washed once (immortalized cell lines) or at least twice (primary airway epithelial cells, to remove mucus) with phosphate–buffered saline (PBS) and inoculated for 1 h with virus dissolved in infectious medium (CCM34 medium containing 5% Penicillin–Streptomycin–Glutamine, 0,2% BSA and 1 μg/ml L–1–tosylamido–2–phenylethyl chloromethyl ketone (TPCK)–treated trypsin) (immortalized cell lines) or in PBS (primary airway epithelial cells) for Influenza infection. For SARS–CoV–2, HuH7 cells were washed once with phosphate–buffered saline (PBS) and inoculated for 1 h with virus dissolved in Opti–MEM™ I Reduced Serum Medium. For the infections proper amount of virus using the multiplicity of infection (MOI) was applied. MOI of 1 means 1 infectious particle per cell. Then the inoculum containing the virus was added to the cells, which were gently rocked for every 15 min to ensure even distribution of the inoculum, and after 1 hour the inoculum was removed and replaced with fresh medium for further incubation at 37°C.

5.2.3 Production of viral stocks

A/PR/8/34, A/HAM/2009, A/WSN/33 PB2 627 E/K were propagated on MDCK cells. Cells were seeded in T175 flasks and infected one day after with 0.01 MOI. Upon infection, infectious medium was added. Cell supernatants were collected 2 days post infection and stored at –80°C. Influenza stocks were titrated by plaque assay on MDCK cells. SARS–COV–2 virus and infections were performed by Dr Shalamova L.

5.2.4 Viral titer determination through plaque assay

The plaque assay is a method to determine the virus concentration by the number of plaque forming units (PFU) produced in a cell monolayer. Plaque assay was performed to determine the viral titer of stocks or infected cell supernatants. Virus containing samples were serially diluted (1/10) and used to infect MDCK cells and 24 hours later, the medium was exchanged with 1.5%–Avicel solution per well (1X MEM containing 1.5% Avicel, 5% FBS, 1X P/S/Q, 1 μg/ml TPCK–treated trypsin). Avicel prevents the spread of newly produced viral particles across the monolayer by allowing only infection of the neighboring cells. This leads to the formation of the so–called plaques, which are cell–free dots in the well. Depending on the following staining method, cells were incubated for 24 hours (immunostaining) or 48 hours (crystal

violet). Immunostaining as described previously (Matrosovich et al., 2006), is a method to detect plaques through antibodies detecting viral proteins. Briefly cells, were washed with PBS to remove Avicel solution and fixed with 4% PFA at 4°C for 20 minutes followed by 15 minutes incubation with IF permeabilization buffer RT (room temperature). Wells were then incubated with primary antibody (1:2000 in IF blocking buffer) detecting viral protein for 60 minutes rocked. Cells were then washed 3 times with IF wash buffer and incubated with the secondary antibody specific to the species of the primary one (1:2000 in IF blocking buffer) 60 minutes rocked. Then, cells were washed with IF wash buffer followed by 30 minutes incubation with TrueBlue™ Peroxidase Substrate which stains the plaques blue. The reaction was stopped with tap water washes and plates were dried completely before plaque determination. For the case of crystal violet detection, cells were washed with PBS and stained with crystal violet solution (0.75% crystal violet, 3.75% formaldehyde, 20% ethanol, 1% methanol in ddH_2O) for 20 minutes. For the determination of the viral titer the following form was used.

Titer (in PFU (plaque forming units)/ml) = plaque number / (dilution factor * inoculum volume (in ml))

5.2.5 Inhibitor treatments

Paliperidone (PP) was dissolved in infectious medium for Influenza or cell culture medium for SARS–CoV–2 infections. Cells were treated with PP (10 μg/ml when Influenza followed, 1 μg/ml and 10 μg/ml when SARS–CoV–2 infections followed, stocks dissolved in DMSO) at 1 h post–infection (immortalized cell lines), or at 1 h and at 48 h post infection (primary cells).

5.2.6 Cell viability assay

Cell viability assays are used to measure the fitness of the cells and consequently the toxicity of chemical compounds. For the course of this study, neutral red staining was used which is a eurhodin dye, which is incorporated into the lysosomes of live cells, while dead cells or those undergoing cell death cannot incorporate the dye (Repetto et al., 2008). Briefly, cells were treated with different concentration of PP for 24 h. Medium was removed and 40 μg/ml neutral red, diluted in cell culture medium, was added for 1 h at 37° C. Cells were then fixed with 4% paraformaldehyde in PBS,

followed by incubation with neutral red destain solution (1% acetic acid solution containing 30% ethanol). Optical density determined at wavelength λ=540 nm.

5.2.7 Real–time qPCR

Real–Time quantitative Reverse Transcription PCR is a method that enables reliable detection and measurement of RNA transcripts in a sample of interest. This is possible upon binding of fluorescent probes to the single stranded DNA or dyes by intercalating between the bases of DNA molecules. This leads to the release of energy as fluorescence, with the fluorescence intensity being directly dependent on the concentration of double stranded DNA, which is measured upon each cycle of PCR. The fluorescence intensity is plotted to a ΔRn, which is the fluorescent signal at each time point, to the number of PCR cycles. A signal that is above a threshold is considered as signal of the amplified DNA and is defined as threshold cycle (CT). In order to calculate the relative fold gene expression of samples the 2^–(ΔΔCT) method is used.

ΔΔCT = ΔCT (treated sample) – ΔCT (untreated sample)

Where Δ means the difference of two numbers. The **ΔCT** of a sample is defined as the difference of the CT values of the gene of interest and the housekeeping gene, which is typically a constitutively expressed gene. Upon calculation of the upper equation, in order to calculate the fold gene expression, the following equation is used:

Fold gene expression = 2^–(ΔΔCT)

For the course of this study, total RNA was isolated from cells using the RNeasy Mini Kit (Qiagen) which uses the system of silica–membrane spin–column technology. Upon determination of the RNA concentration with a DS–11+ Spectrophotometer, Two–step probe qRT–PCR or Two–step SYBR® green qRT–PCR followed. For both two–step qRT–PCR, RNA isolated from cell lysates was first transcribed into copy DNA (cDNA). For this, the PrimeScript™ RT reagent Kit with gDNA Eraser from Takara was used according to manufacturer's instructions. With this kit, potentially contaminating genomic DNA is eliminated in a first step, followed by reverse transcription of the RNA into cDNA by a reverse transcriptase in a second step. Polymerase chain reaction with the SYBR Premix Ex Taq (Tli RNaseH Plus) master mix with the following protocol were performed (table 22).

Table 22: Polymerase chain reaction conditions with the SYBR Premix Ex Taq (Tli RNaseH Plus)

Initial Denaturation	95°C 30sec	
Denaturation	95°C 5 sec	40 cycles
Anneal and elongation	60°C 30sec	
Melt curve stage	95°C 15sec	
	60°C 15sec	
	+ 0.3°C increase	
	95°C 15sec	

The Premix Ex Taq (Probe qPCR) master mix was used with the following protocol (table 23).

Table 23: Polymerase chain reaction conditions with the Premix Ex Taq (Probe qPCR)

Initial Denaturation	95°C 20sec	
Denaturation	95°C 1 sec	40 cycles
Anneal and elongation	60°C 20sec	

Values were normalized against GAPDH (in the course of Influenza infection) and 18S ribosomal RNA (in the course of SARS–CoV 2) using the ΔΔCT method (Livak and Schmittgen 2001).

5.2.8 Viral polymerase activity (RdRp activity) (minigenome assay)

Transcription and replication of Influenza virus genome is accomplished by the viral RNA–dependent RNA polymerase (RdRp). The activity of the polymerase can be examined through minigenome assays, where fluorescence–encoding reporter viral RNAs are replicated by the *in situ* reconstituted viral polymerase (TeVelthuis et al., 2018, Lutz et al., 2005). For the course of this study HEK 293T cells were transiently transfected with viral polymerase encoding constructs, PB1 (250 ng), PA (25 ng), NP (250 ng), and dual luciferase expressing reporter constructs, firefly luciferase–encoding viral RNA (50 ng) and Renilla luciferase reporter gene (18.75 ng). Furthermore, constructs encoding the avian signature PB2 627E (250 ng), or mammalian PB2 627K (250 ng) were transiently transfected to reconstitute the polymerase function. 4 hours later, media was removed and media containing PP (10 μg/ml) was used as treatment.

24 hours later, cells were lysed in 1X PLB, and Firefly and Renilla luciferase levels were measured with Dual Luciferase Reporter Assay System (Promega) and a LB 942 TriStar2 multimode reader (Berthold Technologies) according to manufacturer's recommendations. Firefly Luciferase was normalized to Renilla luciferase transfection control and DMSO (Dimethyl sulfoxide) stimulation levels were set as 100%.

5.2.9 Immunoblotting

SDS–PAGE (sodium dodecyl sulfate–polyacrylamide gel electrophoresis) is a method that allows separation of proteins by mass on a matrix, which is a polyacrylamide gel. Furthermore, SDS is used to confer to the proteins charge and a similar charge to mass ratio with a concomitant protein denaturation induced by heat and β–mercaptoethanol. Upon loading of the denatured protein solution and application of constant electric charge, the proteins migrate towards the anode, with the speed being dependent on the mass of each protein. Due to the fragile nature of the matrix, the proteins are transferred to a PVDF (polyvinylidene difluoride) membrane using electric current. The negatively charged proteins move towards the anode where the membrane is situated, leading to the transfer of proteins to a thin membrane. After blocking of the membrane with a dilute solution of proteins, most commonly used are non–fat dry milk and BSA (bovine serum albumin), to avoid non–specific binding, the primary antibody, produced from certain animal species, against a certain protein of interest and a secondary antibody are applied. The secondary antibody is species–specific, dependent on primary antibody, and is linked with the horseradish peroxidase. A chemo–luminescent substrate is cleaved by horseradish peroxidase producing luminescence, which can be detected using photographic film or camera. Thus, the signal can be analyzed by densitometry to specifically quantify the amount of a target protein.

For the course of this study, cells were scraped off in PBS, centrifuged for 5 min at 800 g, and lysed using 0.5% Triton X–100 in PBS for 10 min at 4°C. After 10 min centrifugation at 10,000 g (4°C), supernatants were boiled for 5 min in sample buffer (62.5 mM Tris–HCl pH 6.8, 25% Glycerol, 2% SDS, 0.01% Bromophenol Blue, 5% β–Mercaptoethanol), separated by SDS–PAGE 10 or 12% separating gel and 3% stacking gel (prepared as table 24) and transferred to a PVDF membrane using a semidry blot transfer apparatus (Bio–Rad).

Table 24: Casting polyacrylamide gel protocol

Reagent	**3% stacking gel (for 2 gels volume in ml)**	**10% separating gel (for 2 gels volume in ml)**	**12% separating gel(for 2 gels volume in ml)**
ddH_2O	2.56	4.1	3.4
Rotiphorese® Gel 30 (37.5:1)	0.4	3.3	4
Rotiphorese®–PAGE Matrix Buffer plus	1	2.5	2.5
10% APS solution	0.04	0.1	0.1
TEMED	0.004	0.006	0.006

After incubation with 10% nonfat milk in Tris–buffered saline (TBS; 10 mM Tris, pH 8.0, 150 mM NaCl) for 60 min, the membrane was washed once with TBS / 0.1% Tween–20 (TBS–T) and incubated with the respective antibodies at 4°C for 18 h. Membranes were washed three times in TBS–T for 10 min each and incubated with a 1:10,000 dilution of horseradish peroxidase–conjugated anti–mouse (Thermo Fisher, 31430) or anti–rabbit (Thermo Fisher, 31460) antibodies for 1 h. Blots were washed with TBS–T three times and once with TBS and developed with the ECL system (Super–Signal™ West Femto Chemiluminescent Substrate) according to the manufacturer's protocols.

5.2.10 RIG–I activation assays

Upon recognition to its ligands, RIG–I undergoes a conformational switch followed by oligomerization. By limited protein digestion with trypsin, the conformational switch of RIG–I and thus protection from the digestion by the emergence of fragment that is resistant to digestion can be visualized through immunoblotting (Weber and Weber 2014). Thus briefly, upon cell lysis and protein isolation, half of each lysate was left untreated (input control) while the other half was subjected to limited protease digestion. Thereby, samples were digested for 10 min with 0.2 µg/µl TPCK–treated trypsin (Sigma–Aldrich) at 37°C. Then 4–fold sample buffer (200 mM Tris–HCl pH 6.8, 8% SDS, 40% glycerol, 25% β–Mercaptoethanol, 0.4%

Bromophenol Blue) was added and samples were boiled for 5 min at 100°C. Samples were subjected to 12% SDS–PAGE and immunoblot analysis using mouse monoclonal anti–RIG–I antibody (Adipogen ALME–1). Band intensities were quantified on a ChemiDoc system (Bio–Rad) using Image Lab 5.2.1 (Bio–Rad). Activated RIG–I represents the ratio of trypsin–resistant RIG–I to undigested RIG–I.

5.2.11 Co–immunoprecipitation assay

The co–immunoprecipitation assay is used to identify protein–protein interactions by targeting a protein with a specific antibody. With the usage of beads, an antibody can immobilize the target protein with its potential interactors. Upon elution and western blot, these potential interactors can be identified. So briefly, for the course of this study, cells were seeded in 6 well plate format ($1*10^6$ each well) and 6 hours post infection were scraped off with PBS followed by centrifugation for 5 min at 800 g. Pellets were resuspended in RIPA buffer (50 mM Tris–HCl pH 7.5, 0.15 M NaCl, 1% NP40) containing protease inhibitors (c0mplete protease inhibitor cocktail, Roche, 04693116001) and incubated for 10 min at 4°C and stored at –20°C. For coupling, 25 µl of Dynabeads™ Protein G for Immunoprecipitation per sample were resuspended in RIPA buffer and incubated with the corresponding antibodies using the so–called sandwich method. During this, the beads are coupled initially with the proper secondary antibody overnight 4°C with slow tilt rotation, followed by the primary antibody overnight at 4°C with slow tilt rotation, with final incubation with the supernatants also overnight at 4°C with slow tilt rotation. Thus, supernatants were immunoprecipitated using mouse monoclonal anti–p53 (Calbiochem, OP43), rabbit polyclonals anti–NP (Genetex GTX125989) and anti–PB2 (Genetex GTX125926) as described (Krischuns et al., 2018). Mouse monoclonal anti–p53 (1:1000) and rabbit polyclonals anti–NP (1:1000), anti–PB2 (1:200), and anti–beta tubulin (Abcam, ab6046), (1:1000) were used for immunoblotting.

5.2.12 Immunofluorescence

Immunofluorescence is an assay that enables the visualization of a protein in cells. With the use of a fluorescence microscope and immunostaining and by using fluorophores, the location and distribution of certain proteins can be detected and visualized. Thus, for the course of this study, and to detect the expression of the protein in stably expression cell lines, cells ($1*10^5$ cells per well) were seeded and in the

following day were rinsed with ice–cold PBS and fixed with 4% paraformaldehyde for 20 min at room temperature followed by permeabilization with 0.5% Triton X–100 solution. The cells were subjected to immunofluorescence staining with FLAG–M2 (1:500) antibody diluted in PBS containing 1% FCS solution for 1 h at room temperature. The cells were then washed with cold 1% FCS in PBS three times for 5 min each, and incubated with Alexa Fluor 488 Donkey anti–mouse IgG (1:200) (Invitrogen) at room temperature for 1 h. For nuclear staining, cells were incubated with 4′,6–diamidino–2–phenylindole (DAPI) which is a DNA–specific fluorescent probe (1:1000) (Sigma) (Kapuscinski 1995). Cells were evaluated on a qualitative fluorescent microscope (IX70; Olympus, Tokyo, Japan) and photomicrographs were taken using a monochromatic camera (DFC3000G; Leica, Wetzlar, Germany). Fluorescence intensities from images of three randomly selected microscopic fields of cells were acquired (LAS.X.13, Leica).

5.2.13 Transfections

Transient transfection is used to introduce nucleic acids into the cells, which are not incorporated into the genome and thus are available for a short period of time. Although transient transfection leads to a limited–time expression of proteins, the high copy number of the transfected material leads to high expression of the target translated protein. In this study, transient transfection was performed with TransIT–LT1 according to the manufacturer's protocol (Mirus Bio LLC). Briefly, HEK 293T cells were seeded and in the following day, the required plasmid amount (diluted in Optimem™ I Reduced Serum Medium) was mixed with 3µl of TransIT–LT1 per 1 mg of DNA in serum free medium for 15 min. This mix was gently applied to the attached cells and cells were incubated for 1 (minigenome) or 2 (RIG–I mutants antiviral assay) days at 37°C.

5.2.14 Generation of stable cell lines

In order to accomplish constant and long–term expression of a certain protein, lentiviral stable cell line system is used. Besides the advantage of the constant expression there is also universal expression of the incorporated nucleic acid, with the elimination of expression variance since the nucleic acid is incorporated into the cell´s chromosome. Furthermore, cells that have not taken up the nucleic acid of interest can be excluded through antibiotic selection, since generated stable cell lines express

antibiotic resistant genes. Thus, stable cell lines expressing the genes of interest from an integrated lentiviral vector (Clontech, Thermo Fischer, Zufferey et al., 1998). Briefly a mix of plasmids pLP1HIV, pLP2REV, pLP3 VSV with either pE 2xFLAG GST, pE WT RIG–I or pE DC RIG–I were transiently transfected to HEK293T cells. Upon 2 days of incubation, supernatants containing newly produced virions carrying the gene of interest, were isolated and used to infect A549 WT and RIG–I KO cells (Schilling et al., 2020) for 2 days. Selection of transduced cells was accomplished through puromycin resistance. Cells were then cultured under constant puromycin selection.

5.2.15 Plasmid DNA isolation

To prepare a working stock of plasmid DNA for various experimental applications, bacteria expressing the plasmid of interest were picked from the LB–agar plates or glycerol stocks (stored at –80°C) with a 10 µl pipette tip and used to inoculate a 50 ml LB medium solution containing 100 ng/ml ampicillin. After overnight incubation at 37°C while rotating at approx. 120 rpm, the bacteria culture was transferred to a 50 ml falcon tube and pelleted for 30 min at 4,000×g at 4°C. Plasmid DNA isolation was carried out with the E.Z.N.A.® Plasmid DNA Midi Kit from Omega bio–tek according to manufacturer's instructions. Plasmid DNA concentration was measured with a DS–11+ Spectrophotometer.

5.2.16 Cloning and prokaryotic cell culture

For the transfection experiment, both transient and stable, as well as the polymerase activity assay, the gene of interest have to be incorporated in a bacterial vector backbone. Thus, with molecular cloning the desired gene of interest is fused into a vector backbone to produce the construct of interest. Initially, the gene of interest is amplified using PCR. The primers used were designed to be complementary on the respective end of the gene of interest (15–20 nucleotides) including a restriction site for a certain restriction enzyme, followed by a buffer sequence to enable better restriction enzyme binding. Here the Phusion® polymerase system was used (table 25).

Table 25: Phusion® system master mix

Reagent	**Volume for one reaction (µl)**
ddH_2O	12.3
5X Phusion® HF buffer	4

dNTPs (2 mM)	2
Primer, forward (20 μM)	0.5
Primer, reverse (20 μM)	0.5
Phusion® DNA Polymerase	0.2
Template DNA (2 ng/μl)	0.5
DMSO	0.5

With the PCR conditions given in table 26.

Table 26: Phusion® system PCR conditions

Initial denaturation	98°C 30sec	
Denaturation	98°C 10sec	35 cycles
Annealing	Depending ofTm of primers 30sec	
Elongation	72°C Depending of the length of gene of interest	
Final elongation	72°C 10 min	
Hold	4°C ∞	

Primer Melting Temperature (Tm) is defined as the temperature which induces annealing of a dsDNA molecule to ssDNA. In order to remove any template DNA samples were digested with *DpnI* restriction enzyme (table 27) for 90 minutes at 37°C, followed by enzyme inactivation for 20 minutes at 80°C.

Table 27: *DpnI* restriction digestion conditions

Reagent	**Volume for one reaction (μl)**
10X CutSmart buffer	2
DNA	17
DpnI	1

Afterwards, the product of the reaction and the corresponding vector were digested with restriction enzymes to create appropriate ligation “sticky” (5’ or 3’ overhang) or blunt (no overhang) ends (table 28) for 90 minutes at 37°C, followed by enzyme inactivation for 20 min at 65°C. These enzymes act as a defense mechanism for bacteria and archaea, by recognizing and cleaving a target sequence, often comprised by 4–8 base pairs (usually palindromic).

Table 28: Restriction enzymes digestion mix

Reagent	**Volume for one reaction (µl)**
Nuclease free ddH_2O	Up to 20 µl
Cutsmart buffer (10X)	2
Restriction Enzyme 1	20 Units
Restriction Enzyme 2	20 Units
DNA	1 µg

To insert the amplified and cut DNA sequence into the linearized backbone vector, the Rapid Ligation DNA kit was used (table 29) for 5 minutes 22°C, with optimal ratio of insert/vector being 3:1 using the Ligation Calculator tool (http://www.insilico.uni–duesseldorf.de/Lig_Input.html).

Table 29: Ligation master mix

Reagent	**Volume for one reaction (µl)**
Linear vector DNA	Dependent on ng amount
Insert DNA	Dependent on ng amount
5X ligation buffer	4 µl
T4 DNA ligase	1 µl
ddH_2O	Up to 20 µl

The product of the ligation was, afterwards, transformed into *Escherichia coli (E. coli)* bacteria. Bacteria were carefully thawed on ice and 2µl of the ligation reaction was added to the bacteria solution followed by 30 min incubation on ice. Cells were then heat shocked at 42°C for 30 sec and 400 µl LB medium was added followed by incubation of 60 min at 37°C while shaking at 400 rpm. 200 µl of this reaction was plated on LB agar plates containing 100 ng/ml ampicillin to promote the amplification of only the expected bacteria containing the construct of interest. Bacterial plates were incubated overnight at 37°C.

In order to confirm that the proper insert was inserted into the vector backbone and amplified in bacteria, a colony PCR was performed (table 30, 31). Depending on the construct, a set of primers was used, preferably those which were used for amplification.

Table 30: Colony PCR master mix

Reagent	**Volume for one reaction (µl)**
ddH_2O	15.2
10X buffer	2
dNTPs (2mM each)	2
Primer 1 (10 µM)	0.2
Primer 2 (10 µM)	0.2
Template (colony)	Colony
Jumpstart Taq polymerase	0.4

Table 31: Colony PCR conditions

Initial denaturation	94°C 60 sec	
Denaturation	94°C 30 sec	30 cycles
Annealing	Depending of Tm of primers 30sec	
Extension	72°C Depending of the length of gene of interest	
Final extension	72°C 10min	
Hold	4°C	

Colonies were picked using a 10µl tip and swirled into the PCR reaction. Afterwards the reaction was loaded with 6X orange DNA loading dye and separated on agarose gel (1% in 1X TAE buffer) for approx. 45 min at 100 V. As a ladder sequence the O'GeneRuler™ 1 kb Plus DNA Ladder was used.

In order to further confirm the positive colonies from the previous step, constructs were sequenced through Sanger sequencing. For this, colonies were incubated overnight in LB medium and DNA was isolated (see 5.2.15) the following day. The resulting DNA was sent to Microsynth Seqlab using the single tube sequencing service in a tube containing 1.35 mg of DNA and 1.5 µl of corresponding primer (10 mM). The resulting sequences were analyzed with SnapGene viewer and the BlastN suite.

5.2.17 Statistical analysis

For statistical analyses, an independent two–tailed paired Student's t test was used. P values lower than 0.05 were considered statistically significant. Calculations were performed using Microsoft Excel software. Graphpad Prism and Microsoft Excel softwares were used for plotting the graphs and the EC50 calculator online tool (AAT Bioquest) was used to calculate the EC50 values.

6 Results

6.1 Effect of Paliperidone on the viability of cells

Paliperidone was suggested as an ideal lead for new antivirals against FLUAV, as it was predicted *in silico* to target the evolutionary conserved sites of PB2 (Patel and Kukol 2017). Thus, the hypothesis that Paliperidone might have antiviral activity against FLUAV was tested. Initially, the tolerance of cells to Paliperidone had to be determined. In order to accomplish this, the Neutral Red Dye, an eurhodin dye, which is incorporated into the lysosomes of live cells (Repetto et al., 2008), was used after a spectrum of concentrations from 2.34 µM to 0.492 mM (1 µg/ml to 200 µg/ml) of Paliperidone in A549, MDCK and (0.5 µg/ml to 100 µg/ml) of Paliperidone in HuH7 cells. The time points represent the longest time points used for the next experiments. Thus, for A549 cells, 24 hours of incubation was examined while in MDCK cells 72 hours and HuH7 cells 48 hours of incubation were used. Since the concentrations that reduced cell viability indicate toxicity, they were not further investigated. As shown in fig. 9, Paliperidone could be administered to the A549 and HuH7 cells without showing toxic effect up to the concentration of 50 µg/ml, while in MDCK cells 25 µg/ml concentration could be used. Interestingly, but not significantly in some replicate experiments a higher viability compared to the untreated cells was observed suggesting that at these concentrations Paliperidone does not seem to be toxic to these cells.

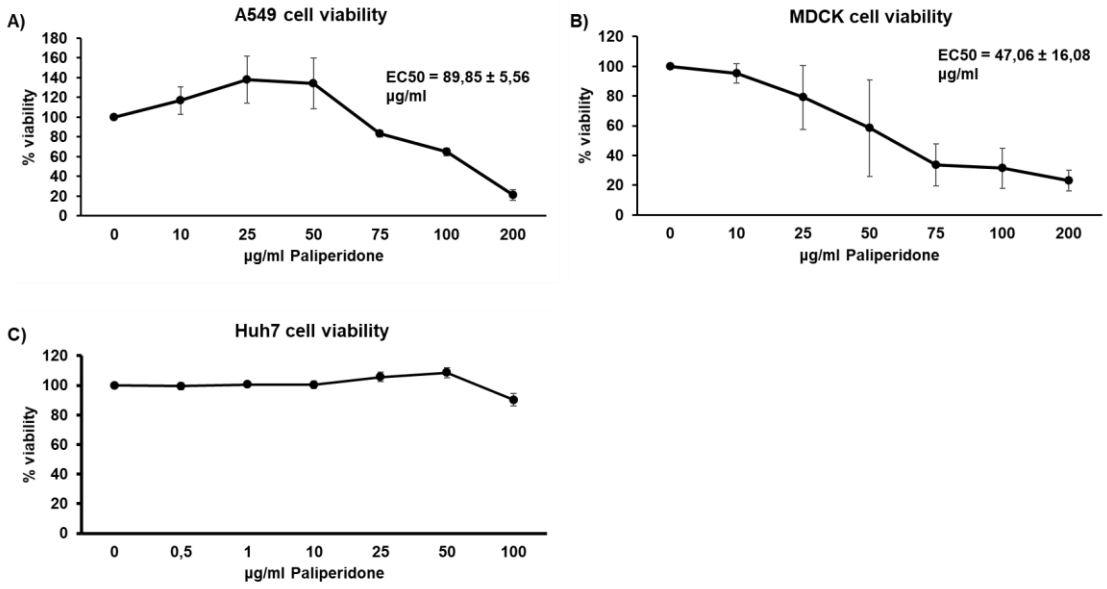

Figure 9: Effect of Paliperidone on cell viability.

A549 (A), MDCK (B) or HuH7 (C) cells were treated with the indicated amount of Paliperidone for 24 (A), 72 (B) or 48 (C) hours, and subjected to cell viability assay with the Neutral Red dye. Mean values with standard deviation from three biological replicates are shown.

Thus, the potential antiviral activity of Paliperidone against A/PR/8/34 was examined. In a preliminary experiment the non–toxic concentrations of Paliperidone were tested in A549 cells and early viral replication through RNA levels of M segment A/PR/8/34 were assessed. To test this RNA was isolated from cells at 6 hours post infection, as it has been shown that at this time point, infected cells begin to produce new influenza viruses (Baccam et al., 2006). The cells were infected for 1 h at a multiplicity of infection (MOI) of 1, and then treated with the indicated concentrations of Paliperidone to reflect therapeutic conditions. 6 h later levels of viral RNA were determined. As a marker for the de novo synthesized viral RNA, the positive–strand sequence (mRNA and antigenome) of the viral genome segment 7 was determined, while the newly produced viral RNA was examined with the negative strand of segment 7. Paliperidone was solubilized in DMSO and thus was used as control. In this study, preliminary data showed that Paliperidone has inhibitory effect on influenza A replication at a concentration of 10 µg/ml (fig. 10). Thus, this concentration was chosen for further investigations.

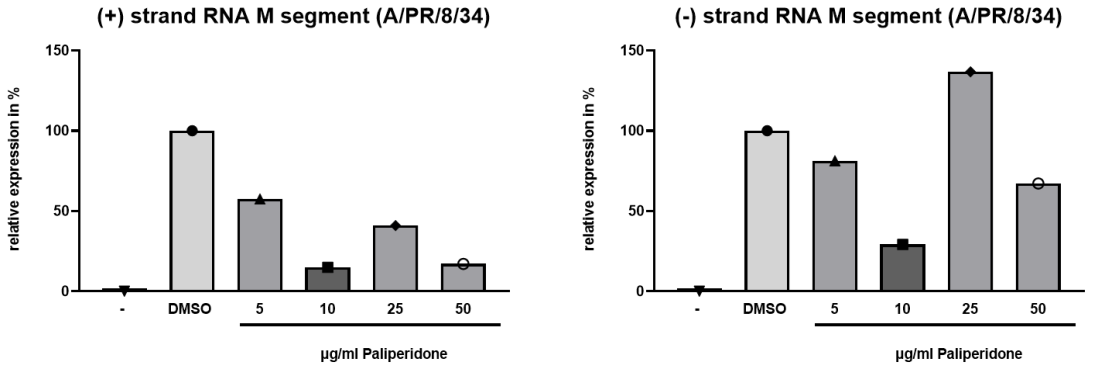

Figure 10: Effect of Paliperidone on the early infection phase of FLUAV strain A/PR/8/34.

qRT–PCR analysis of M segment levels (positive and negative strand) of A/PR/8/34. A549 cells were infected with A/PR/8/34 (MOI 1, 1hour) and were untreated (–) or treated with DMSO or Paliperidone (5, 10, 25, 50 µg/ml). 6 hours later RNA was isolated from A549 cells for qRT–PCR

analysis. Relative values from one replicate are shown, with the DMSO set to 100%. Individual values from one biological replicate are shown.

6.2 Effect of Paliperidone on the early infection phase of FLUAV strain A/PR/8/34

Since, in a preliminary experiment Paliperidone proved to inhibit early viral replication of A/PR/8/34 (fig. 10), a broad examination of its inhibitory effect was assessed. Initially, early viral replication through RNA levels of M segment and protein synthesis of NP were assessed 6 hours post infection. The cells were infected for 1 h at a multiplicity of infection (MOI) of 1, and then treated with 10 μg/ml Paliperidone, and 6 h later levels of viral RNA and protein were determined. As a marker for the de novo synthesized viral RNA, the positive–strand sequence (mRNA and antigenome) of the viral genome segment 7 was determined, while the newly produced viral RNA was examined with the negative strand of segment 7. Protein synthesis was examined with the levels of NP protein. As shown in fig 11. Paliperidone, at early infection, diminishes significantly only the synthesis of the negative strand of the M segment RNA, with NP and PB2 protein levels being also diminished compared to the DMSO control.

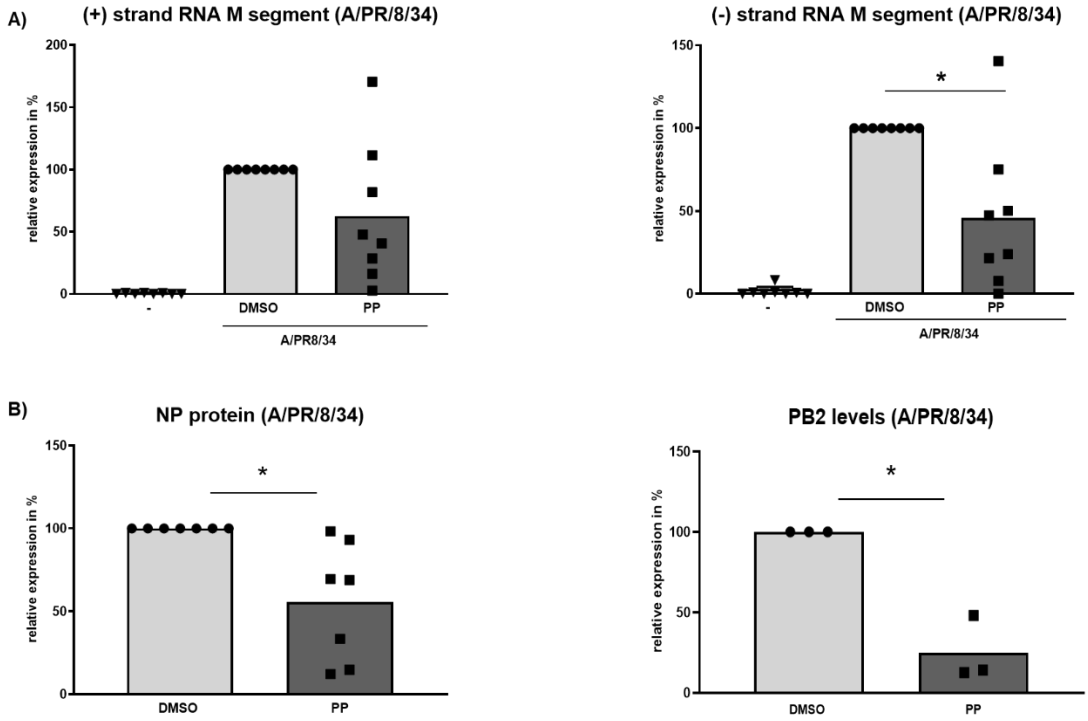

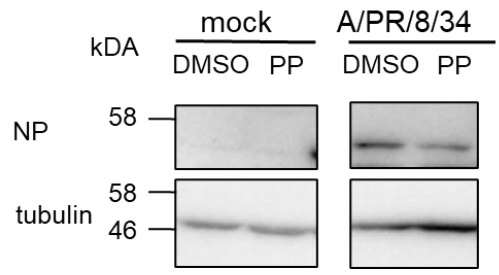

Figure 11: Effect of Paliperidone on the early infection phase of FLUAV strain A/PR/8/34.

A) qRT–PCR analysis of M segment levels (positive and negative strand) of A/PR/8/34. A549 cells were infected with A/PR/8/34 (MOI 1, 1hour) and were untreated (–) or treated with DMSO or Paliperidone (10 µg/ml). 6 hours later RNA was isolated for qRT–PCR analysis. Mean and individual values from eight biological replicates are shown. DMSO was set as 100%. Two–tailed paired Student's t test indicated significance* $p<0.05$. B) Western Blot analysis of NP and PB2 protein levels normalised to β–tubulin. A549 cells were infected with A/PR/8/34 (MOI 1, 1hour) and were treated with DMSO or Paliperidone (10 µg/ml). 6 hours later total protein lysate was isolated for Western blot analysis for the indicated antigens. Representative blot of staining is shown. Numbers indicate the molecular weight of the protein in kilo Dalton (kDA). Bands were quantified with Image Lab 5.2.1 software. Mean and individual values from seven for NP and three for PB2 biological replicates are shown. DMSO was set as 100%. Two–tailed paired Student's t test indicated significance * $p<0.05$.

RIG–I is the major sensor for FLUAV infection. Upon recognition of its ligands (triphosphorylated (5′ppp) dsRNA), RIG–I is activated undergoing conformational switch, activating downstream signalling (Weber et al., 2015). To examine if the early antiviral effect of Paliperidone affects RIG–I recognition of FLUAV and concomitantly its activation and signalling, the RIG–I activation was assessed though conformational switch assay. The cells were infected for 1 h at MOI of 1, then treated with 10 µg/ml Paliperidone, and 1 h later levels of the trypsin resistant fragment of RIG–I, indicative of a conformational switch, was examined. As shown in fig.12, paliperidone induces RIG–I activation in mock conditions, Despite that fact, even though a pattern of induction regarding RIG–I trypsin resistant fragments under infection with Paliperidone treatment was observed, compared to DMSO treatment, this was not statistically significant. Conclusively, while Paliperidone shows significant inhibitory effect against A/PR/8/34, it does not cause any effect on RIG–I activation itself during infection.

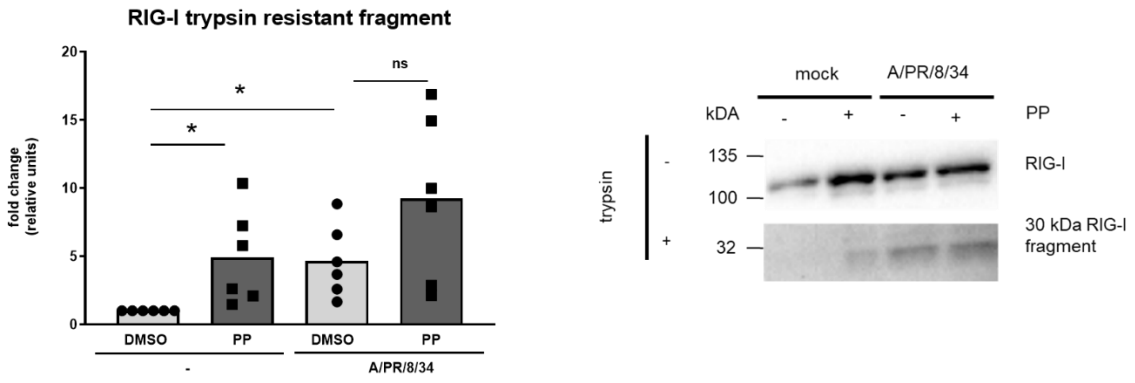

Figure 12: Effect of Paliperidone on RIG–I activation.

Western blot analysis of RIG–I conformational switch assay. A549 cells were infected with A/PR/8/34 (MOI 1, 1hour) and were treated with DMSO or Paliperidone (10 µg/ml). 1 hour later total protein lysate was isolated for Western blot analysis for the indicated antigens. In order to quantify RIG–I trypsin resistant fragments were divided to total RIG–I protein. Representative blot of staining is shown. Numbers indicate the molecular weight of the protein in kilo Dalton (kDA). Bands were quantified with Image Lab 5.2.1 software. Mean and individual values from seven biological replicates are shown. DMSO was set as 100%. Two–tailed paired Student's t test indicated significance * $p<0.05$.

6.3 Effect of Paliperidone on interferon signalling

Paliperidone showed early inhibitory effect against A/PR/8/34 (fig. 10, 11). On the other side, even though a trend of RIG–I activation during infection was observed, this was not significant (fig. 12). Activation of RIG–I leads to the initiation of interferon signalling which ultimately lead to the production of ISGs (Panne 2008, Loo et al. 2008). Thus, next, the potential effect of Paliperidone on interferon signalling was tested. Therefore, the cells were infected for 1 h at MOI of 1, then treated with 10 µg/ml Paliperidone, and 6 h later the mRNA levels of IRF3, IRF7 and ISG56 and the protein levels of IRF3 were tested. As shown in fig 14. no significant effect was observed in any interferon regulatory or stimulated gene tested after Paliperidone treatment, compared to the DMSO control.

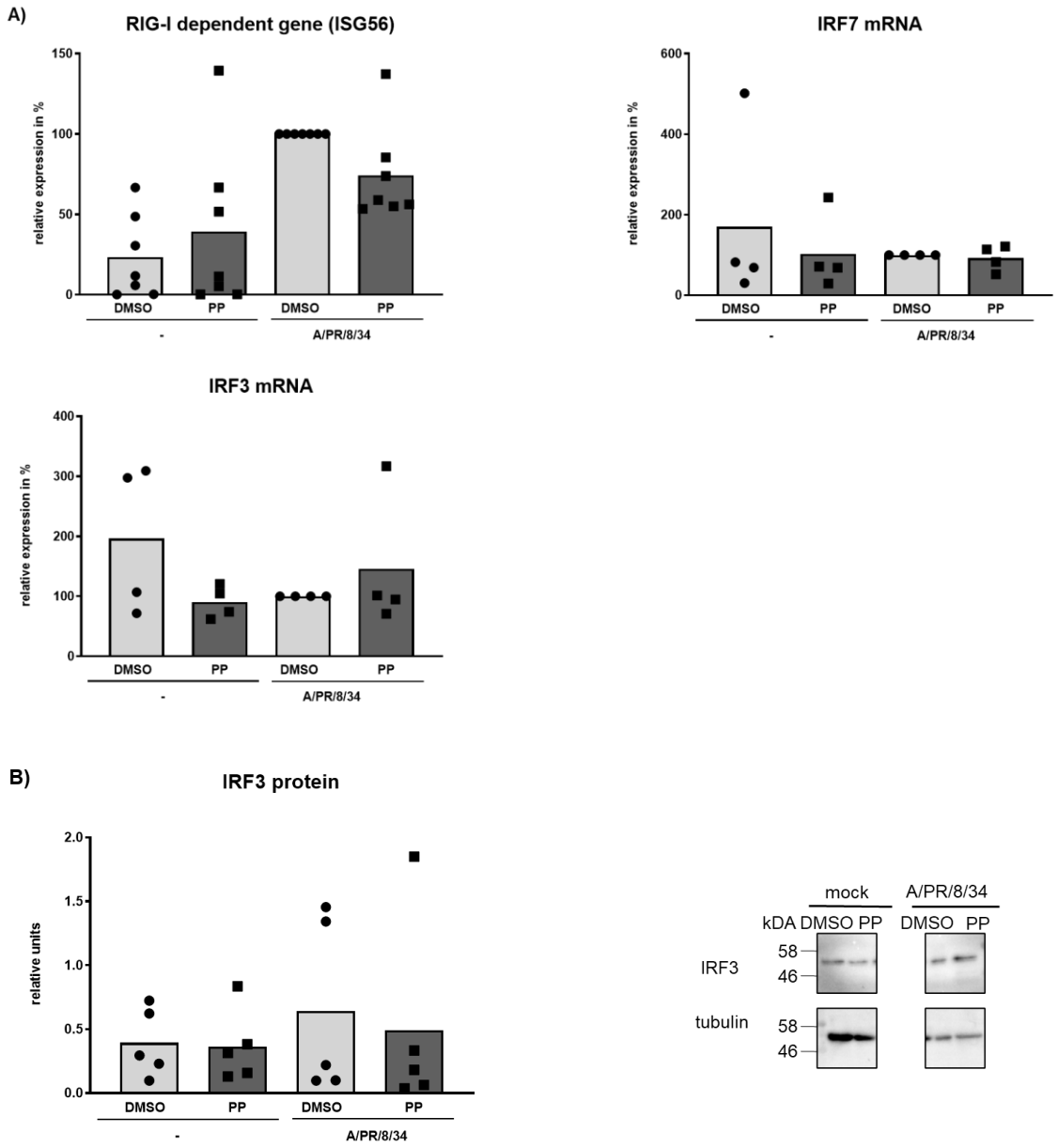

Figure 13: Effect of Paliperidone on interferon signalling during the early infection phase of A/PR/8/34.

A) qRT–PCR analysis of ISG56, IRF7 and IRF3 mRNA levels. A549 cells were infected with A/PR/8/34 (MOI 1, 1hour) and were untreated (–) or treated with DMSO or Paliperidone (10 µg/ml). 6 hours later RNA was isolated for qRT–PCR analysis. Mean and individual values from seven (ISG56) and four (IRF7/3) biological replicates are shown. DMSO was set as 100%. B) Western blot analysis of IRF3 protein levels. A549 cells were infected with A/PR/8/34 (MOI 1, 1hour) and were untreated (–) or treated with DMSO or Paliperidone (10 µg/ml). 6 hours protein lysate was isolated for WB analysis for the indicated antigens. Representative blot of staining is shown. Numbers indicate the molecular weight of the protein in kilo Dalton (kDA). Bands were quantified with Image Lab 5.2.1 software. Mean and individual values from five biological replicates are shown. Two–tailed paired Student's t test indicated significance * $p<0.05$.

6.4 Effect of Paliperidone on other H1N1 strains

Since Paliperidone inhibits early viral RNA replication and protein synthesis of FLUAV H1N1 strain A/PR/8/34, its potential effect against other H1N1 strains was evaluated. To do this, the cells were infected for 1 h at a multiplicity of infection (MOI) of 1, then treated with 10 μg/ml Paliperidone, and 6 h later levels of viral and cellular interferon regulatory gene RNAs and protein were determined. Cellular interferon regulatory genes which were tested, were IRF3/7, while protein synthesis was examined with the levels of NP protein. The strains examined were a) A/HAM/2009 pandemic strain, b) A/WSN/33 bearing the mammalian adaptation signature in PB2 segment in position 627K (A/WSN/33 PB2 627K), and c) A/WSN/33 bearing the avian adaptation signature in PB2 segment in position 627E (A/WSN/33 PB2 627E). Contrary to its inhibitory effect observed for A/PR/8/34, Paliperidone inhibited only NP protein synthesis of A/HAM/2009 compared to the DMSO control without affecting the RNA synthesis (fig. 14B). Furthermore, Paliperidone showed inhibitory effect against the strain A/WSN/33 PB2 627K but only on the synthesis of negative strand of M segment RNA levels (fig. 14A) without affecting protein levels compared to the DMSO control. No effect was observed on IRF3/7 mRNA and IRF3 protein levels (fig. 14).

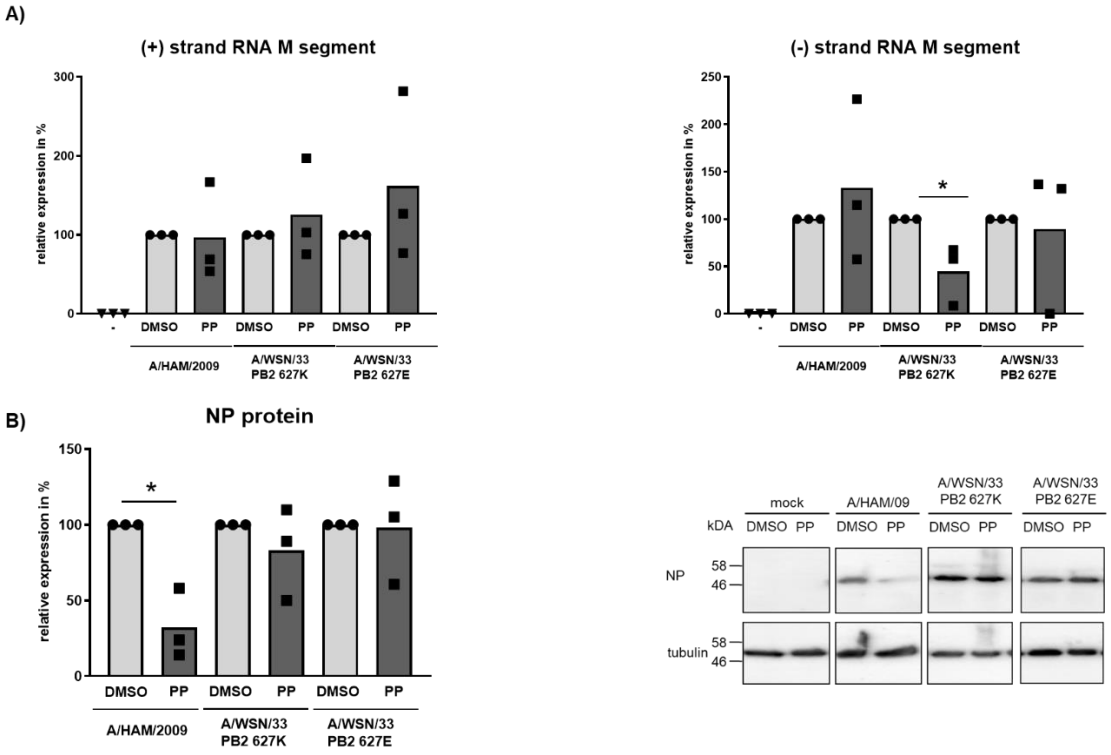

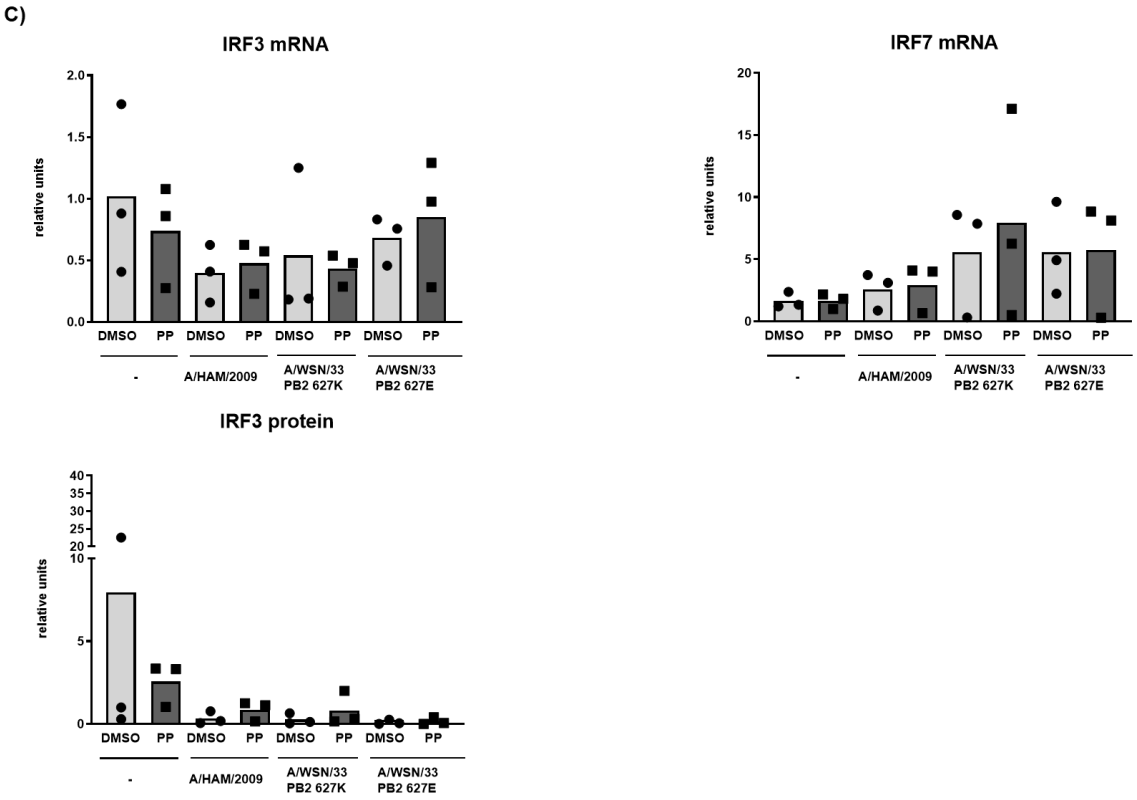

Figure 14: Effect of Paliperidone on the early infection phase of other H1N1 strains.

A) qRT–PCR analysis of M segment levels (positive and negative strand) of A/HAM/2009, A/WSN/33 PB2 627K and A/WSN/33 PB2 627E. A549 cells were infected with A/PR/8/34 (MOI 1, 1hour) and were untreated (–) or treated with DMSO or Paliperidone (10 µg/ml). 6 hours later RNA was isolated for qRT–PCR analysis. Mean and individual values from three biological replicates are shown. DMSO was set as 100%. Two–tailed paired Student's t test indicated significance * $p<0.05$. B) Western Blot analysis of NP protein levels normalised to β–tubulin. A549 cells were infected with A/HAM/2009, A/WSN/33 PB2 627K variant and A/WSN/33 PB2 627E variant (MOI 1, 1hour) and were treated with DMSO or Paliperidone (10 µg/ml). 6 hours later total protein lysate was isolated for Western blot analysis for the indicated antigens. Representative blot of staining is shown. Numbers indicate the molecular weight of the protein in kilo Dalton (kDA). Bands were quantified with Image Lab 5.2.1 software. Mean and individual values from five biological replicates are shown. Two–tailed paired Student's t test indicated significance * $p<0.05$. C) qRT–PCR and WB analysis of IRF7, IRF3 mRNA and IRF3 protein levels. A549 cells were infected with A/HAM/2009, A/WSN/33 PB2 627K variant and A/WSN/33 PB2 627E variant (MOI 1, 1hour) and were untreated (–) or treated with DMSO or Paliperidone (10 µg/ml). 6 hours later RNA was isolated for qRT–PCR analysis and protein lysate was isolated for WB analysis for the indicated antigens. Bands were quantified with Image Lab 5.2.1 software. Mean and individual values from three biological replicates are shown.

Surprisingly, Paliperidone did not show any inhibition in both strands of RNA M segment levels and NP protein synthesis of A/WSN/33 PB2 627E. This insensitivity of the avian adapted strain to Paliperidone on RNA and protein levels led to the hypothesis that Paliperidone can affect the polymerase activity of only mammalian adaptation bearing strains. Thus, the activity of viral polymerase of strains carrying the avian and mammalian signature was tested through minigenome assay. In this assay fluorescence–encoding reporter viral RNAs are replicated by the *in situ* reconstituted viral polymerase (TeVelthuis et al., 2018, Lutz et al., 2005). To do this, cells were transiently co–transfected with constructs encoding the viral polymerase, construct encoding viral RNA tagged with firefly luciferase encoding gene and a Renilla expressing construct. 4 hours later cells were treated with Paliperidone (10 mg/ml) and 24 hours later the expression of both luciferases was examined indicating the replication of viral RNA (firefly) and control for transient transfection (Renilla). As shown in fig. 15, Paliperidone was unable to affect the activity of the polymerase carrying the avian adapted signature, while the activity of the mammalian adapted signature polymerase was reduced.

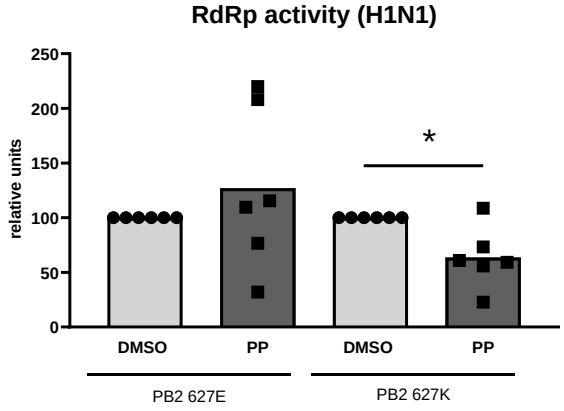

Figure 15: Effect of Paliperidone on the viral RNA–dependent RNA polymerase activity of H1N1 strains.

Minigenome analysis of viral polymerase activity, of PB2 627E variant and PB2 627K variant. HEK 293T cells were transiently transfected with viral polymerase encoding constructs, PB1, PA, NP, and luciferase expressing reporter genes, Firefly encoding viral RNA, Renilla reporter gene. Furthermore, constructs encoding the avian signature PB2 627E, or mammalian PB2 627K were transiently transfected to reconstitute the polymerase function. 4 hours later media was removed and media containing PP (10 μg/ml) was used as treatment. 24 hours later, firefly and Renilla luciferase levels were determined using Dual Luciferase Reporter Assay System (Promega) and a LB 942 TriStar2

multimode reader (Berthold Technologies). Firefly luciferase was normalized to Renilla luciferase. Mean and individual values from six biological replicates are shown. DMSO was set as 100%. Two–tailed paired Student's t test indicated significance * $p<0.05$.

Conclusively, Paliperidone does not exert any effect against the avian adapted strain A/WSN/33 PB2 627E. Nevertheless, interestingly, Paliperidone inhibits both mammalian adapted strains A/WSN/33 PB2 627K and A/HAM/2009 in viral RNA and protein level, without any effect on the interferon signalling. Furthermore, Paliperidone fails to affect the polymerase activity of the avian adapted strain, in contrast with the mammalian adapted strain where polymerase activity is significantly inhibited by Paliperidone.

6.5 Effect of Paliperidone on the full viral replication cycle

Paliperidone inhibits the viral RNA replication, protein synthesis of different H1N1 strains (fig. 11, 14) as well as the viral polymerase activity (fig. 15). Therefore, next, the effect of Paliperidone in viral growth kinetics was examined. Thus, MDCK cells were infected with the four previously mentioned H1N1 virus strains (A/PR/8/34, A/HAM/2009, A/WSN/33 PB2 627K and A/WSN/33 PB2 627E) and treated with Paliperidone. Supernatants were collected in time course manner (8, 24, 48, 72 hours post infection) and titrated with immunoplaque assay. As shown in fig. 16 Paliperidone showed inhibitory effect only in early infection (8 hours) against strain A/PR/8/34.

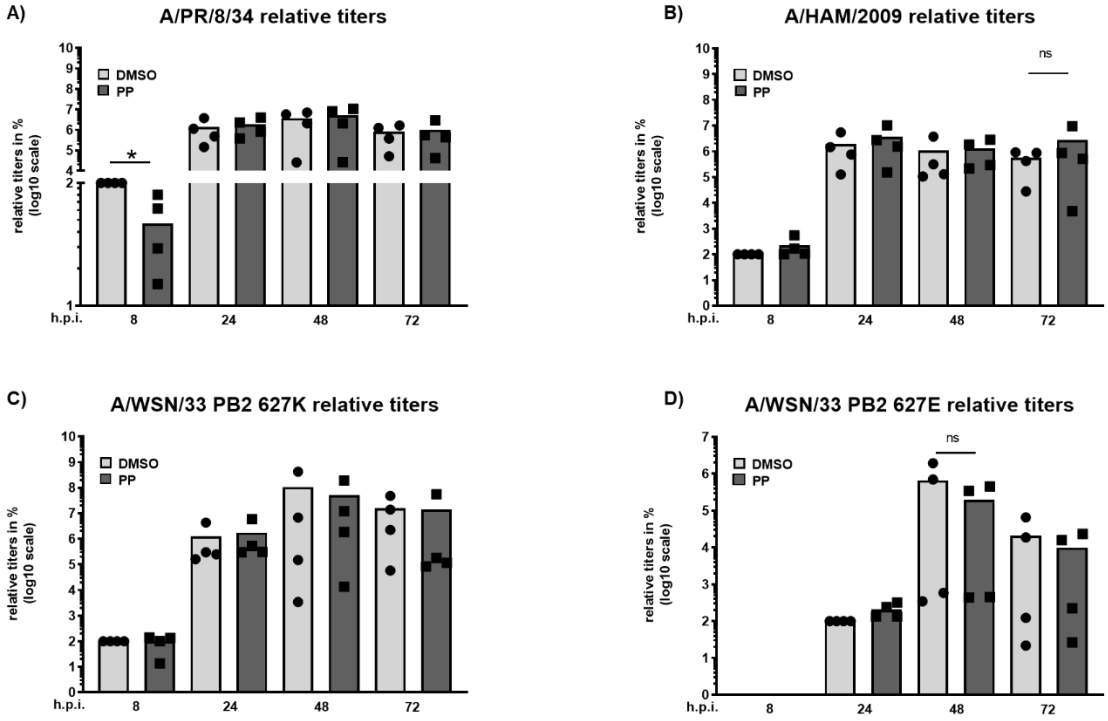

Figure 16: Effect of Paliperidone on the viral replication cycle in MDCK cells.

Canine MDCK cells were infected with A) A/PR/8/34, B) A/HAM/09, C) A/WSN/33 PB2 627 K, D) A/WSN/33 PB2 627 E at an MOI of 0.01, and 1 h later treated with 10 µg/ml Paliperidone or the DMSO control. At the time points indicated, supernatants were harvested and titrated by immunoplaque assay. Titers of the earliest measurable time point were set to 100%. Mean and individual values from four biological replicates are shown. Two–tailed paired Student's t test indicated significance * $p<0.05$.

Even though viral growth is optimal in MDCK cells (Krammer et al., 2018), this does not represent the natural infection conditions (Peteranderl et al., 2016) with one example being that these cells are deficient in the antiviral type I interferon (IFN) (Seitz et al., 2010). To continue the analyses using conditions closer to the infection in humans, primary bronchial cells derived from patient donors were employed, a system found to have the best predictive value for the *in vivo* situation (Ilyushina et al., 2012). The strain to infect the cells was A/PR/8/34, the H1N1 strain with the most obvious sensitivity towards Paliperidone at the early infection phase. Indeed, also in primary human bronchial cells, Paliperidone delays the replication of A/PR/8/34 at 8 and 24 h.p.i, (fig. 17). At later time points, however, the antiviral effect seems slightly reversed (48 and 72 h.p.i.), although statistical significance was not reached. Thus, also under *ex vivo* conditions, Paliperidone inhibits the replication of FLUAV A/PR/8/34 until 24 hours post infection.

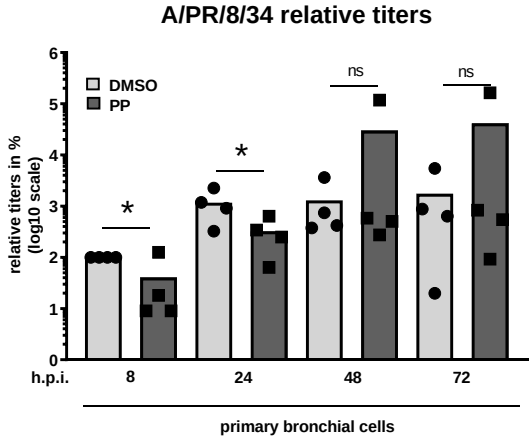

Figure 17: Effect of Paliperidone on the viral replication cycle in human primary bronchial cells.

Cells were infected at an MOI of 1, Paliperidone treatment and subsequent analyses were done as described for figure 15. Titers of the earliest measurable time point were set to 100%. Mean and individual values from four biological replicates are shown. One–tailed unpaired Student's t test indicated significance * $p<0.05$.

6.6 Influence of Paliperidone on PB2–NP binding

Paliperidone was predicted to dock into a deep pocket on PB2 that is evolutionary conserved and overlaps with a domain important for NP binding (Patel and Kukol 2017). Therefore, using strain A/PR/8/34 where the early inhibitory effects were observed, by co–immunoprecipitation assays, the *in silico* finding of the PB2–NP complex disassembly (Patel and Kukol 2017) was examined *in vitro*. A549 cells were infected for 6 h at an MOI of 1, lysed, and the viral proteins were immunoprecipitated using antisera directed against either NP or PB2. As shown by immunoblotting (fig. 18A), both viral proteins were detectable in the input control, as expected, and Paliperidone treatment reduced their signals. Interestingly, application of Paliperidone resulted in less PB2 in the NP immunoprecipitates, and conversely there was less NP in the PB2 immunoprecipitates. Along these lines, quantification of the immunoblot signals from independent experimental replicates, normalized to the signal of the respective immunoprecipitated viral protein, revealed that Paliperidone reduces the binding of PB2 to NP, whereas the ratio of the two proteins in the input lysates remained unaffected (fig. 18B). Thus, as predicted *in silico* (Patel and Kukol 2017), Paliperidone indeed disturbs the interaction of FLUAV A/PR/8/34 PB2 with NP.

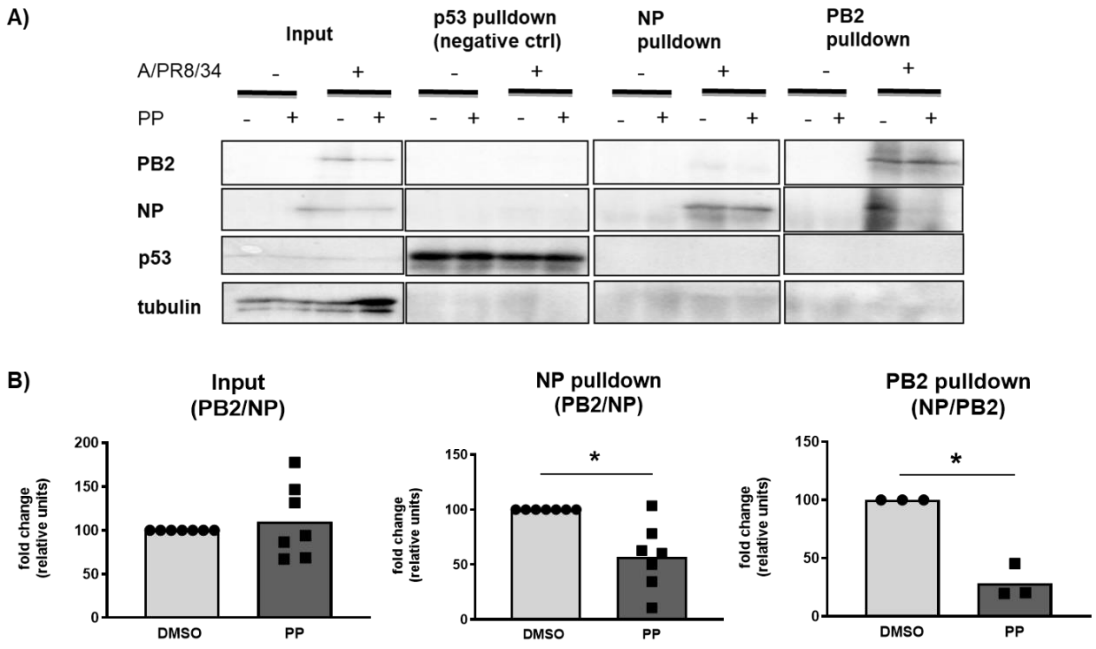

Figure 18: Influence of Paliperidone on PB2–NP interaction.

A) Human A549 cells were infected at an MOI of 1, and 1 h later treated with 10 µg/ml Paliperidone or the solvent DMSO as control. A further 6 h later, total protein was extracted and 10% of lysate was used as input while p53 pulldown was used as a negative control pulldown. Representative blots of stainings are shown. B) Ratios of quantified immunoblot signals for PB2 and NP. Bands were quantified with Image Lab 5.2.1 software. Mean and individual values from seven (input and NP pulldown) and three (PB2 pulldown) biological replicates are shown. DMSO was set as 100%. Two–tailed paired Student's t test indicated significance * $p<0.05$.

6.7 Involvement of RIG–I

It was previously shown that a destabilization of the polymerase complex renders FLUAV more prone to be sensed and inhibited by RIG–I immediately after the viral nucleocapsids have entered the cell (Weber et al., 2015). Given that Paliperidone interferes with the binding of PB2 to NP, as well as the observation that its antiviral activity seems to be restricted to the early phase of infection, the hypothesis of RIG–I involvement in the effect of Paliperidone were examined. In order to investigate this, A549 cell lines bearing CRISPR/Cas9–generated knockouts either in RIG–I, the related PRR MDA5, or the adapter molecule MAVS that relays the antiviral signalling initiated by RIG–I and MDA5 to the induction of the IFN promoter were used. Cells were infected for 1 h at MOI of 1, then treated with 10 µg/ml Paliperidone, and 6 h later levels of viral RNA and protein were determined. As a marker for the *de novo* synthesized viral RNA, the positive–strand sequence (mRNA and antigenome) of the viral genome segment 7 was used, while the newly produced viral RNA was examined with the negative strand of segment 7. Protein synthesis was examined through the levels of NP. According to fig. 19 while in MDA5 KO cells Paliperidone showed inhibitory effect regarding the positive strand of M segment compared to the vehicle control, knock out all three proteins abolished the inhibitory effect of Paliperidone against FLUAV regarding the negative strand of M segment. On the other hand, examination of NP protein levels showed, that Paliperidone boosts NP protein synthesis when RIG–I is absent, while in MDA5 KO cells Paliperidone did not exert any inhibitory effect. In contrast, knock out of MAVS led to inhibition of synthesis of NP protein levels under Paliperidone comparable to the inhibition shown in A549 CTRL KO cells compared to the vehicle control. Conclusively, RIG–I is involved in the inhibitory effect of Paliperidone against A/PR/8/34, while MDA5 and MAVS are

partially involved in the inhibitory effect in RNA (negative strand) (fig. 19A), and protein (fig. 19B) respectively.

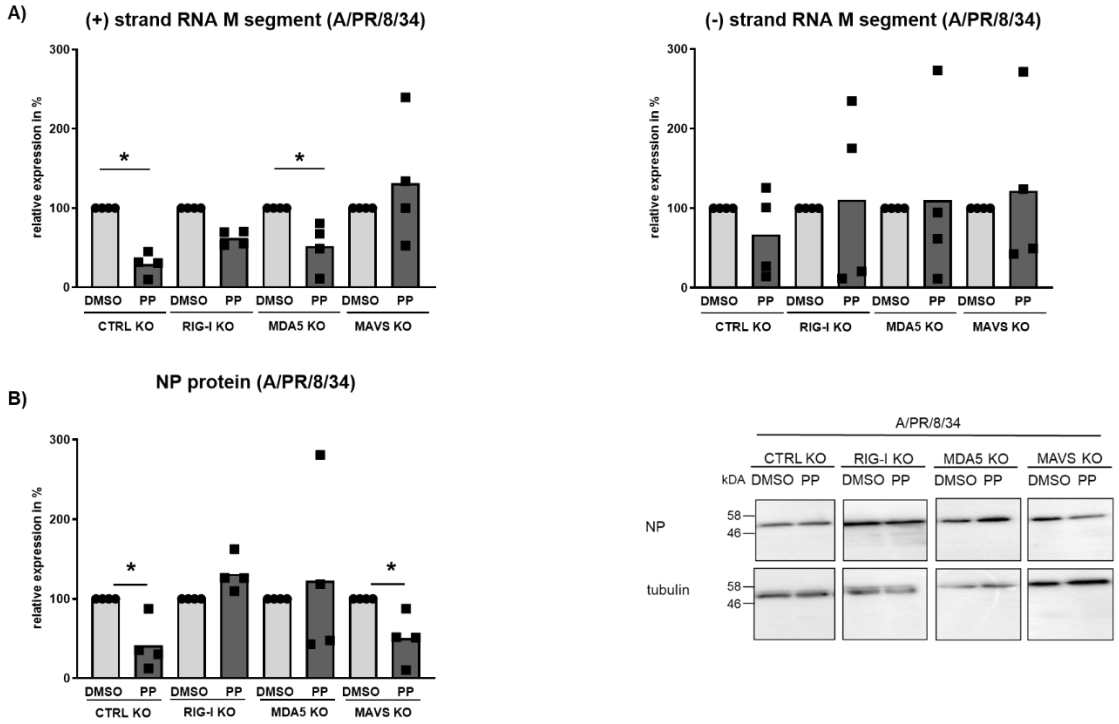

Figure 19: Involvement of RIG–I.

A) qRT–PCR analysis of M segment levels of A/PR/8/34. A549 control KO (CTRL KO), A549 RIG–I KO (RIG–I KO), A549 MDA5 KO (MDA5 KO) and A549 MAVS KO (MAVS KO) cells were infected with A/PR/8/34 (MOI 1, 1hour) and were treated with DMSO or Paliperidone (10 µg/ml). 6 hours later RNA was isolated for qRT–PCR analysis. Mean and individual values from four biological replicates are shown. DMSO was set as 100%. Two–tailed paired Student's t test indicated significance * $p<0.05$. B) Western Blot analysis of NP protein levels. A549 control KO (CTRL KO), A549 RIG–I KO (RIG–I KO), A549 MDA5 KO (MDA5 KO) and A549 MAVS KO (MAVS KO) cells were infected with A/PR/8/34 (MOI 1, 1hour) and were treated with DMSO or Paliperidone (10 µg/ml). 6 hours later total protein lysate was isolated for Western blot analysis for the indicated antigens. Representative blot of staining of NP is shown. Numbers indicate the molecular weight of the protein in kilo Dalton (kDA). Bands were quantified with Image Lab 5.2.1 software. Mean and individual values from four biological replicates are shown. DMSO was set as 100%. Two–tailed paired Student's t test indicated significance * $p<0.05$.

6.8 Influence of Paliperidone on cell signalling proteins.

Paliperidone is a centrally active dopamine D2 and serotonin 5–HT2A antagonist (Karlsson et al., 2005). D2 receptors modulate many signalling pathways, some of which are the PI3K/AKT, adenylate cyclase, phospholipases, ion channels,

mitogen activated protein (MAP) kinases, and the Na^+/H^+ exchanger (Huff et al., 1998). AKT is known between others as a regulator of cell survival by regulating apoptosis (Li et al., 2019) and senescence (Rössig et al., 2001, Shtutman et al., 2017). p21 protein is a senescence marker, inducing cell cycle arrest (Shtutman et al., 2019). It is known that Paliperidone reverts the chemically induced inhibition of AKT in neuronal cells (Peng et al., 2013, Peng et al., 2014). On the other hand, several studies indicated that AKT is modulated and required by FLUAV (Ehrhardt et al., 2007, Hirata et al., 2014, Murray et al., 2012.). According to a study (Ma et al., 2022), p21 exhibited Influenza inhibiting effect, by binding to FLUAV´s PA protein and competing out its binding to PB1. Thus, in order to test the effect of Paliperidone on these cellular signalling mediators during infection, A549 cells were infected for 6 h at an MOI of 1, lysed and the levels of AKT and p21 were tested. Paliperidone exerted a minor but not significant increase in AKT levels (phosphorylated/total) and a significant inhibition p21 levels compared to the vehicle control under infection. These indicate that paliperidone enhances cell survival but inhibits the anti–FLUAV p21 protein (fig. 20).

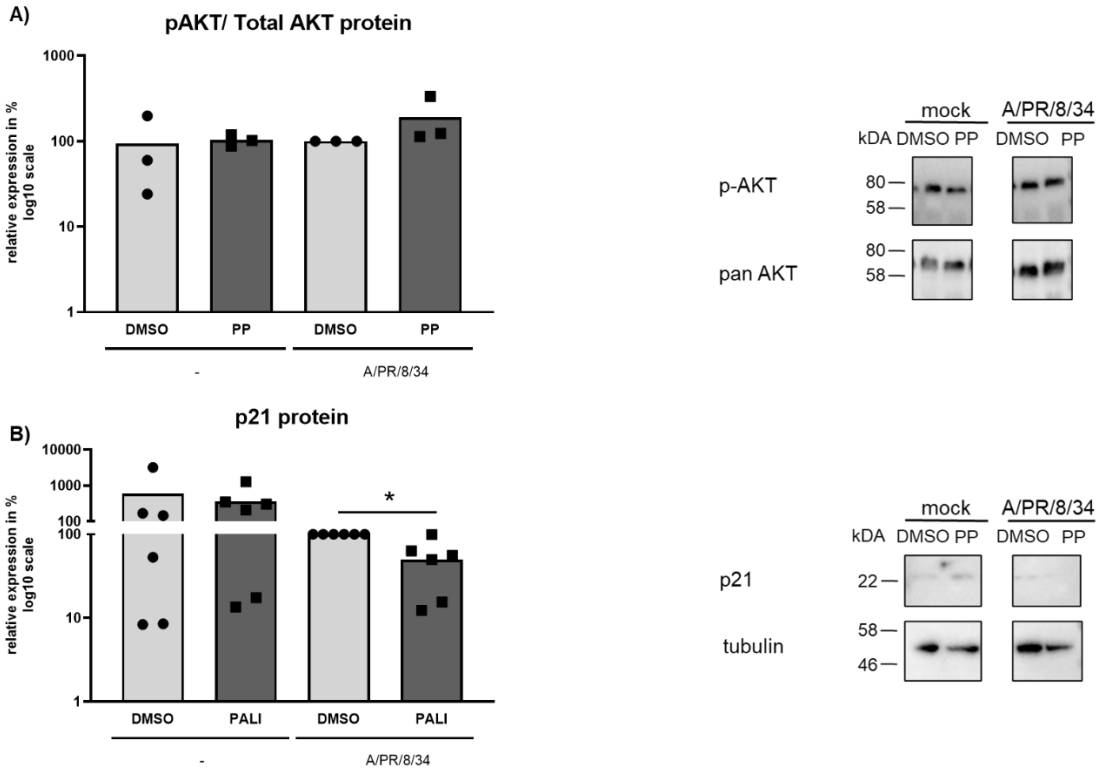

Figure 20: Influence of Paliperidone on cell survival signalling molecules.

Western Blot analysis of A) phospho– AKT normalized to total (pan) AKT and B) p21 protein levels normalised to β–tubulin. A549 cells were infected with A/PR/8/34 (MOI 1, 1hour) and were

treated with DMSO or Paliperidone (10 µg/ml). 6 hours later total protein lysate was isolated for Western blot analysis for the indicated antigens. Representative blot of staining is shown. Numbers indicate the molecular weight of the protein in kilo Dalton (kDA). Bands were quantified with Image Lab 5.2.1 software. Mean and individual values from three (A), six (B) biological replicates are shown. DMSO was set as 100%. Two–tailed paired Student's t test indicated significance * $p<0.05$.

6.9 Effect of Paliperidone on SARS–CoV–2

Paliperidone was suggested as a potential inhibitor candidate against SARS–CoV–2 as it was predicted, *in silico*, that it has high affinity binding to 3CLpro, the main protease of SARS–CoV–2, leading to the enzymatic inhibition (Gul et al., 2020). Thus, its potential antiviral activity against SARS–CoV–2 was examined. Initially, viral replication through RNA levels of E gene and protein synthesis of N were assessed 48 hours post infection. Furthermore, at 48 hours post infection the effect on full viral replication cycle was determined. The cells were infected for 1 h at MOI of 0.005, then treated with a range of Paliperidone concentrations (1, 10 µg/ml), and 48 h later levels of E gene, N protein and viral titers were determined. Paliperidone inhibited viral transcription of E gene (fig. 21A), but failed to affect titer levels of SARS–CoV–2 (fig. 21B) and N protein (fig. 21C).

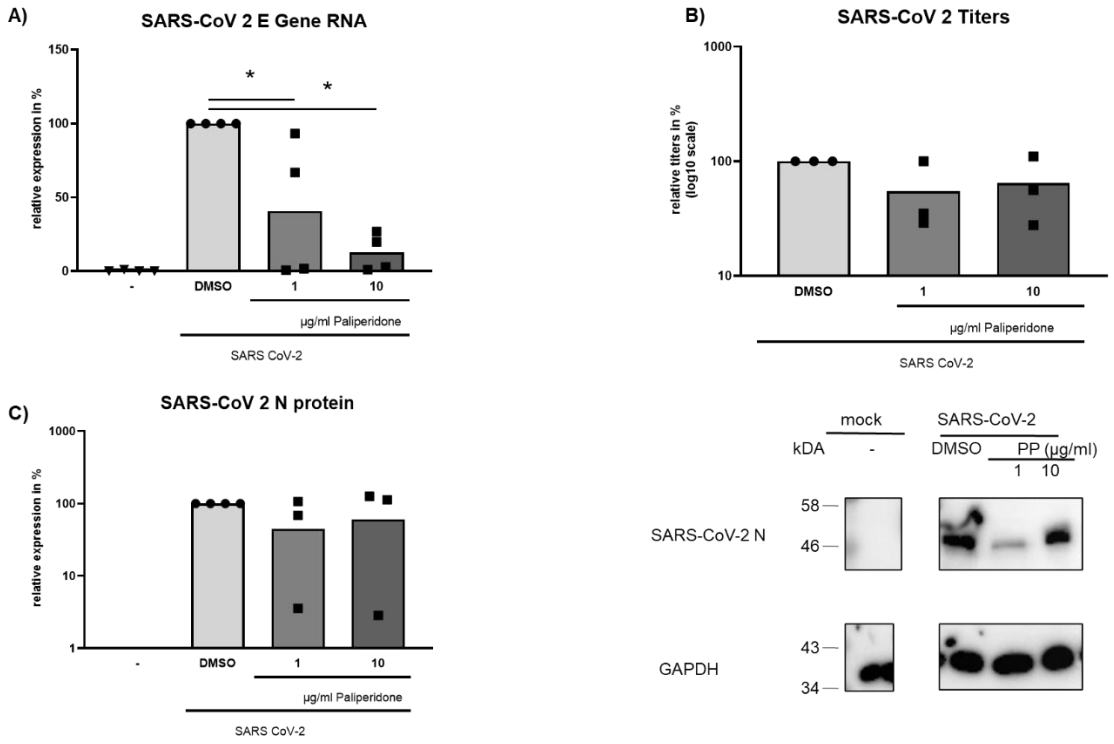

Figure 21: Effect of Paliperidone on SARS–CoV–2.

A) qRT–PCR analysis of E gene levels of SARS–CoV–2. HuH7 cells were infected with SARS–CoV–2 at an MOI of 0.005, and 1 h later treated with the indicated amount of Paliperidone or the solvent DMSO as control. At 48 hours post infection, RNA was isolated and levels of E gene was determined by qRT–PCR. Mean and individual values from four biological replicates are shown. DMSO was set as 100%. Two–tailed paired Student's t test indicated significance * $p<0.05$. B) Western blot analysis of N protein levels of SARS–CoV–2. HuH7 cells were infected with SARS–CoV–2 at an MOI of 0.005, and 1 h later treated with the indicated amount of Paliperidone or the solvent DMSO as control. At 48 hours post infection, total protein lysates were isolated and protein levels were determined by SDS PAGE and Western blotting for the indicated antigens. Representative blot of staining is shown. Numbers indicate the molecular weight of the protein in kilo Dalton (kDA). Bands were quantified with Image Lab 5.2.1 software. Mean and individual values from three biological replicates are shown. DMSO was set as 100%. C) Full viral replication analysis of SARS–CoV–2. HuH7 cells were infected with SARS–CoV–2 at an MOI of 0.005, and 1 h later treated with the indicated amount of Paliperidone or the solvent DMSO as control. At 48 hours post infection, supernatants were isolated and titrated by plaque assay. Mean and individual values from three biological replicates are shown. DMSO was set as 100%.

To conclude, in this study, Paliperidone exhibited early inhibitory effect against H1N1, which was strain dependent. This inhibitory effect did not affect the interferon signalling, whatsoever, even though it was RIG–I dependent. On the other hand, the *in silico* prediction (Patel and Kukol 2017) on Paliperidone inhibiting the interaction of NP with PB2 proteins was proved here *in vitro* affecting also viral polymerase activity. Furthermore, Paliperidone exhibited minor effect against SARS–CoV–2.

6.10 Effect of RIG–I mutants on A/PR/8/34

RIG–I is the major sensor for FLUAV infection (Weber et al., 2015), as well as recently proved to also sense SARS–CoV–2 (Yamada et al., 2021). RIG–I shows both direct antiviral activity and induction of interferon signalling (Chan and Gack 2015). Thus, in this study, the direct antiviral activity through signalling–deficient RIG–I was examined against both viruses in another complementary approach. In this approach, since evidence show that the signalling deficient RIG–I mutant K270A shows inhibitory effect against FLUAV (Weber et al., 2015, Yao et al., 2015), here this and other signalling altered RIG–I mutants, were tested for their inhibitory capacity against A/PR/8/34. These RIG–I mutants tested here were the signalling deficient RIG–I ΔCARD, and the ATP binding/ATP–ase deficient helicase mutants RIG–I K270A, RIG–I K270A/E373Q, and RIG–I T409A/S411A (fig. 22) (Lassig et al., 2015, Louber et al., 2015, Kumar et al., 2009).

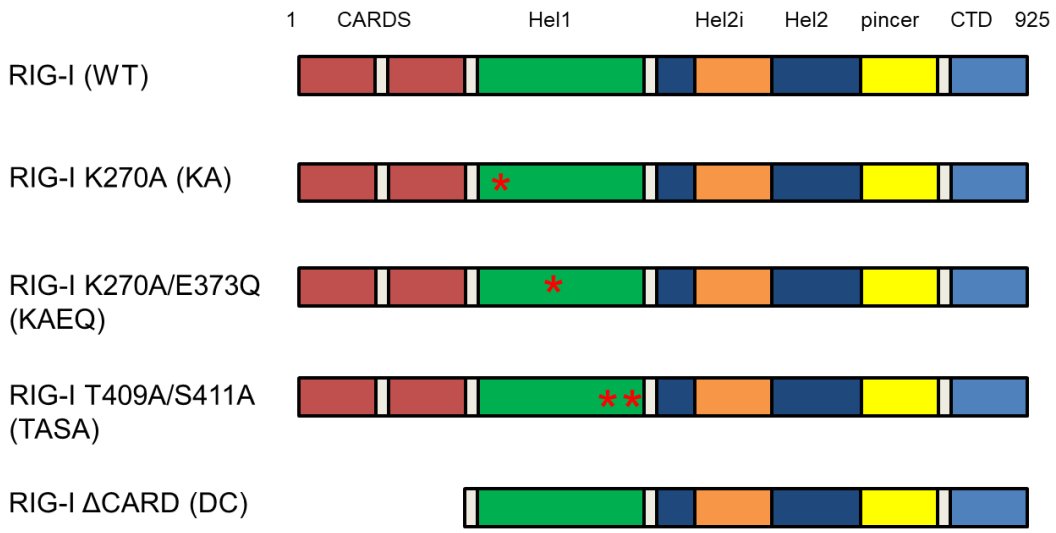

Figure 22: RIG–I constructs tested and their respective mutations.

Constructs expressing RIG–I WT= WT, RIGI–I K270A= KA, RIG–I K270A/E373Q= KAEQ, RIG–I T409A/S411A= TASA, RIG–I ΔCARD=DC were used for following analysis.

Cells were transfected with constructs containing the wild type or mutant RIG–I and upon 2 days cells were infected with A/PR/8/34 strain for 6 hours before cellular RNA was isolated. Initially, these mutants were tested for their inhibitory capability against A/PR/8/34 and signalling capacity. As a marker for the *de novo* synthesized virus RNA, the positive–strand sequence (mRNA and antigenome) of the viral genome segment 7 was examined, while the newly produced viral RNA was examined with the negative strand of segment 7. The RIG–I dependent gene ISG56 was used as a RIG–I mediated signalling indicator. As shown in fig. 23 as expected RIG–I WT and K270A reduced the levels of M segment. In addition, all RIG–I mutants showed the same or even better inhibitory effect on the levels of M segment compared to the GFP control. On the other hand, examination of the levels of ISG56 upon transfection and infection, showed that the K270A show minor ISG56 induction. Contrary to that, both the double mutants induced ISG56, while the ΔCARD mutant did not induce the RIG–I dependent gene in both mock and infected cells (fig. 23A).

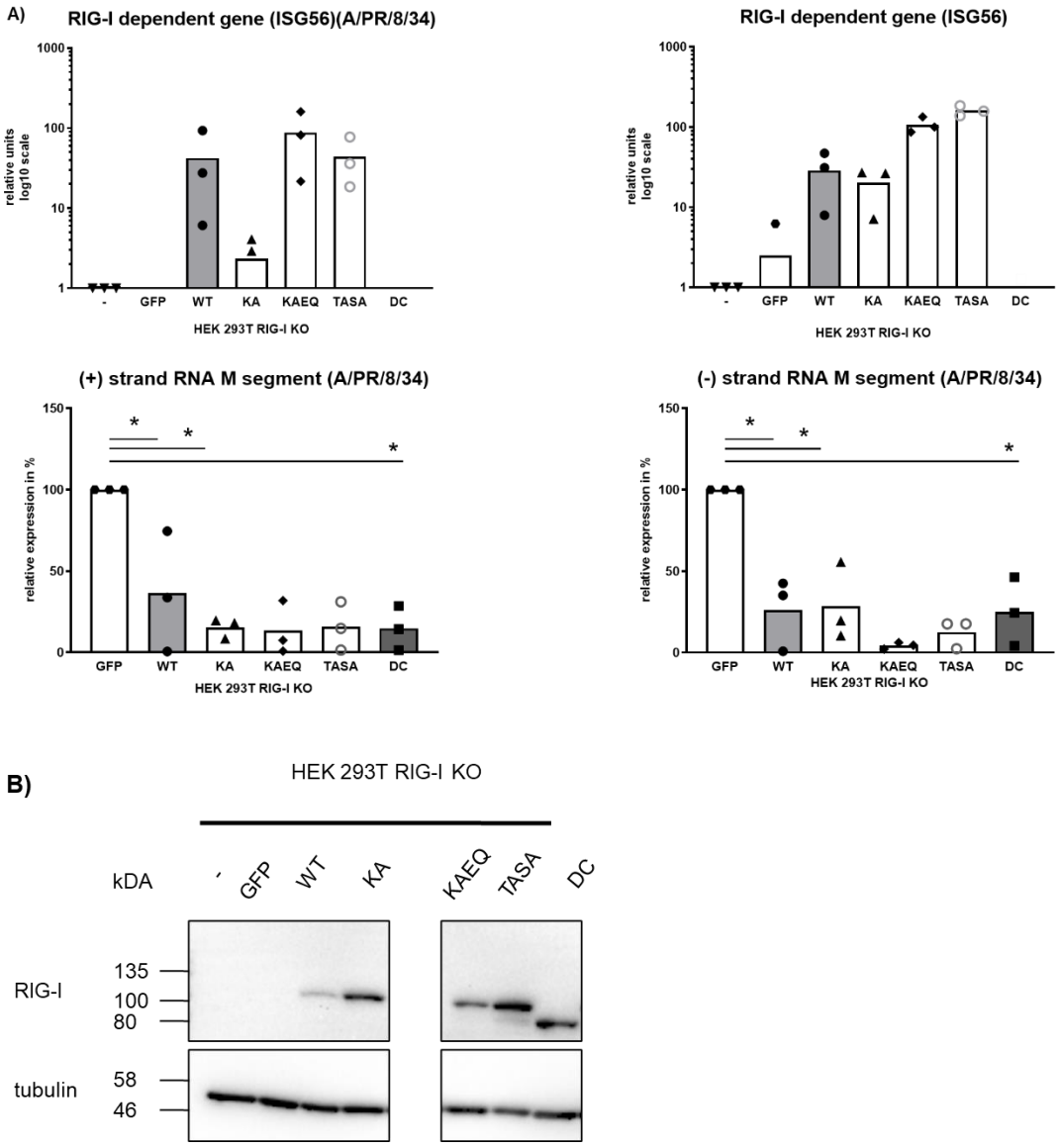

Figure 23: Effect of RIG–I mutants on A/PR/8/34.

A) qRT–PCR analysis of M segment levels (positive and negative strand) of A/PR/8/34 and cellular ISG56 levels. HEK 293T RIG–I KO cells transiently transfected with expressing constructs green fluorescence protein (GFP), RIG–I WT= WT, RIGI–I K270A= KA, RIG–I K270A/E373Q= KAEQ, RIG–I T409A/S411A= TASA, RIG–I ΔCARD=DC were infected with A/PR/8/34 (MOI 1, 1hour). 6 hours later RNA was isolated for qRT–PCR analysis. Mean and individual values from three biological replicates are shown. GFP was set as 100%. Two–tailed paired Student's t test indicated significance * $p<0.05$. B) Western Blot analysis of RIG–I expression. HEK 293T RIG–I KO cells transiently expressing green fluorescence protein (GFP) transfection RIG–I WT= WT, RIGI–I K270A= KA, RIG–I K270A/E373Q= KAEQ, RIG–I T409A/S411A= TASA, RIG–I ΔCARD=DC were infected with A/PR8/34 (MOI 1, 1hour). 6 hours later total protein lysate was isolated for immunoblot analysis for the indicated antigens. Numbers indicate the molecular weight of the protein in kilo Dalton (kDA). Representative blot is shown.

Even though the RIG–I mutants K270A/E373Q, and T409A/S411A inhibited A/PR/8/34 on RNA levels (fig. 23A), they show constitutive signalling activity. Thus, for the course of this study the signalling deficient RIG–I ΔCARD (DC) was assessed against a set of viruses. For this approach, the lung–alveolar adeno–carcinoma cell line A549 was used for a better representation of human lung infection. Thereby, WT A549 cells were compared to RIG–I KO cells reconstituted with FLAG–tagged RIG–I WT or RIG–I DC through lentiviral infection. A549 RIG–I KO cells reconstituted with the unrelated FLAG–tag glutathione S–transferase (GST) was used as a control (fig. 24).

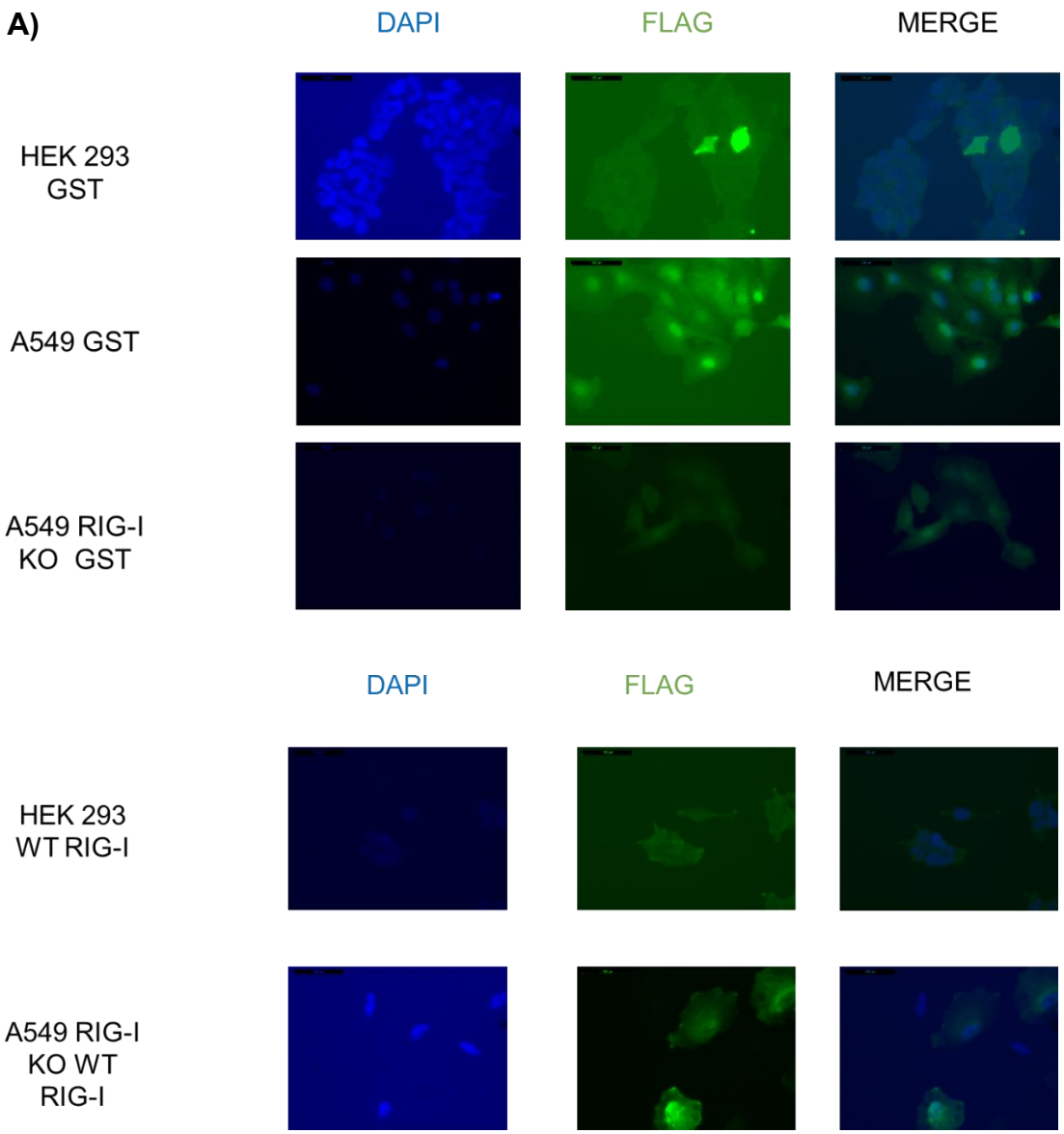

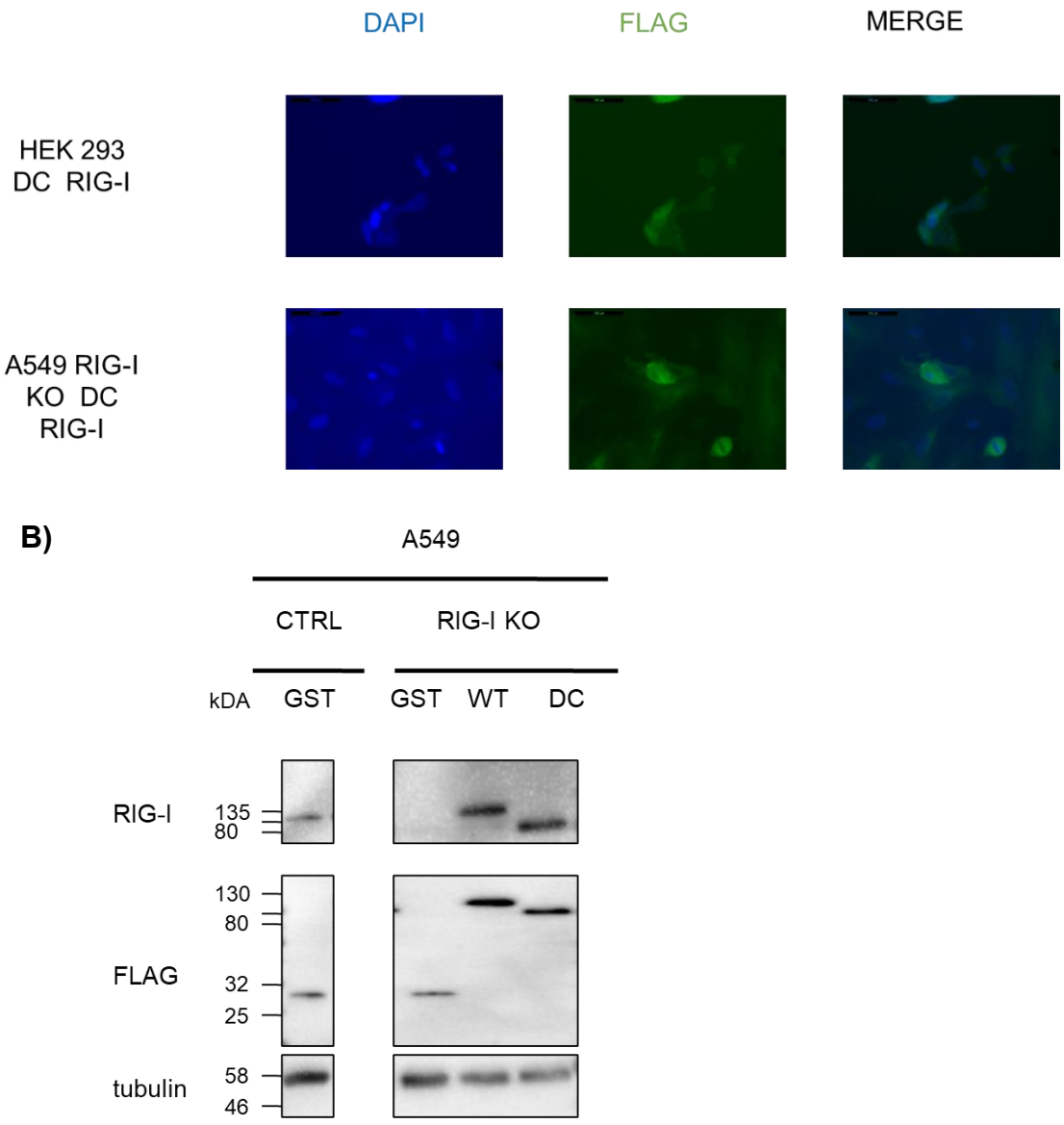

Figure 24: Expression of target proteins in the generated stable cell lines.

A) A549 control (CTRL) cell line stably expressing GST and RIG–I KO cell line stably expressing GST, RIG–I WT, and RIG–I DC and HEK293T cells transiently transfected with constructs expressing GST, RIG–I WT and RIG–I DC used as control for staining were seeded. 24h post transfection cells were fixed with paraformaldehyde and stained using anti–FLAG tag primary antibody and DAPI. Confocal microscopy was performed using Olympus IX70 Inverted Fluorescence Phase Contrast Microscope and the accompanying software. B) WB analysis of FLAG and RIG–I protein. A549 WT and RIG–I KO total protein lysates were isolated and levels of FLAG, RIG–I and tubulin proteins were determined. 6 hours later total protein lysate was isolated for immunoblot analysis for the indicated antigens. Numbers indicate the molecular weight of the protein in kilo Dalton (kDA). Representative blot is shown from one biological replicate. A549 control cells line=CTRL, A549RIG–I KO cell line=RKO, GST= glutathione–S–transferase, RIG–I WT= WT, RIG–I ΔCARD= DC

In order to test the effect of RIG–I against A/PR/8/34 on this system, briefly, the stably expressing cells, mentioned before, were infected with A/PR/8/34 strain (MOI 1) and 6 hours later RNA and protein were isolated. Furthermore, in a time course manner (8, 24, 48 hours post infection) the effect of RIG–I on full viral replication cycle was also determined. The cells were infected for 1 h at MOI of 0.001 and viral titers were determined. These RIG–Is were tested for both their capability of being inhibitory against A/PR/8/34 and signalling capacity. As a marker for the *de novo* synthesized virus RNA, the positive–strand sequence (mRNA and antigenome) of the viral genome segment 7 was tested, while the newly produced viral RNA was examined with the negative strand of segment 7. The RIG–I dependent gene ISG56 was used as a RIG–I mediated signalling indicator. Protein synthesis was examined with the levels of NP and PB2 protein. As shown in fig. 25A, although there was no significant reduction of viral transcription of M segment from both RIG–I WT and RIG–I DC compared to GST control, the newly produced viral RNA was reduced by both RIG–I WT and RIG–I DC compared to GST control (fig. 25A last graph). The RIG–I dependent gene was induced in the RIG–I KO when only RIG–I WT was expressed. Both NP and PB2 protein levels remained unaffected by both RIG–I´s compared to GST control (fig.25B). Furthermore, the viral A/PR/8/34 titers remained unaffected by RIG–I WT and RIG–I DC compared to GST control (fig. 25C).

A)

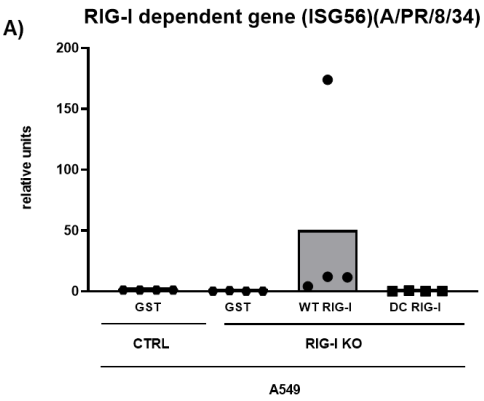
RIG-I dependent gene (ISG56)(A/PR/8/34)
relative units
200
150
100
50
0
GST
GST
WT RIG-I
DC RIG-I
CTRL
RIG-I KO
A549

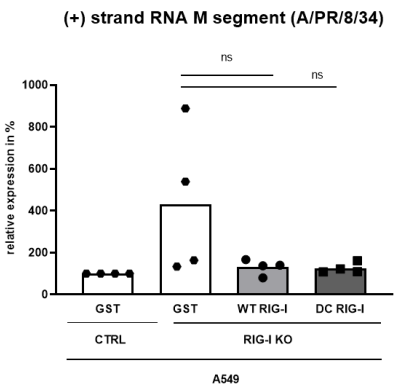
(+) strand RNA M segment (A/PR/8/34)
ns
ns
relative expression in %
1000
800
600
400
200
0
GST
GST
WT RIG-I
DC RIG-I
CTRL
RIG-I KO
A549

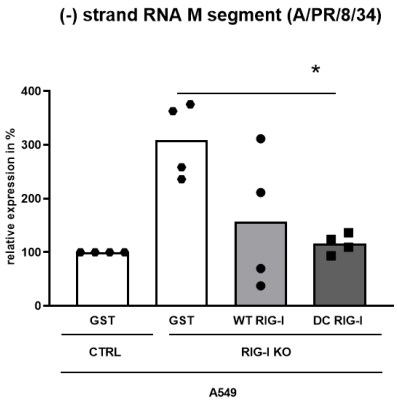
(-) strand RNA M segment (A/PR/8/34)
*
relative expression in %
400
300
200
100
0
GST
GST
WT RIG-I
DC RIG-I
CTRL
RIG-I KO
A549

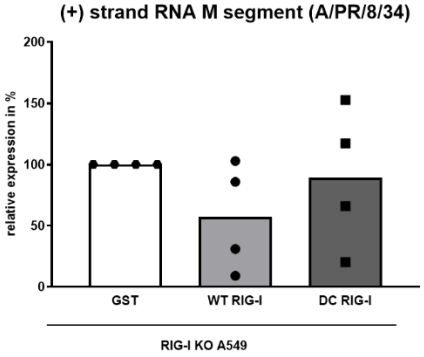
(+) strand RNA M segment (A/PR/8/34)
relative expression in %
200
150
100
50
0
GST
WT RIG-I
DC RIG-I
RIG-I KO A549

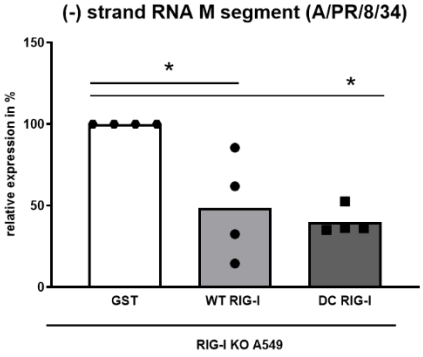
(-) strand RNA M segment (A/PR/8/34)
*
*
relative expression in %
150
100
50
0
GST
WT RIG-I
DC RIG-I
RIG-I KO A549

B)

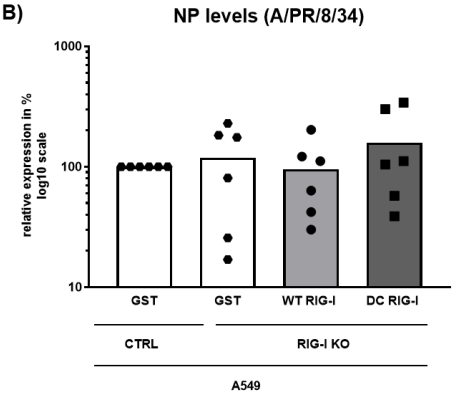
NP levels (A/PR/8/34)
relative expression in %
log10 scale
1000
100
10
GST
GST
WT RIG-I
DC RIG-I
CTRL
RIG-I KO
A549

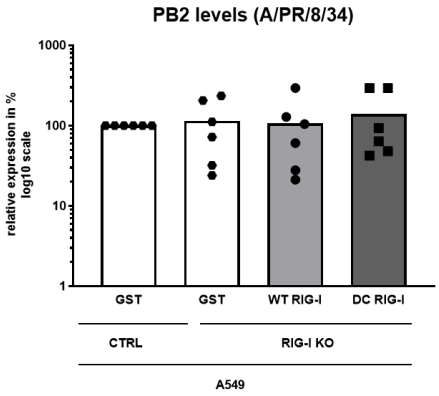
PB2 levels (A/PR/8/34)
relative expression in %
log10 scale
1000
100
10
1
GST
GST
WT RIG-I
DC RIG-I
CTRL
RIG-I KO
A549

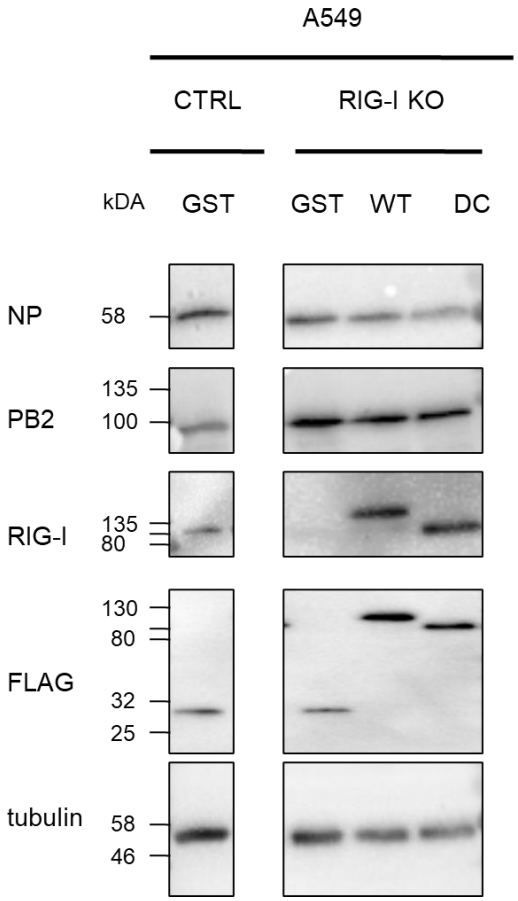
A549
CTRL
RIG-I KO
kDA
GST
GST
WT
DC
NP
58
PB2
135
100
RIG-I
135
80
FLAG
130
80
32
25
tubulin
58
46

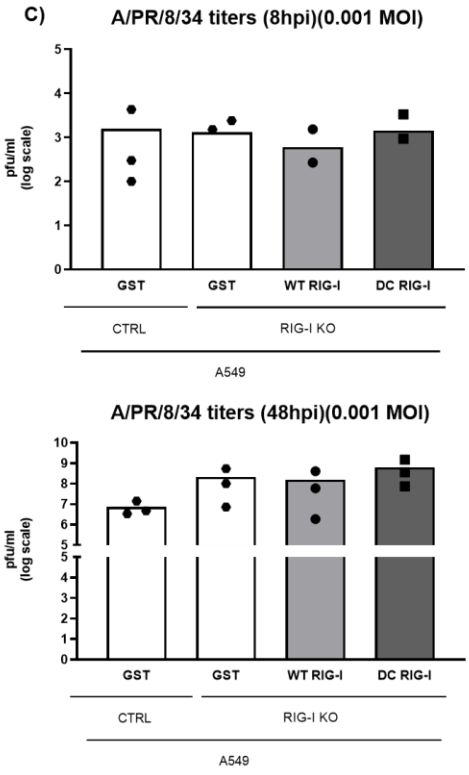
C)
A/PR/8/34 titers (8hpi)(0.001 MOI)
pfu/ml
(log scale)
GST
GST
WT RIG-I
DC RIG-I
CTRL
RIG-I KO
A549

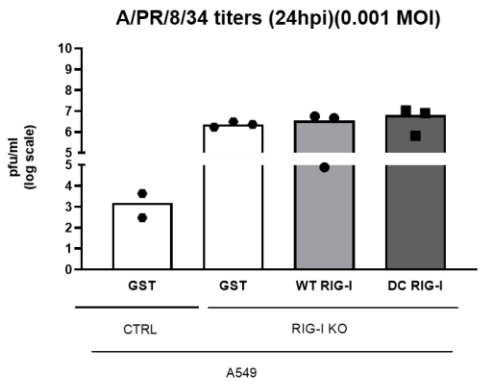
A/PR/8/34 titers (24hpi)(0.001 MOI)
pfu/ml
(log scale)
GST
GST
WT RIG-I
DC RIG-I
CTRL
RIG-I KO
A549

A/PR/8/34 titers (48hpi)(0.001 MOI)
pfu/ml
(log scale)
GST
GST
WT RIG-I
DC RIG-I
CTRL
RIG-I KO
A549

Figure 25: Effect of RIG–I mutant A/PR/8/34.

A) qRT–PCR analysis of M segment levels (positive and negative strand) of A/PR/8/34 and cellular ISG56 levels. Stably expressing GST or WT (wild type) RIG–I or DC (ΔCARD) RIG–I A549 control cell line (CTRL) or RIG–I KO cells were infected with A/PR/8/34 (MOI 1, 1hour). 6 hours later RNA was isolated for qRT–PCR analysis. Mean and individual values from four biological replicates are shown. CTRL GST or RIG–I KO GST was set as 100%. Two–tailed paired Student's t test indicated significance * $p<0.05$. B) Western Blot analysis of NP and PB2 protein levels normalised to β–tubulin. Stably expressing GST or WT (wild type) RIG–I or DC (ΔCARD) RIG–I A549 control cell line (CTRL) or RIG–I KO cells were infected with A/PR8/34 (MOI 1, 1hour). 6 hours later total protein lysate was isolated for Western blot analysis for the indicated antigens. Representative blot of staining is shown. Numbers indicate the molecular weight of the protein in kilo Dalton (kDA). Bands were quantified with Image Lab 5.2.1 software. Mean and individual values from six biological replicates are shown. CTRL GST was set as 100%. C) Stably expressing GST or WT (wild type) RIG–I or DC (ΔCARD) RIG–I A549 control cell line (CTRL) or RIG–I KO cells were infected at an MOI of 0.001. At the time points indicated, supernatants were harvested and titrated by immunoplaque assay. Mean and individual values from three biological replicates are shown. CTRL GST was set as 100%.

6.11 Effect of RIG–I mutants on avian signature strain A/WSN/33

Since RIG–I DC, like RIG–I WT, inhibits early viral RNA replication of strain A/PR/8/34, its potential effect against other FLUAV virus was tested. Thus, the effect of RIG–I on A/WSN/33 bearing the avian adaptation signature in PB2 segment at position 627 (A/WSN/33 PB2 627E) was evaluated. The avian adaptive mutation PB2 627E is known to negatively impact NP binding but positively impact the RIG–I activation (Labadie et al., 2007, Weber et al., 2015, Rameix–Welti et al., 2009). Thus, the cells were infected for 1 h at MOI of 1, and 6 h later levels of cellular ISG56, viral RNA and protein were determined. As a marker for the *de novo* synthesized viral RNA, the positive–strand sequence (mRNA and antigenome) of the viral genome segment 7 was used, while the newly produced viral RNA was examined with the negative strand of segment 7. The RIG–I dependent gene ISG56 was used as a RIG–I mediated signalling indicator. Viral protein synthesis was examined through levels of NP protein. In addition, the effect of RIG–I on full viral replication cycle was also determined at 1 and 2 days after infection. The cells were infected for 1 h MOI of 0.001, and at the indicated time points, viral titers were determined. Again, ISG56 was induced in the RIG–I KO when only RIG–I WT was expressed. Surprisingly, under these conditions, viral RNA, protein and titer levels of A/WSN/33 PB2 627E were unaffected by RIG–I WT and RIG–I DC (fig. 26)

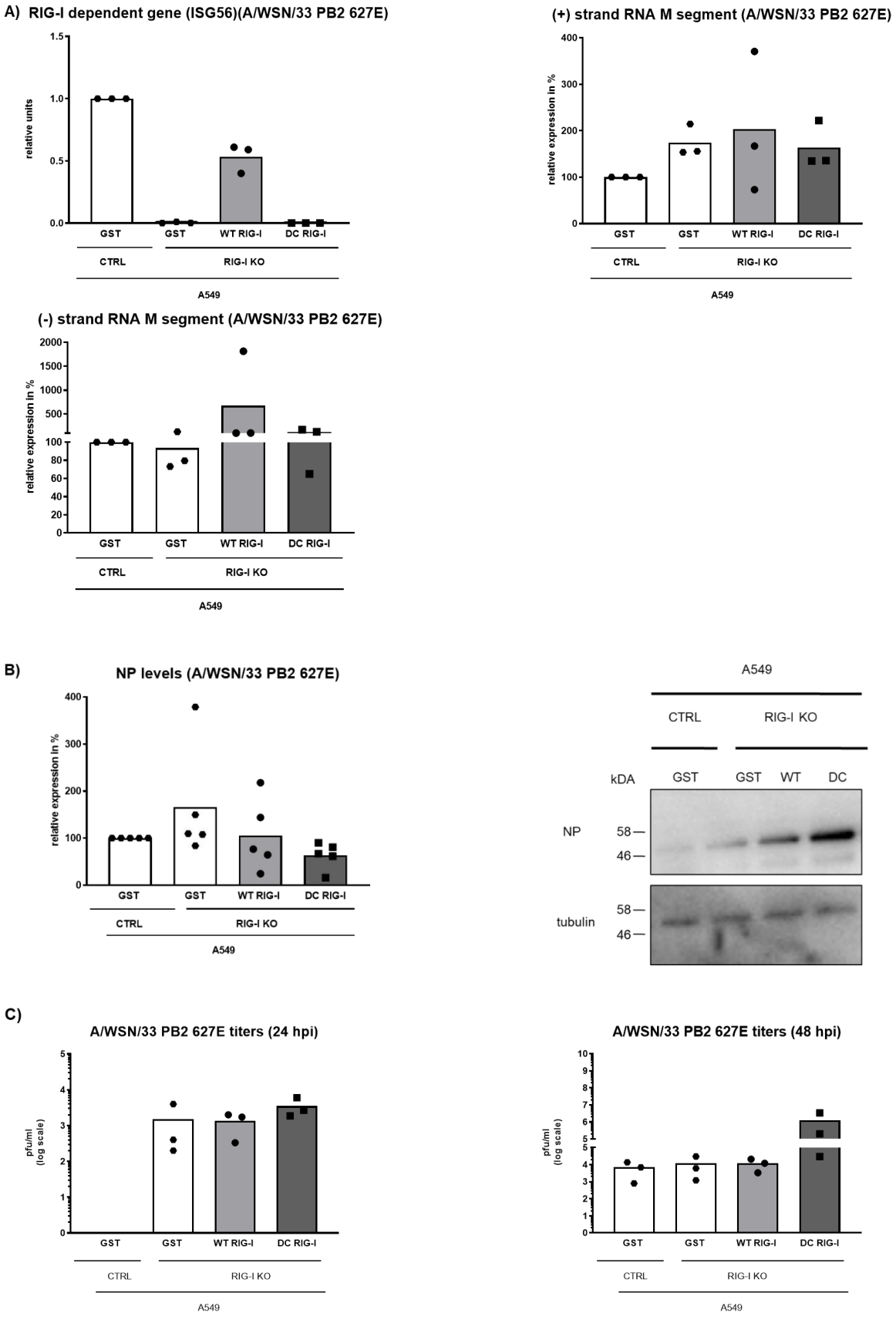

Figure 26: Effect of RIG–I mutant on avian strain A/WSN/33 PB2 627E.

A) qRT–PCR analysis of cellular ISG56 levels and M segment levels (positive and negative strand) of A/WSN/33 PB2 627E. Stably expressing GST or WT (wild type) RIG–I or DC (ΔCARD) RIG–I A549 control cell line (CTRL) or RIG–I KO cells were infected with A/WSN/33 PB2 627E (MOI 1, 1hour). 6 hours later RNA was isolated for qRT–PCR analysis. Mean and individual values from three biological replicates are shown. CTRL GST was set as 100%. B) Western Blot analysis of NP levels normalised to β–tubulin. Stably expressing GST or WT (wild type) RIG–I or DC (ΔCARD) RIG–I A549 control cell line (CTRL) or RIG–I KO cells were infected with A/WSN/33 PB2 627E (MOI 1, 1hour). 6 hours later total protein lysate was isolated for Western blot analysis for the indicated antigens. Representative blot of staining is shown. Numbers indicate the molecular weight of the protein in kilo Dalton (kDA). Bands were quantified with Image Lab 5.2.1 software. Mean and individual values from three biological replicates are shown. CTRL GST was set as 100%. C) Stably expressing GST or WT (wild type) RIG–I or DC (ΔCARD) RIG–I A549 control cell line (CTRL) or RIG–I KO cells were infected at an MOI of 0.001. At the time points indicated, supernatants were harvested and titrated by immunoplaque assay. Mean and individual values from three biological replicates are shown. CTRL GST was set as 100%.

6.12 Effect of RIG–I mutants on SARS–CoV–2 virus

Recently, RIG–I was described as a sensor of viral SARS–CoV–2 RNA, inhibiting viral replication in an IFN–independent manner (Yamada et al., 2021). Conversely, other reports indicate that even though RIG–I senses SARS–CoV–2 RNA, viral components hamper its downstream activation leading to infectivity (Kouwaki et al., 2021, Chen et al., 2020). Thus, the effect of RIG–I was also tested against SARS–CoV–2. For this, cells were infected for 1 h at a multiplicity of infection (MOI) of 0.5, and 48 h later levels of viral RNA and protein were addressed. As a marker for viral RNA, the E gene was assessed while protein synthesis was examined with the levels of N protein. As shown in fig. 27 under these conditions, viral RNA and protein levels of SARS–CoV–2 remained unaffected by RIG–I DC and RIG–I WT compared to the GST control.

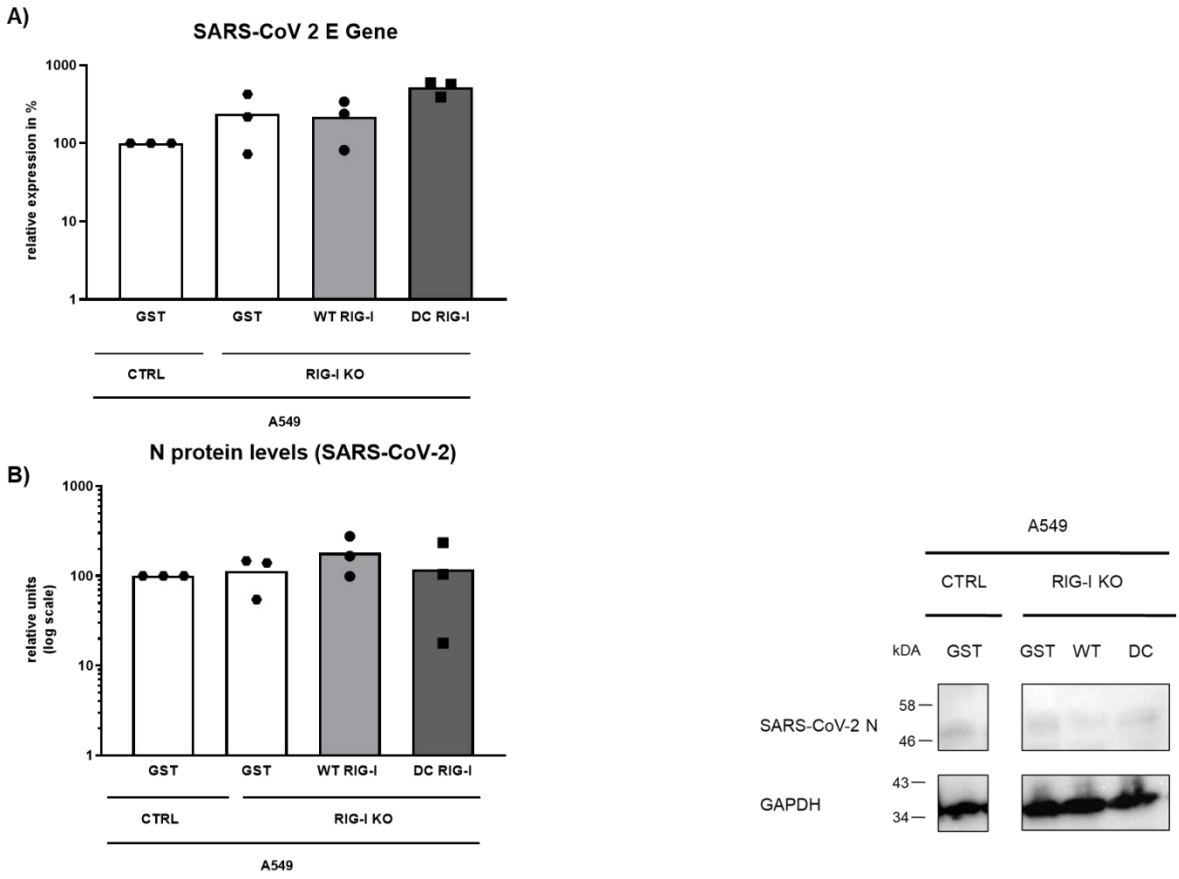

Figure 27: Effect of RIG–I mutant on SARS–CoV–2.

A) qRT–PCR analysis of E gene levels of SARS–CoV–2. Stably expressing GST or WT (wild type) RIG–I or DC (ΔCARD) RIG–I A549 control cell line (CTRL) or RIG–I KO cells were infected with SARS–CoV–2 (MOI 0.5, 1hour). 48 hours later RNA was isolated for qRT–PCR analysis. Mean and individual values from three biological replicates are shown. CTRL GST was set as 100%. B) Western Blot analysis of N protein levels normalised to β–tubulin. Stably expressing GST or WT (wild type) RIG–I or DC (ΔCARD) RIG–I A549 control cell line (CTRL) or RIG–I KO cells were infected with SARS–CoV–2 (MOI 0.5, 1hour). 48 hours later total protein lysate was isolated for Western blot analysis for the indicated antigens. Representative blot of staining is shown. Numbers indicate the molecular weight of the protein in kilo Dalton (kDA). Bands were quantified with Image Lab 5.2.1 software. Mean and individual values from three biological replicates are shown. CTRL GST was set as 100%.

To conclude, in this study, RIG–I signalling deficient mutant DC exhibited early inhibitory effect against A/PR/8/34 in a transient transfection system. In this system HEK293T cells were used, but due to their organ origin and fragility the A549 lung adenocarcinoma cell line was used. With this cell line, a stable transfection system was used. In this system RIG–I WT and DC inhibited only the early RNA replication of

A/PR/8/34. Furthermore, both RIG–Is did not show any effect on H1N1 strain A/WSN/33 PB2 627E and SARS–CoV–2.

7 Discussion

7.1 Influenza and SARS–CoV–2 viruses remain a burden

Despite the vaccinations against Influenza and SARS–CoV–2, the number of infections is still a burden (Świerczyńska et al., 2022, Iacopetta et al., 2022). In addition, Influenza antivirals are available but have several limitations. Amantadine, the first anti–Influenza drug (Huber et al., 1999, Tokimatsu and Nasu, 2000), an M2 ion–channel blocker, had a dose–dependent effect but the therapy had to be initiated within the first two days of infection (Tokimatsu and Nasu 2000). In addition, since 2006, due to the emergence of amantadine–resistant strains, this therapeutic strategy is not recommended (Dong et al., 2015). On the other hand, the current therapeutic strategy against FLUAV is neuraminidase inhibitors (Bassetti et al., 2019). Even though the toxicity levels are low and the emergence of viral resistance is unlikely, the administration has to be again within the first two days (Moscona 2005). Thus, antiviral agents are most effective if administered early in the disease course, but have only a modest impact upon the duration of clinical symptoms (McNicholl and McNicholl 2001).

7.2 Paliperidone as a potential lead antiviral compound and its limitations

This leads to an urgent need of more effective inhibitors against FLUAV. Paliperidone, an FDA–approved drug against schizophrenia (PubChem. 2020), was suggested as an ideal lead for new antivirals (Patel and Kukol 2017). This hypothesis was addressed in this study using different strains of FLUAV H1N1. Indeed, for the case of A/PR/8/34, Paliperidone was able to mildly inhibit early viral RNA and consistently protein synthesis at 6 hours post infection and virus yields at 8 hours post infection. The latter was also observed on a relevant *ex vivo* infection system based on human primary bronchial cells until 24 hours post infection. However, this effect was not observed on longer infection periods. Furthermore, Paliperidone was tested against the avian adapted A/WSN/33 PB2 627E, the mammalian adapted A/WSN/33 PB2 627K and pandemic A/HAM/2009 strains. Under these conditions, Paliperidone exerted inhibitory effect against strain A/WSN/33 PB2 627K only on the newly produced viral RNA. Furthermore, Paliperidone was inhibitory against A/HAM/2009 only on the protein synthesis level failing to affect the avian adapted strain A/WSN/33 PB2 627E. This was in consistency with the viral polymerase activity data, where the

mammalian polymerase activity was inhibited by Paliperidone in contrast with the avian one. However, inhibition of virus titers was not observed. The early antiviral effects of Paliperidone observed did not alter the levels of interferon signalling, whatsoever. Mechanistically, in this study it was demonstrated that Paliperidone disturbs the interaction between the A/PR/8/34 polymerase subunit PB2 and the nucleoprotein NP, thus being in line with the *in silico* prediction that the compound docks onto a domain on PB2 involved in NP binding (Patel and Kukol 2017). This exact mechanism might explain the early and not later effect of Paliperidone in the course of infection. This docking might be strong enough to keep Paliperidone molecules bound to PB2 proteins, inhibiting Paliperidone to bind to other PB2 molecules. Repeated administration of Paliperidone, which would be necessary to uphold the inhibition, might lead to toxic effects due to minor or lack of metabolism of the compound within the cells. On the other hand, it is, therefore, conceivable that concentrations of Paliperidone, chosen to be below the toxicity threshold, were not sufficient for a sustained antiviral effect. Nonetheless, these data validated the *in silico* predictions and suggest that Paliperidone could serve as starting point for the development of new anti–influenza drugs.

The question why other H1N1 strains were not as affected as A/PR/8/34 remains unclear. *In silico* prediction showed a hydrogen bond formed between a nitrogen atom of Paliperidone and the oxygen atom of PB2 Glu241, and hydrophobic interactions with additional 16 surrounding residues of the target site (Patel and Kukol 2017). Comparing those PB2 relevant sites between the FLUAV strain A/VietNam/1203/2004 (H5N1) that was used for the structure modelling and the ones investigated here (A/PR/8/34, A/HAM/2009, A/WSN/33) revealed almost 100% amino acid sequence conservation (Fig. 28).

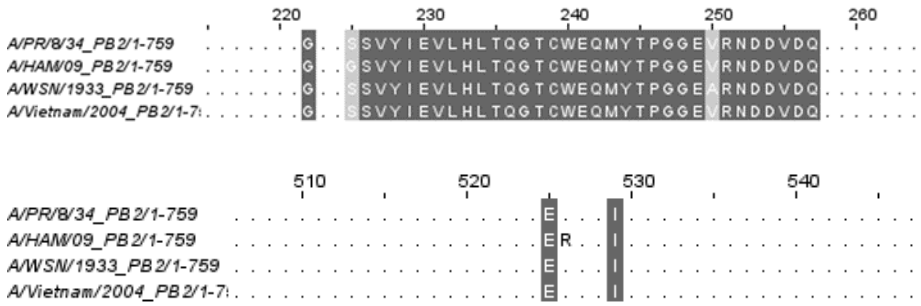

Figure 28. Evolutionary conservation of the amino acids in PB2 proposed to bind Paliperidone.

Alignment of PB2 amino acid sequences proposed to be critical for Paliperidone binding. Sequences of FLUAV strains A/PR/8/34 H1N1, A/HAM/2009 H1N1, A/WSN/33 H1N1 and A/VietNam/2004 H5N1 are shown. Putative Paliperidone–interacting PB2 residues are highlighted depending on their degree of evolutionary conservation. Sequences were obtained from NCBI Protein and analyzed with Clustal Omega tool.

It appears therefore unlikely that the PB2 sequence itself is responsible for the observed differences in sensitivity, although a definite proof for Paliperidone binding has yet to be provided. In line with this interpretation, also the avian adaptive mutation PB2 627E, though known to impact NP binding and RIG–I activation (Labadie et al., 2007, Weber et al., 2015, Rameix–Welti et al., 2009), did not sensitize the virus to Paliperidone. Even though the residues with which Paliperidone interacts show high conservation, the structural conformation of the protein might be altered due to the change of amino acid at position 627 (Yamada et al., 2010). This, in connection with the interaction of NP protein, showing variability between strains, might lead to the steric hindrance of interaction of Paliperidone with avian adapted PB2 and ultimately escaping inhibition by Paliperidone.

Even though PB2 proteins of the strains tested are highly conserved, the exact site of Paliperidone blocking NP interacting with PB2 protein is unclear. Four domains of NP were found to interact with PB2 (NP aa 1–161, 255–340, 340–465, 340–498) with the interaction described as dynamic (Biswas et al., 1998). These regions of NP show both highly conserved and variable residues (Kukol and Hughes 2014). In that study the level of conservation of 4430 NPs tested was 59%, with variability of the residues being at 21%. Therefore, NP protein residue variability might be responsible for the differences in sensitivity of different strains to Paliperidone observed in this study.

The effect of Paliperidone against A/PR/8/34 depends on the presence of the virus sensor RIG–I. RIG–I is an RNA helicase that can recognize the “panhandle” promoter of FLUAV nucleocapsids (Weber et al., 2015). This short double–stranded sequence results from imperfect base pairing between the 5’ and 3’ ends of the viral genomic RNA. Although the genome ends are normally hidden inside the tripartite

polymerase structure (Pflug 2014), a certain background to activate RIG–I is detectable, and can be boosted by the PB2 627E mutation that lowers the affinity to NP, by or biochemical interference (Weber et al., 2015). Despite the impact on PB2–NP binding, no significant increase of RIG–I activation by Paliperidone was detected, perhaps because the impact of the compound is too subtle to be detected by the conformational switch assay.

Upon RIG–I activation a signalling cascade is initiated leading to Interferon and ISGs expression (Yoneyama et al., 2015, Rehwinkel and Gack 2020, Loo et al., 2008, Poeck et al., 2010). Paliperidone did not alter interferon signalling regulators and products (ISG56, IRF7/3). Interferon signalling might be protective but excessive activation might be detrimental and lead to damage (Guo and Thomas 2017). To this context, Paliperidone, even though leads to early inhibition of some H1N1 strains, does not alter interferon signalling.

Besides the fact that Paliperidone was proved to disrupt the interaction between NP and PB2 *in vitro* in this study, Paliperidone is a D2 and 5–HT2A receptor antagonist. These receptors affect major signalling modulators in the cells such as AKT signalling (Boyd and Mailman, 2012). Paliperidone, as an antagonist, reverts the D2 receptor–mediated AKT inhibition, and this effect is shown in cellular models of schizophrenia (Peng et al., 2014). On the other side, FLUAV manipulates a variety of cellular signalling pathways with one being PI3K/AKT (Ehrhardt et al., 2007, Hirata et al., 2014, Murray et al., 2012). AKT is known among others as a regulator of cell survival by regulating apoptosis (Li et al., 2019) and senescence (Rössig et al., 2001, Shtutman et al., 2017). p21 protein is a senescence marker, inducing cell cycle arrest (Shtutman et al., 2019), and recently its FLUAV restricting and interferon inducing role was described (Ma et al., 2022) (Figure 29).

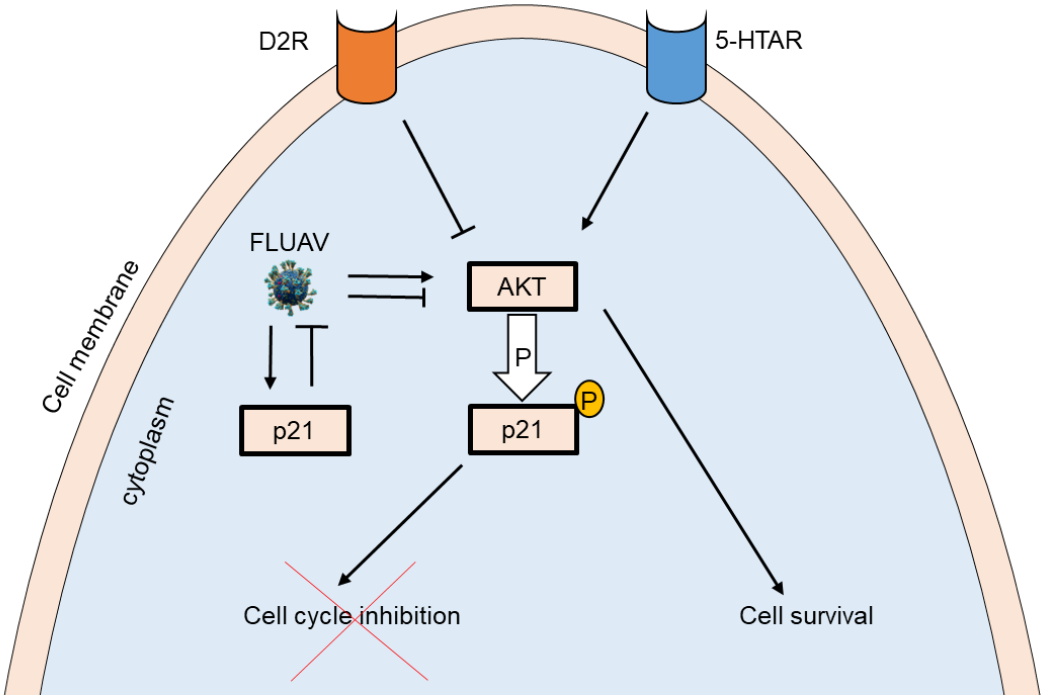

Figure 29: D2, 5–HT2A receptors and FLUAV affect major signalling cascades.

Dopamine 2 receptor (D2R) and the serotonin receptor 5–HTAR supress and induce AKT accordingly (Boyd and Mailman, 2012). The senescence marker p21 is phosphorylated by AKT (Rössig et al., 2001, Shtutman et al., 2017) leading to cell cycle progression and cell survival. FLUAV also affects AKT (Ehrhardt et al., 2007, Hirata et al., 2014, Murray et al., 2012) and induces p21, with latter being an inhibitor of FLUAV (Ma et al., 2022).

In this study here, Paliperidone did not exert any effect on levels of AKT but induced cell survival under FLUAV infection (microscopic observation, data not shown). Furthermore, Paliperidone was inhibitory on p21 levels, pinpointing a possible explanation of the loss of effect on late infection, in accordance with the anti–FLUAV effect of p21 (Ma et al., 2022). In addition, in connection with the NP residue variability, this could synergize to the strain–specific effect of Paliperidone observed, which is interesting for further examination.

To summarize, on this part of the study, Paliperidone inhibits on certain levels H1N1 viruses early in the course of infection without affecting the interferon signalling. This effect is accounted to its ability to fit in the NP binding domain of PB2, disrupting the formation of the complex. Future research optimizing Paliperidone on its anti–

FLUAV effect would be of interest and further tests should be put into consideration on animals for its inhibitory capacity against FLUAV.

The COVID–19 pandemic, caused by the coronavirus SARS–CoV–2, has become a global concern, with infections and death numbers continuing to grow (accessed on August 9, 2022 WHO Coronavirus (COVID–19) Dashboard) even though vaccines are available. Taking into account that SARS–CoV–2 is still a burden, there is still an urgent need to identify new compounds with potent anti–SARS–CoV–2 activity (Xu et al., 2021). Recently, antipsychotics were examined in cohort studies for their anti–SARS–CoV–2 effect with the contradictory results. Evidence showed that antipsychotics showed decreased chance of infection (Nemani et al., 2022) in accordance with another study where lower prevalence of infection and less severe outcomes in individuals treated with antipsychotics were observed (Canal–Rivero et al., 2021). Contrary to that, in another study, mortality rate of SARS–CoV–2 was higher in individuals prescribed with antipsychotics (Austria et al., 2021). A screening of potential inhibitors against SARS–CoV–2 3CLpro protease was carried out, with docking models revealing the high affinity of Paliperidone binding to 3CLpro *in silico*, suggesting Paliperidone as a potential inhibitor candidate against SARS–CoV–2 (Gul et al., 2020). This viral–inhibitory hypothesis was addressed *in vitro* in this study. Even though both Paliperidone concentrations tested here showed inhibition of viral RNA levels, protein expression and viral yields remained unaffected. This minor effect might indicate that concentrations of Paliperidone, chosen to be below the toxicity threshold, were not sufficient for a sustained antiviral effect. It would be of interest to examine cells treated with Paliperidone prior to infection, in order to mimic the antipsychotic treatment before SARS–CoV–2 infection *in vitro* (Nemani et al., 2022, Canal–Rivero et al., 2021 and Austria et al., 2021) and eventually examine the potential antiviral effect. The steric hindrance mechanism of 3CLpro protease inhibition as described (Gul et al. 2020) would be also of interest to be addressed. This would be possible by assessing the 3CLpro enzyme activity (Mody et al., 2022, Heilmann et al., 2022) after Paliperidone treatment.

7.3 RIG–I direct activity against FLUAV and SARS–CoV–2 and system limitations

In the course of FLUAV and SARS–CoV–2 infection, the severity of the disease is an interplay between the virulence and the excessive immune activation produced as resistance from the host (Liu et al., 2016, Song et al., 2020). RIG–I is the major sensor for FLUAV infection (Weber, 2015). RIG–I recognition of its ligands and subsequent activation leads to the production of chemokines and cytokines (Onomoto et al., 2021), with excess activation leading to detrimental effects (Yamada et al., 2018). Evidence indicate that RIG–I has direct antiviral effect since RIG–I signalling deficient mutants show FLUAV restricting effects (Weber et al., 2015). Thus, this study, as a complementary approach, focused on testing the antiviral capacity of signalling–deficient RIG–I mutants, initially, against FLUAV. The mutants tested here were the ligand dependent–signalling deficient K270A (Lassig et al., 2015, Yoneyama et al., 2005), and the K270A/E373Q. Furthermore, the T409A/S411A, which signalling capacity is ligand dependent (Louber et al., 2015) and the signalling deficient ΔCARD were tested. Initially these constructs were tested for their signalling capacity and inhibitory effect on RNA levels. Indeed, here, RIG–I helicase mutant K270A exerted same levels of antiviral activity against A/PR/8/34 as RIG–I WT in RNA levels. This is in accordance with another study (Weber et al., 2015) where K270A was inhibitory against A/PR/8/34 on protein level. Furthermore, here, the same antiviral effect as RIG–I WT was observed by the signalling deficient RIG–I ΔCARD.

It is worth mentioning that K270A mutation exhibited minor signalling capability, mainly under non–infection conditions. The same effect was also observed in other studies (Louber et al., 2015 and Ranjith–Kumar et al., 2009) after stimulation with RIG–I ligands. This effect might be explained by the fact that ATP binding activity, which is absent in RIG–I K270A is required for the specificity for RNA recognition (Lässig and Hopfner 2017). Also, in this study, the RIG–I K270A/E373Q showed constitutively active signalling in accordance with another study (Louber et al., 2015) in which mutation at position E373Q led to constitutive signalling. For T409A/S411A mutation studies show that depending on the stimulation there is both a defect (Louber et al., 2015) but also capability of signalling (Ranjith–Kumar et al., 2009) with the latter also observed here, indicating the dependence on the nature of activating ligands. Moreover, in this study was shown that the CARDs domains are

indispensable for signalling, in accordance with another study (Kowalinski et al., 2011). Independent on the RIG–I signalling capacity, all constructs used here, interestingly, were inhibitory, against A/PR/8/34 RNA transcription and replication.

The antiviral effect was observed in transiently transfected HEK 293T RIG–KO cells. Even though HEK 293T cells are used for FLU vaccine, reverse genetics and viral yields (Le Ru et al., 2010, Milián et al., 2017), their organ origin (kidney) as well as their fragility, led to the change of cell system to the alveolar adenocarcinoma A549 cell line. Furthermore, for sustained expression of RIG–I, lentiviral–based stable expression cell lines were used. Since here the mutation on RIG–I at position K270A led to minor expression of the RIG–I–dependent gene ISG56, and the aim of this study was to examine the potential direct antiviral activity and thus signalling–deficient RIG–I mutations, RIG–I ΔCARD was further evaluated in antiviral tests. Also, for the following tests GST (Glutathione–S–transferase) was used as a control due to the cytotoxicity and immunogenicity observed with GFP (Ansari et al., 2016). Even though A/PR/8/34 RNA viral replication was also inhibited in this system, as in the transient transfection system, the inhibitory effect was not observed in viral transcription, viral protein and titer levels. This might be due to the nature of system used. The amount of copy numbers of nucleotide material is high in the transient transfection, leading to high protein expression. In contrast, in the stable expression system, single or low copy numbers of genetic material found, lead to low protein expression. Thus, the lower expression of RIG–I due to the stable transfection system itself, might not be enough to exert the same antiviral effect as in the transient transfection system. Also, the virus A/WSN/33 PB2 627E known for its sensitivity to RIG–I (Weber et al., 2015) was not sensitive to any of the RIG–I constructs supporting the fact that the amount of protein in this stable transfection system compared to the transient transfection system used in Weber et al., 2015, is not enough to exert the antiviral effect.

Notably, the FLUAV strains used here contain functional NS1 protein. As the major virulence factor of influenza viruses, NS1 targets posttranslational modification of RIG–I, which is required for its activation (Jureka et al., 2020) and downstream signalling (Rajsbaum et al., 2012). Thus, the surprising absence of inhibitory effect of RIG–I WT found here might be due the low levels of the protein expression in the stable transfection system being incapable to overcome the inhibiting action of NS1.

Recent evidence indicate that RIG–I senses SARS–CoV–2 RNA. RIG–I′s inhibitory effect is still unclear with evidence indicating both inhibition (Yamada et al., 2021) and exacerbation of the severity of infection through inflammation (Thorne et al., 2021). Furthermore, other evidence indicate that absence of RIG–I leads to higher viral replication of SARS–CoV–2 (Yang et al., 2021). Also, the virus itself exhibits mechanisms to escape RIG–I–mediated immune response (Kouwaki et al., 2021) indicating a possible antiviral role of RIG–I. RIG–I, expressed in a transient transfection system was proved to be inhibitory against SARS–CoV–2 in an IFN–independent manner (Yamada et al., 2021). In this study, in stable transfection system, none of the RIG–I proteins expressed showed inhibitory effect against SARS–CoV–2. This is once more an indication that the levels of expressed RIG–I in this stable transfection system used here, were below threshold to show inhibitory effect. In addition to that, the absence of antiviral effect of RIG–I WT observed here might be due to the action of Orf9b protein, which inhibits the interaction of RIG–I and MAVS hindering IFN signalling (Kouwaki et al., 2021).

In conclusion, for the course of this study, the FDA–approved schizophrenia drug Paliperidone was shown to disrupt the interaction of Influenza polymerase subunit PB2 with the nucleoprotein NP, as predicted *in silico* (Patel and Kukol 2017). This led to early inhibition of strain A/PR/8/34. Furthermore, effects were restricted to strains carrying the mammalian signature at PB2 protein at position 627. The strain dependent effect could be accounted to the residue variability of NP protein while the early effect might be result of the relative low concentration used here together with the p21 Paliperidone induced inhibition. Furthermore, Paliperidone exhibited mild inhibitory effect against SARS–CoV–2 as suggested *in silico* (Gul et al., 2020). These indicate that Paliperidone might be of interest for further optimization and investigation for its potential antiviral effect against FLUAV and SARS–CoV–2.

In another complementary approach, RIG–I′s direct antiviral activity was examined. Thus, RIG–I WT and signalling deficient RIG–I ΔCARD were examined for their antiviral effect. Even though initial findings showed that these proteins are inhibitory against A/PR/8/34 in a transient transfection system, they failed to show a strong or any effect in a stable transfection system. That could be accounted to the fact that the nature of the system used leads to lower levels of protein of interest expression. This absence of effect was also observed with another FLUAV strain and SARS–CoV–

2. This indicates that this system is not suitable for its use in antiviral assays. Besides that, due to the initial data, it would be interesting to examine the effect of RIG–I WT and ΔCARD, in a transient transfection system, against different strains of FLUAV and SARS–CoV–2 virus.

8 References

Aggarwal S, Bradel–Tretheway B, Takimoto T, Dewhurst S, Kim B. Biochemical characterization of enzyme fidelity of influenza A virus RNA polymerase complex. PLoS One. 2010 Apr 29;5(4):e10372. doi: 10.1371/journal.pone.0010372. PMID: 20454455; PMCID: PMC2861597.

Albo C, Valencia A, Portela A. Identification of an RNA binding region within the N–terminal third of the influenza A virus nucleoprotein. J Virol. 1995 Jun;69(6):3799–806. doi: 10.1128/JVI.69.6.3799–3806.1995. PMID: 7745727; PMCID: PMC189097.

Anchisi S, Guerra J, Garcin D. RIG–I ATPase activity and discrimination of self–RNA versus non–self–RNA. mBio. 2015 Mar 3;6(2):e02349. doi: 10.1128/mBio.02349–14. PMID: 25736886; PMCID: PMC4358010.

Ansari AM, Ahmed AK, Matsangos AE, Lay F, Born LJ, Marti G, Harmon JW, Sun Z. Cellular GFP Toxicity and Immunogenicity: Potential Confounders in in Vivo Cell Tracking Experiments. Stem Cell Rev Rep. 2016 Oct;12(5):553–559. doi: 10.1007/s12015–016–9670–8. PMID: 27435468; PMCID: PMC5050239.

Austria B, Haque R, Mittal S, Scott J, Vengassery A, Maltz D, Li W, Greenwald B, Freudenberg–Hua Y. Mortality in association with antipsychotic medication use and clinical outcomes among geriatric psychiatry outpatients with COVID–19. PLoS One. 2021 Oct 21;16(10):e0258916. doi: 10.1371/journal.pone.0258916. PMID: 34673821; PMCID: PMC8530340.

Baccam P, Beauchemin C, Macken CA, Hayden FG, Perelson AS. Kinetics of influenza A virus infection in humans. J Virol. 2006 Aug;80(15):7590–9. doi: 10.1128/JVI.01623–05. PMID: 16840338; PMCID: PMC1563736.

Baddock HT, Brolih S, Yosaatmadja Y, Ratnaweera M, Bielinski M, Swift LP, Cruz–Migoni A, Fan H, Keown JR, Walker AP, Morris GM, Grimes JM, Fodor E, Schofield CJ, Gileadi O, McHugh PJ. Characterization of the SARS–CoV–2 ExoN (nsp14ExoN–nsp10) complex: implications for its role in viral genome stability and inhibitor identification. Nucleic Acids Res. 2022 Feb 22;50(3):1484–1500. doi: 10.1093/nar/gkab1303. PMID: 35037045; PMCID: PMC8860572.

Baer A, Kehn–Hall K. Viral concentration determination through plaque assays: using traditional and novel overlay systems. J Vis Exp. 2014 Nov 4;(93):e52065. doi: 10.3791/52065. PMID: 25407402; PMCID: PMC4255882.

Bassetti M, Castaldo N, Carnelutti A. Neuraminidase inhibitors as a strategy for influenza treatment: pros, cons and future perspectives. Expert OpinPharmacother. 2019 Oct;20(14):1711–1718. doi: 10.1080/14656566.2019.1626824. Epub 2019 Jun 6. PMID: 31169040.

Baudin F, Bach C, Cusack S, Ruigrok RW. Structure of influenza virus RNP. I. Influenza virus nucleoprotein melts secondary structure in panhandle RNA and exposes the bases to the solvent. EMBO J. 1994 Jul 1;13(13):3158–65. PMID: 8039508; PMCID: PMC395207.

Baum A, Sachidanandam R, García–Sastre A. Preference of RIG–I for short viral RNA molecules in infected cells revealed by next–generation sequencing. Proc Natl Acad Sci U S A. 2010 Sep 14;107(37):16303–8. doi: 10.1073/pnas.1005077107. Epub 2010 Aug 30. Erratum in: Proc Natl Acad Sci U S A. 2011 Feb 15;108(7):3092. PMID: 20805493; PMCID: PMC2941304.

Beckham SA, Brouwer J, Roth A, Wang D, Sadler AJ, John M, Jahn–Hofmann K, Williams BR, Wilce JA, Wilce MC. Conformational rearrangements of RIG–I receptor on formation of a multiprotein:dsRNA assembly. Nucleic Acids Res. 2013 Mar 1;41(5):3436–45. doi: 10.1093/nar/gks1477. Epub 2013 Jan 15. PMID: 23325848; PMCID: PMC3597671.

Biswas SK, Boutz PL, Nayak DP. Influenza virus nucleoprotein interacts with influenza virus polymerase proteins. J Virol. 1998 Jul;72(7):5493–501. doi: 10.1128/JVI.72.7.5493–5501.1998. PMID: 9621005; PMCID: PMC110190.

Bortolotti D, Gentili V, Rizzo S, Schiuma G, Beltrami S, Strazzabosco G, Fernandez M, Caccuri F, Caruso A, Rizzo R. TLR3 and TLR7 RNA Sensor Activation during SARS–CoV–2 Infection. Microorganisms. 2021 Aug 26;9(9):1820. doi: 10.3390/microorganisms9091820. PMID: 34576716; PMCID: PMC8465566.

Boulo S, Akarsu H, Ruigrok RW, Baudin F. Nuclear traffic of influenza virus proteins and ribonucleoprotein complexes. Virus Res. 2007 Mar;124(1–2):12–21. doi: 10.1016/j.virusres.2006.09.013. Epub 2006 Nov 1. PMID: 17081640.

Boyd KN, Mailman RB. Dopamine receptor signalling and current and future antipsychotic drugs. Handb Exp Pharmacol. 2012;(212):53–86. doi: 10.1007/978–3–642–25761–2_3. PMID: 23129328; PMCID: PMC4711768.

Brisse M, Ly H. Comparative Structure and Function Analysis of the RIG–I–Like Receptors: RIG–I and MDA5. Front Immunol. 2019 Jul 17;10:1586. doi: 10.3389/fimmu.2019.01586. PMID: 31379819; PMCID: PMC6652118.

Bui M, Whittaker G, Helenius A. Effect of M1 protein and low pH on nuclear transport of influenza virus ribonucleoproteins. J Virol. 1996 Dec;70(12):8391–401. doi: 10.1128/JVI.70.12.8391–8401.1996. PMID: 8970960; PMCID: PMC190928.

Canal–Rivero M, Catalán–Barragán R, Rubio–García A, Garrido–Torres N, Crespo–Facorro B, Ruiz–Veguilla M; IBIS Translational Psychiatry Group. Lower risk of SARS–CoV2 infection in individuals with severe mental disorders on antipsychotic treatment: A retrospective epidemiological study in a representative Spanish population. Schizophr Res. 2021 Mar;229:53–54. doi: 10.1016/j.schres.2021.02.002. Epub 2021 Feb 19. PMID: 33631466; PMCID: PMC7894093.

Chan YK, Gack MU. RIG–I works double duty. Cell Host Microbe. 2015 Mar 11;17(3):285–287. doi: 10.1016/j.chom.2015.02.014. PMID: 25766287; PMCID: PMC5072393.

Chen J, Malone B, Llewellyn E, Grasso M, Shelton PMM, Olinares PDB, Maruthi K, Eng ET, Vatandaslar H, Chait BT, Kapoor TM, Darst SA, Campbell EA. Structural Basis for Helicase–Polymerase Coupling in the SARS–CoV–2 Replication–Transcription Complex. Cell. 2020 Sep 17;182(6):1560–1573.e13. doi: 10.1016/j.cell.2020.07.033. Epub 2020 Jul 28. PMID: 32783916; PMCID: PMC7386476.

Chen K, Xiao F, Hu D, Ge W, Tian M, Wang W, Pan P, Wu K, Wu J. SARS–CoV–2 Nucleocapsid Protein Interacts with RIG–I and Represses RIG–Mediated IFN–β Production. Viruses. 2020 Dec 30;13(1):47. doi: 10.3390/v13010047. PMID: 33396605; PMCID: PMC7823417.

Chen Y, Su C, Ke M, Jin X, Xu L, Zhang Z, Wu A, Sun Y, Yang Z, Tien P, Ahola T, Liang Y, Liu X, Guo D. Biochemical and structural insights into the mechanisms of SARS coronavirus RNA ribose 2'–O–methylation by nsp16/nsp10 protein complex. PLoS Pathog. 2011 Oct;7(10):e1002294. doi: 10.1371/journal.ppat.1002294. Epub 2011 Oct 13. PMID: 22022266; PMCID: PMC3192843.

Civril F, Bennett M, Moldt M, Deimling T, Witte G, Schiesser S, Carell T, Hopfner KP. The RIG–I ATPase domain structure reveals insights into ATP–dependent antiviral signalling. EMBO Rep. 2011 Oct 28;12(11):1127–34. doi: 10.1038/embor.2011.190. PMID: 21979817; PMCID: PMC3207106.

Compans RW, Content J, Duesberg PH. Structure of the ribonucleoprotein of influenza virus. J Virol. 1972 Oct;10(4):795–800. doi: 10.1128/JVI.10.4.795–800.1972. PMID: 4117350; PMCID: PMC356535.

Corman VM, Landt O, Kaiser M, Molenkamp R, Meijer A, Chu DK, Bleicker T, Brünink S, Schneider J, Schmidt ML, Mulders DG, Haagmans BL, van der Veer B, van den Brink S, Wijsman L, Goderski G, Romette JL, Ellis J, Zambon M, Peiris M, Goossens H, Reusken C, Koopmans MP, Drosten C. Detection of 2019 novel coronavirus (2019–nCoV) by real–time RT–PCR. Euro Surveill. 2020 Jan;25(3):2000045. doi: 10.2807/1560–7917.ES.2020.25.3.2000045. Erratum in: Euro Surveill. 2020 Apr;25(14): Erratum in: Euro Surveill. 2020 Jul;25(30): Erratum in: Euro Surveill. 2021 Feb;26(5): PMID: 31992387; PMCID: PMC6988269.

Cui S, Eisenächer K, Kirchhofer A, Brzózka K, Lammens A, Lammens K, Fujita T, Conzelmann KK, Krug A, Hopfner KP. The C–terminal regulatory domain is the RNA 5'–triphosphate sensor of RIG–I. Mol Cell. 2008 Feb 1;29(2):169–79. doi: 10.1016/j.molcel.2007.10.032. PMID: 18243112.

Davidson M, Emsley R, Kramer M, Ford L, Pan G, Lim P, Eerdekens M. Efficacy, safety and early response of paliperidone extended–release tablets (paliperidone ER): results of a 6–week, randomized, placebo–controlled study. Schizophr Res. 2007 Jul;93(1–3):117–30. doi: 10.1016/j.schres.2007.03.003. Epub 2007 Apr 26. Erratum in: Schizophr Res. 2007 Nov;96(1–3):273–4. PMID: 17466492.

de Graaf M, Fouchier RA. Role of receptor binding specificity in influenza A virus transmission and pathogenesis. EMBO J. 2014 Apr 16;33(8):823–41. doi: 10.1002/embj.201387442. Epub 2014 Mar 25. Erratum in: EMBO J. 2014 Jul 17;33(14):1614. PMID: 24668228; PMCID: PMC4194109.

De Maio F, Lo Cascio E, Babini G, Sali M, Della Longa S, Tilocca B, Roncada P, Arcovito A, Sanguinetti M, Scambia G, Urbani A. Improved binding of SARS–CoV–2 Envelope protein to tight junction–associated PALS1 could play a key role in COVID–19 pathogenesis. Microbes Infect. 2020 Nov–Dec;22(10):592–597. doi: 10.1016/j.micinf.2020.08.006. Epub 2020 Sep 4. PMID: 32891874; PMCID: PMC7473260.

de Wit E, van Doremalen N, Falzarano D, Munster VJ. SARS and MERS: recent insights into emerging coronaviruses. Nat Rev Microbiol. 2016 Aug;14(8):523–34. doi: 10.1038/nrmicro.2016.81. Epub 2016 Jun 27. PMID: 27344959; PMCID: PMC7097822.

Deng X, Baker SC. An "Old" protein with a new story: Coronavirus endoribonuclease is important for evading host antiviral defenses. Virology. 2018 Apr;517:157–163. doi: 10.1016/j.virol.2017.12.024. Epub 2018 Jan 4. PMID: 29307596; PMCID: PMC5869138.

Devarkar SC, Schweibenz B, Wang C, Marcotrigiano J, Patel SS. RIG–I Uses an ATPase–Powered Translocation–Throttling Mechanism for Kinetic Proofreading of RNAs and Oligomerization. Mol Cell. 2018 Oct 18;72(2):355–368.e4. doi: 10.1016/j.molcel.2018.08.021. Epub 2018 Sep 27. PMID: 30270105; PMCID: PMC6434538.

Dong G, Peng C, Luo J, Wang C, Han L, Wu B, Ji G, He H. Adamantane–resistant influenza a viruses in the world (1902–2013): frequency and distribution of M2 gene mutations. PLoS One. 2015 Mar 13;10(3):e0119115. doi: 10.1371/journal.pone.0119115. PMID: 25768797; PMCID: PMC4358984.

Draft landscape and tracker of COVID–19 candidate vaccines. www.who.int/publications/m/item/draft–landscape–of–covid–19–candidate–vaccines [accessed August 10, 2022].

Drożdżal S, Rosik J, Lechowicz K, Machaj F, Szostak B, Przybyciński J, Lorzadeh S, Kotfis K, Ghavami S, Łos MJ. An update on drugs with therapeutic potential for SARS–CoV–2 (COVID–19) treatment. Drug Resist Updat. 2021 Dec;59:100794. doi: 10.1016/j.drup.2021.100794. Epub 2021 Dec 9. PMID: 34991982; PMCID: PMC8654464.

Dyall J, Gross R, Kindrachuk J, Johnson RF, Olinger GG Jr, Hensley LE, Frieman MB, Jahrling PB. Middle East Respiratory Syndrome and Severe Acute Respiratory Syndrome: Current Therapeutic

Options and Potential Targets for Novel Therapies. Drugs. 2017 Dec;77(18):1935–1966. doi: 10.1007/s40265–017–0830–1. PMID: 29143192; PMCID: PMC5733787.

Ehrhardt C, Wolff T, Pleschka S, Planz O, Beermann W, Bode JG, Schmolke M, Ludwig S. Influenza A virus NS1 protein activates the PI3K/Akt pathway to mediate antiapoptoticsignalling responses. J Virol. 2007 Apr;81(7):3058–67. doi: 10.1128/JVI.02082–06. Epub 2007 Jan 17. PMID: 17229704; PMCID: PMC1866065.

Fairman–Williams ME, Guenther UP, Jankowsky E. SF1 and SF2 helicases: family matters. CurrOpin Struct Biol. 2010 Jun;20(3):313–24. doi: 10.1016/j.sbi.2010.03.011. Epub 2010 Apr 22. PMID: 20456941; PMCID: PMC2916977.

Felsenstein S, Herbert JA, McNamara PS, Hedrich CM. COVID–19: Immunology and treatment options. Clin Immunol. 2020 Jun;215:108448. doi: 10.1016/j.clim.2020.108448. Epub 2020 Apr 27. PMID: 32353634; PMCID: PMC7185015.

Fodor E, Pritlove DC, Brownlee GG. The influenza virus panhandle is involved in the initiation of transcription. J Virol. 1994 Jun;68(6):4092–6. doi: 10.1128/JVI.68.6.4092–4096.1994. PMID: 8189550; PMCID: PMC236924.

Frazier MN, Dillard LB, Krahn JM, Perera L, Williams JG, Wilson IM, Stewart ZD, Pillon MC, Deterding LJ, Borgnia MJ, Stanley RE. Characterization of SARS2 Nsp15 nuclease activity reveals it's mad about U. Nucleic Acids Res. 2021 Sep 27;49(17):10136–10149. doi: 10.1093/nar/gkab719. PMID: 34403466; PMCID: PMC8385992.

Gack MU, Shin YC, Joo CH, Urano T, Liang C, Sun L, Takeuchi O, Akira S, Chen Z, Inoue S, Jung JU. TRIM25 RING–finger E3 ubiquitin ligase is essential for RIG–I–mediated antiviral activity. Nature. 2007 Apr 19;446(7138):916–920. doi: 10.1038/nature05732. PMID: 17392790.

Gao Y, Yan L, Huang Y, Liu F, Zhao Y, Cao L, Wang T, Sun Q, Ming Z, Zhang L, Ge J, Zheng L, Zhang Y, Wang H, Zhu Y, Zhu C, Hu T, Hua T, Zhang B, Yang X, Li J, Yang H, Liu Z, Xu W, Guddat LW, Wang Q, Lou Z, Rao Z. Structure of the RNA–dependent RNA polymerase from COVID–19 virus. Science. 2020 May 15;368(6492):779–782. doi: 10.1126/science.abb7498. Epub 2020 Apr 10. PMID: 32277040; PMCID: PMC7164392.

González S, Zürcher T, Ortín J. Identification of two separate domains in the influenza virus PB1 protein involved in the interaction with the PB2 and PA subunits: a model for the viral RNA polymerase structure. Nucleic Acids Res. 1996 Nov 15;24(22):4456–63. doi: 10.1093/nar/24.22.4456. PMID: 8948635; PMCID: PMC146260.

Gordon DE, Jang GM, Bouhaddou M, Xu J, Obernier K, White KM, O'Meara MJ, Rezelj VV, Guo JZ, Swaney DL, Tummino TA, Hüttenhain R, Kaake RM, Richards AL, Tutuncuoglu B, Foussard H, Batra J, Haas K, Modak M, Kim M, Haas P, Polacco BJ, Braberg H, Fabius JM, Eckhardt M, Soucheray M, Bennett MJ, Cakir M, McGregor MJ, Li Q, Meyer B, Roesch F, Vallet T, Mac Kain A,

Miorin L, Moreno E, Naing ZZC, Zhou Y, Peng S, Shi Y, Zhang Z, Shen W, Kirby IT, Melnyk JE, Chorba JS, Lou K, Dai SA, Barrio–Hernandez I, Memon D, Hernandez–Armenta C, Lyu J, Mathy CJP, Perica T, Pilla KB, Ganesan SJ, Saltzberg DJ, Rakesh R, Liu X, Rosenthal SB, Calviello L, Venkataramanan S, Liboy–Lugo J, Lin Y, Huang XP, Liu Y, Wankowicz SA, Bohn M, Safari M, Ugur FS, Koh C, Savar NS, Tran QD, Shengjuler D, Fletcher SJ, O'Neal MC, Cai Y, Chang JCJ, Broadhurst DJ, Klippsten S, Sharp PP, Wenzell NA, Kuzuoglu–Ozturk D, Wang HY, Trenker R, Young JM, Cavero DA, Hiatt J, Roth TL, Rathore U, Subramanian A, Noack J, Hubert M, Stroud RM, Frankel AD, Rosenberg OS, Verba KA, Agard DA, Ott M, Emerman M, Jura N, von Zastrow M, Verdin E, Ashworth A, Schwartz O, d'Enfert C, Mukherjee S, Jacobson M, Malik HS, Fujimori DG, Ideker T, Craik CS, Floor SN, Fraser JS, Gross JD, Sali A, Roth BL, Ruggero D, Taunton J, Kortemme T, Beltrao P, Vignuzzi M, García–Sastre A, Shokat KM, Shoichet BK, Krogan NJ. A SARS–CoV–2 protein interaction map reveals targets for drug repurposing. Nature. 2020 Jul;583(7816):459–468. doi: 10.1038/s41586–020–2286–9. Epub 2020 Apr 30. PMID: 32353859; PMCID: PMC7431030.

Grein J, Ohmagari N, Shin D, Diaz G, Asperges E, Castagna A, Feldt T, Green G, Green ML, Lescure FX, Nicastri E, Oda R, Yo K, Quiros–Roldan E, Studemeister A, Redinski J, Ahmed S, Bernett J, Chelliah D, Chen D, Chihara S, Cohen SH, Cunningham J, D'Arminio Monforte A, Ismail S, Kato H, Lapadula G, L'Her E, Maeno T, Majumder S, Massari M, Mora–Rillo M, Mutoh Y, Nguyen D, Verweij E, Zoufaly A, Osinusi AO, DeZure A, Zhao Y, Zhong L, Chokkalingam A, Elboudwarej E, Telep L, Timbs L, Henne I, Sellers S, Cao H, Tan SK, Winterbourne L, Desai P, Mera R, Gaggar A, Myers RP, Brainard DM, Childs R, Flanigan T. Compassionate Use of Remdesivir for Patients with Severe Covid–19. N Engl J Med. 2020 Jun 11;382(24):2327–2336. doi: 10.1056/NEJMoa2007016. Epub 2020 Apr 10. PMID: 32275812; PMCID: PMC7169476

Gul S, Ozcan O, Asar S, Okyar A, Barıs I, Kavakli IH. In silico identification of widely used and well–tolerated drugs as potential SARS–CoV–2 3C–like protease and viral RNA–dependent RNA polymerase inhibitors for direct use in clinical trials. J Biomol Struct Dyn. 2021 Oct;39(17):6772–6791. doi: 10.1080/07391102.2020.1802346. Epub 2020 Aug 5. PMID: 32752938; PMCID: PMC7484590.

Güler G, Özdemir H, Omar D, Akdoğan G. Coronavirus disease 2019 (COVID–19): Biophysical and biochemical aspects of SARS–CoV–2 and general characteristics. Prog Biophys Mol Biol. 2021 Sep;164:3–18. doi: 10.1016/j.pbiomolbio.2021.05.007. Epub 2021 May 24. PMID: 34033836; PMCID: PMC8142027.

Guo XJ, Thomas PG. New fronts emerge in the influenza cytokine storm. Semin Immunopathol. 2017 Jul;39(5):541–550. doi: 10.1007/s00281–017–0636–y. Epub 2017 May 29. PMID: 28555383; PMCID: PMC5580809.

Hackstadt T, Chiramel AI, Hoyt FH, Williamson BN, Dooley CA, Beare PA, de Wit E, Best SM, Fischer ER. Disruption of the Golgi Apparatus and Contribution of the Endoplasmic Reticulum to the SARS–CoV–2 Replication Complex. Viruses. 2021 Sep 9;13(9):1798. doi: 10.3390/v13091798. PMID: 34578379; PMCID: PMC8473243.

Hagemeijer MC, Rottier PJ, de Haan CA. Biogenesis and dynamics of the coronavirus replicative structures. Viruses. 2012 Nov 21;4(11):3245–69. doi: 10.3390/v4113245. PMID: 23202524; PMCID: PMC3509692.

Hamming I, Timens W, Bulthuis ML, Lely AT, Navis G, van Goor H. Tissue distribution of ACE2 protein, the functional receptor for SARS coronavirus. A first step in understanding SARS pathogenesis. J Pathol. 2004 Jun;203(2):631–7. doi: 10.1002/path.1570. PMID: 15141377; PMCID: PMC7167720.

Hamming PHE, Overeem NJ, Huskens J. Influenza as a molecular walker. ChemSci. 2019 Nov 14;11(1):27–36. doi: 10.1039/c9sc05149j. Erratum in: ChemSci. 2020 Feb 18;11(9):2567. PMID: 32153750; PMCID: PMC7021193.

Han L, Zhuang MW, Deng J, Zheng Y, Zhang J, Nan ML, Zhang XJ, Gao C, Wang PH. SARS–CoV–2 ORF9b antagonizes type I and III interferons by targeting multiple components of the RIG–I/MDA–5–MAVS, TLR3–TRIF, and cGAS–STING signalling pathways. J Med Virol. 2021 Sep;93(9):5376–5389. doi: 10.1002/jmv.27050. Epub 2021 May 9. PMID: 33913550; PMCID: PMC8242602.

Hause BM, Collin EA, Liu R, Huang B, Sheng Z, Lu W, Wang D, Nelson EA, Li F. Characterization of a novel influenza virus in cattle and Swine: proposal for a new genus in the Orthomyxoviridae family. mBio. 2014 Mar 4;5(2):e00031–14. doi: 10.1128/mBio.00031–14. PMID: 24595369; PMCID: PMC3958797.

Heilmann E, Costacurta F, Geley S, Mogadashi SA, Volland A, Rupp B, Harris RS, von Laer D. A VSV–based assay quantifies coronavirus Mpro/3CLpro/Nsp5 main protease activity and chemical inhibition. Commun Biol. 2022 Apr 27;5(1):391. doi: 10.1038/s42003–022–03277–0. PMID: 35478219; PMCID: PMC9046202.

Hirata N, Suizu F, Matsuda–Lennikov M, Edamura T, Bala J, Noguchi M. Inhibition of Akt kinase activity suppresses entry and replication of influenza virus. BiochemBiophys Res Commun. 2014 Jul 18;450(1):891–8. doi: 10.1016/j.bbrc.2014.06.077. Epub 2014 Jun 24. PMID: 24971535.

Högner K, Wolff T, Pleschka S, Plog S, Gruber AD, Kalinke U, Walmrath HD, Bodner J, Gattenlöhner S, Lewe–Schlosser P, Matrosovich M, Seeger W, Lohmeyer J, Herold S. Macrophage–expressed IFN–β contributes to apoptotic alveolar epithelial cell injury in severe influenza virus pneumonia. PLoSPathog. 2013 Feb;9(2):e1003188. doi: 10.1371/journal.ppat.1003188. Epub 2013 Feb 28. Erratum in: PLoSPathog. 2016 Jun;12(6):e1005716. PMID: 23468627; PMCID: PMC3585175.

Hsu AC. Influenza Virus: A Master Tactician in Innate Immune Evasion and Novel Therapeutic Interventions. Front Immunol. 2018 Apr 12;9:743. doi: 10.3389/fimmu.2018.00743. PMID: 29755452; PMCID: PMC5932403.

Hu B, Guo H, Zhou P, Shi ZL. Characteristics of SARS–CoV–2 and COVID–19. Nat Rev Microbiol. 2021 Mar;19(3):141–154. doi: 10.1038/s41579–020–00459–7. Epub 2020 Oct 6. Erratum in: Nat Rev Microbiol. 2022 May;20(5):315. PMID: 33024307; PMCID: PMC7537588.

Hu Y, Sneyd H, Dekant R, Wang J. Influenza A Virus Nucleoprotein: A Highly Conserved Multi–Functional Viral Protein as a Hot Antiviral Drug Target. Curr Top Med Chem. 2017;17(20):2271–2285. doi: 10.2174/1568026617666170224122508. PMID: 28240183; PMCID: PMC5967877.

Huber TJ, Dietrich DE, Emrich HM. Possible use of amantadine in depression. Pharmacopsychiatry. 1999 Mar;32(2):47–55. doi: 10.1055/s–2007–979191. PMID: 10333162.

Huff RM, Chio CL, Lajiness ME, Goodman LV. Signal transduction pathways modulated by D2–like dopamine receptors. Adv.Pharmacol. 1998;42:454–457.

Hurt AC, Hardie K, Wilson NJ, Deng YM, Osbourn M, Gehrig N, Kelso A. Community transmission of oseltamivir–resistant A(H1N1)pdm09 influenza. N Engl J Med. 2011 Dec 29;365(26):2541–2. doi: 10.1056/NEJMc1111078. PMID: 22204735.

Iacopetta D, Ceramella J, Catalano A, Saturnino C, Pellegrino M, Mariconda A, Longo P, Sinicropi MS, Aquaro S. COVID–19 at a Glance: An Up–to–Date Overview on Variants, Drug Design and Therapies. Viruses. 2022 Mar 10;14(3):573. doi: 10.3390/v14030573. PMID: 35336980; PMCID: PMC8950852.

Ilyushina NA, Ikizler MR, Kawaoka Y, Rudenko LG, Treanor JJ, Subbarao K, Wright PF. Comparative study of influenza virus replication in MDCK cells and in primary cells derived from adenoids and airway epithelium. J Virol. 2012 Nov;86(21):11725–34. doi: 10.1128/JVI.01477–12. Epub 2012 Aug 22. PMID: 22915797; PMCID: PMC3486302.

Invega, INN–paliperidone EMEA 2007 (https://www.ema.europa.eu/en/documents/scientific–discussion/invega–epar–scientific–discussion_en.pdf.)

Ito T, Suzuki Y, Mitnaul L, Vines A, Kida H, Kawaoka Y. Receptor specificity of influenza A viruses correlates with the agglutination of erythrocytes from different animal species. Virology. 1997 Jan 20;227(2):493–9. doi: 10.1006/viro.1996.8323. PMID: 9018149.

Ito T, Suzuki Y, Suzuki T, Takada A, Horimoto T, Wells K, Kida H, Otsuki K, Kiso M, Ishida H, Kawaoka Y. Recognition of N–glycolylneuraminic acid linked to galactose by the alpha2,3 linkage is associated with intestinal replication of influenza A virus in ducks. J Virol. 2000 Oct;74(19):9300–5. doi: 10.1128/jvi.74.19.9300–9305.2000. PMID: 10982377; PMCID: PMC102129.

Iwasaki A, Pillai PS. Innate immunity to influenza virus infection. Nat Rev Immunol. 2014 May;14(5):315–28. doi: 10.1038/nri3665. PMID: 24762827; PMCID: PMC4104278.

Janeway CA Jr. Approaching the asymptote? Evolution and revolution in immunology. Cold Spring HarbSymp Quant Biol. 1989;54 Pt 1:1–13. doi: 10.1101/sqb.1989.054.01.003. PMID: 2700931.

Jewell NA, Vaghefi N, Mertz SE, Akter P, Peebles RS Jr, Bakaletz LO, Durbin RK, Flaño E, Durbin JE. Differential type I interferon induction by respiratory syncytial virus and influenza a virus in vivo. J Virol. 2007 Sep;81(18):9790–800. doi: 10.1128/JVI.00530–07. Epub 2007 Jul 11. PMID: 17626092; PMCID: PMC2045394.

Jiang F, Ramanathan A, Miller MT, Tang GQ, Gale M Jr, Patel SS, Marcotrigiano J. Structural basis of RNA recognition and activation by innate immune receptor RIG–I. Nature. 2011 Sep 25;479(7373):423–7. doi: 10.1038/nature10537. PMID: 21947008; PMCID: PMC3430514.

Jureka AS, Kleinpeter AB, Tipper JL, Harrod KS, Petit CM. The influenza NS1 protein modulates RIG–I activation via a strain–specific direct interaction with the second CARD of RIG–I. J Biol Chem. 2020 Jan 24;295(4):1153–1164. doi: 10.1074/jbc.RA119.011410. Epub 2019 Dec 16. PMID: 31843969; PMCID: PMC6983837.

Kageyama M, Takahasi K, Narita R, Hirai R, Yoneyama M, Kato H, Fujita T. 55 Amino acid linker between helicase and carboxyl terminal domains of RIG–I functions as a critical repression domain and determines inter–domain conformation. Biochem Biophys Res Commun. 2011 Nov 11;415(1):75–81. doi: 10.1016/j.bbrc.2011.10.015. Epub 2011 Oct 12. PMID: 22020100.

Kallfass C, Lienenklaus S, Weiss S, Staeheli P. Visualizing the beta interferon response in mice during infection with influenza A viruses expressing or lacking nonstructural protein 1. J Virol. 2013 Jun;87(12):6925–30. doi: 10.1128/JVI.00283–13. Epub 2013 Apr 10. PMID: 23576514; PMCID: PMC3676098.

Kandasamy M, Suryawanshi A, Tundup S, Perez JT, Schmolke M, Manicassamy S, Manicassamy B. RIG–I Signalling Is Critical for Efficient Polyfunctional T Cell Responses during Influenza Virus Infection. PLoS Pathog. 2016 Jul 20;12(7):e1005754. doi: 10.1371/journal.ppat.1005754. PMID: 27438481; PMCID: PMC4954706.

Kane J, Canas F, Kramer M, Ford L, Gassmann–Mayer C, Lim P, Eerdekens M. Treatment of schizophrenia with paliperidone extended–release tablets: a 6–week placebo–controlled trial. Schizophr Res. 2007 Feb;90(1–3):147–61. doi: 10.1016/j.schres.2006.09.012. Epub 2006 Nov 7. PMID: 17092691.

Kapuscinski J. DAPI: a DNA–specific fluorescent probe. Biotech Histochem. 1995 Sep;70(5):220–33. doi: 10.3109/10520299509108199. PMID: 8580206.

Karlsson P, Dencker E, Nyberg S, Mannaert E, Boom S, Talluri K, Rossenu S, Eriksson B, Eerdekens M, and Farde L Pharmacokinetics and dopamine D2 and serotonin 5–HT2A receptor occupancy of paliperidone in healthy subjects EurNeuropsychopharmacol 2005

Kato H, Takeuchi O, Mikamo–Satoh E, Hirai R, Kawai T, Matsushita K, Hiiragi A, Dermody TS, Fujita T, Akira S. Length–dependent recognition of double–stranded ribonucleic acids by retinoic acid–inducible gene–I and melanoma differentiation–associated gene 5. J Exp Med. 2008 Jul 7;205(7):1601–10. doi: 10.1084/jem.20080091. PMID: 18591409; PMCID: PMC2442638.

Kato H, Takeuchi O, Sato S, Yoneyama M, Yamamoto M, Matsui K, Uematsu S, Jung A, Kawai T, Ishii KJ, Yamaguchi O, Otsu K, Tsujimura T, Koh CS, Reis e Sousa C, Matsuura Y, Fujita T, Akira S. Differential roles of MDA5 and RIG–I helicases in the recognition of RNA viruses. Nature. 2006 May 4;441(7089):101–5. doi: 10.1038/nature04734. Epub 2006 Apr 9. PMID: 16625202.

Kell AM, Gale M Jr. RIG–I in RNA virus recognition. Virology. 2015 May;479–480:110–21. doi: 10.1016/j.virol.2015.02.017. Epub 2015 Mar 5. PMID: 25749629; PMCID: PMC4424084.

Kocayiğit H, ÖzmenSüner K, Tomak Y, Demir G, Yaylacı S, Dheir H, Güçlü E, Erdem AF. Observational study of the effects of Favipiravir vs Lopinavir/Ritonavir on clinical outcomes in critically Ill patients with COVID–19. J Clin Pharm Ther. 2021 Apr;46(2):454–459. doi: 10.1111/jcpt.13305. Epub 2020 Oct 31. PMID: 33128482.

Komuro A, Horvath CM. RNA– and virus–independent inhibition of antiviral signalling by RNA helicase LGP2. J Virol. 2006 Dec;80(24):12332–42. doi: 10.1128/JVI.01325–06. Epub 2006 Oct 4. PMID: 17020950; PMCID: PMC1676302.

Konno Y, Kimura I, Uriu K, Fukushi M, Irie T, Koyanagi Y, Sauter D, Gifford RJ; USFQ–COVID19 Consortium, Nakagawa S, Sato K. SARS–CoV–2 ORF3b Is a Potent Interferon Antagonist Whose Activity Is Increased by a Naturally Occurring Elongation Variant. Cell Rep. 2020 Sep 22;32(12):108185. doi: 10.1016/j.celrep.2020.108185. Epub 2020 Sep 4. PMID: 32941788; PMCID: PMC7473339.

Kouwaki T, Nishimura T, Wang G, Oshiumi H. RIG–I–Like Receptor–Mediated Recognition of Viral Genomic RNA of Severe Acute Respiratory Syndrome Coronavirus–2 and Viral Escape From the Host Innate Immune Responses. Front Immunol. 2021 Jun 25;12:700926. doi: 10.3389/fimmu.2021.700926. PMID: 34249006; PMCID: PMC8267574.

Kowalinski E, Lunardi T, McCarthy AA, Louber J, Brunel J, Grigorov B, Gerlier D, Cusack S. Structural basis for the activation of innate immune pattern–recognition receptor RIG–I by viral RNA. Cell. 2011 Oct 14;147(2):423–35. doi: 10.1016/j.cell.2011.09.039. PMID: 22000019.

Kramer M, Simpson G, Maciulis V, Kushner S, Vijapurkar U, Lim P, Eerdekens M. Paliperidone extended–release tablets for prevention of symptom recurrence in patients with schizophrenia: a randomized, double–blind, placebo–controlled study. J ClinPsychopharmacol. 2007 Feb;27(1):6–14. doi: 10.1097/JCP.0b013e31802dda4a. Erratum in: J ClinPsychopharmacol. 2007 Jun;27(3):258. PMID: 17224706.

Krammer F, Smith GJD, Fouchier RAM, Peiris M, Kedzierska K, Doherty PC, Palese P, Shaw ML, Treanor J, Webster RG, García–Sastre A. Influenza. Nat Rev Dis Primers. 2018 Jun 28;4(1):3. doi: 10.1038/s41572–018–0002–y. PMID: 29955068; PMCID: PMC7097467.

Krischuns T, Günl F, Henschel L, Binder M, Willemsen J, Schloer S, Rescher U, Gerlt V, Zimmer G, Nordhoff C, Ludwig S, Brunotte L. Phosphorylation of TRIM28 Enhances the Expression of

IFN–β and Proinflammatory Cytokines During HPAIV Infection of Human Lung Epithelial Cells. Front Immunol. 2018 Sep 28;9:2229. doi: 10.3389/fimmu.2018.02229. PMID: 30323812; PMCID: PMC6172303.

Kukol A, Hughes DJ. Large–scale analysis of influenza A virus nucleoprotein sequence conservation reveals potential drug–target sites. Virology. 2014 Apr;454–455:40–7. doi: 10.1016/j.virol.2014.01.023. Epub 2014 Feb 22. PMID: 24725930.

Kumar H, Kawai T, Kato H, Sato S, Takahashi K, Coban C, Yamamoto M, Uematsu S, Ishii KJ, Takeuchi O, Akira S. Essential role of IPS–1 in innate immune responses against RNA viruses. J Exp Med. 2006 Jul 10;203(7):1795–803. doi: 10.1084/jem.20060792. Epub 2006 Jun 19. PMID: 16785313; PMCID: PMC2118350.

Kuzuhara T, Kise D, Yoshida H, Horita T, Murazaki Y, Nishimura A, Echigo N, Utsunomiya H, Tsuge H. Structural basis of the influenza A virus RNA polymerase PB2 RNA–binding domain containing the pathogenicity–determinant lysine 627 residue. J Biol Chem. 2009 Mar 13;284(11):6855–60. doi: 10.1074/jbc.C800224200. Epub 2009 Jan 14. PMID: 19144639; PMCID: PMC2652293.

Labadie K, Dos Santos Afonso E, Rameix–Welti MA, van der Werf S, Naffakh N. Host–range determinants on the PB2 protein of influenza A viruses control the interaction between the viral polymerase and nucleoprotein in human cells. Virology. 2007 Jun 5;362(2):271–82. doi: 10.1016/j.virol.2006.12.027. Epub 2007 Jan 31. PMID: 17270230.

Lamb RA, Choppin PW. The gene structure and replication of influenza virus. Annu Rev Biochem. 1983;52:467–506. doi: 10.1146/annurev.bi.52.070183.002343. PMID: 6351727.

Lamb, RA, Krug RM. Orthomyxoviridae: The viruses and their replication. 1996 In D. M. Knipe, P. M. Howley, & B. N. Fields (Eds.), Fields Virology Lippincott–Raven Press.

Lässig C, Hopfner KP. Discrimination of cytosolic self and non–self RNA by RIG–I–like receptors. J Biol Chem. 2017 Jun 2;292(22):9000–9009. doi: 10.1074/jbc.R117.788398. Epub 2017 Apr 14. PMID: 28411239; PMCID: PMC5454087.

Lässig C, Matheisl S, Sparrer KM, de Oliveira Mann CC, Moldt M, Patel JR, Goldeck M, Hartmann G, García–Sastre A, Hornung V, Conzelmann KK, Beckmann R, Hopfner KP. ATP hydrolysis by the viral RNA sensor RIG–I prevents unintentional recognition of self–RNA. Elife. 2015 Nov 26;4:e10859. doi: 10.7554/eLife.10859. Erratum in: Elife. 2016;5. pii: e14954. doi: 10.7554/eLife.14954. PMID: 26609812; PMCID: PMC4733034.

Lazear HM, Schoggins JW, Diamond MS. Shared and Distinct Functions of Type I and Type III Interferons. Immunity. 2019 Apr 16;50(4):907–923. doi: 10.1016/j.immuni.2019.03.025. PMID: 30995506; PMCID: PMC6839410.

Le Ru A, Jacob D, Transfiguracion J, Ansorge S, Henry O, Kamen AA. Scalable production of influenza virus in HEK–293 cells for efficient vaccine manufacturing. Vaccine. 2010 May 7;28(21):3661–71. doi: 10.1016/j.vaccine.2010.03.029. Epub 2010 Mar 26. PMID: 20347632.

Lei J, Kusov Y, Hilgenfeld R. Nsp3 of coronaviruses: Structures and functions of a large multi–domain protein. Antiviral Res. 2018 Jan;149:58–74. doi: 10.1016/j.antiviral.2017.11.001. Epub 2017 Nov 8. PMID: 29128390; PMCID: PMC7113668.

Lei X, Dong X, Ma R, Wang W, Xiao X, Tian Z, Wang C, Wang Y, Li L, Ren L, Guo F, Zhao Z, Zhou Z, Xiang Z, Wang J. Activation and evasion of type I interferon responses by SARS–CoV–2. Nat Commun. 2020 Jul 30;11(1):3810. doi: 10.1038/s41467–020–17665–9. PMID: 32733001; PMCID: PMC7392898.

Leung DW, Amarasinghe GK. Structural insights into RNA recognition and activation of RIG–I–like receptors. CurrOpin Struct Biol. 2012 Jun;22(3):297–303. doi: 10.1016/j.sbi.2012.03.011. Epub 2012 May 2. PMID: 22560447; PMCID: PMC3383332.

Li D, Ni S, Miao KS, Zhuang C. PI3K/Akt and caspase pathways mediate oxidative stress–induced chondrocyte apoptosis. Cell Stress Chaperones. 2019 Jan;24(1):195–202. doi: 10.1007/s12192–018–0956–4. Epub 2018 Dec 13. PMID: 30543056; PMCID: PMC6363634.

Li JY, Liao CH, Wang Q, Tan YJ, Luo R, Qiu Y, Ge XY. The ORF6, ORF8 and nucleocapsid proteins of SARS–CoV–2 inhibit type I interferon signalling pathway. Virus Res. 2020 Sep;286:198074. doi: 10.1016/j.virusres.2020.198074. Epub 2020 Jun 23. PMID: 32589897; PMCID: PMC7309931.

Lin S, Chen H, Ye F, Chen Z, Yang F, Zheng Y, Cao Y, Qiao J, Yang S, Lu G. Crystal structure of SARS–CoV–2 nsp10/nsp16 2'–O–methylase and its implication on antiviral drug design. Signal Transduct Target Ther. 2020 Jul 29;5(1):131. doi: 10.1038/s41392–020–00241–4. PMID: 32728018; PMCID: PMC7388121.

Liu Q, Zhou YH, Yang ZQ. The cytokine storm of severe influenza and development of immunomodulatory therapy. Cell Mol Immunol. 2016 Jan;13(1):3–10. doi: 10.1038/cmi.2015.74. Epub 2015 Jul 20. PMID: 26189369; PMCID: PMC4711683.

Livak KJ, Schmittgen TD. Analysis of relative gene expression data using real–time quantitative PCR and the 2(–Delta Delta C(T)) Method. Methods. 2001 Dec;25(4):402–8. doi: 10.1006/meth.2001.1262. PMID: 11846609.

Loo YM, Fornek J, Crochet N, Bajwa G, Perwitasari O, Martinez–Sobrido L, Akira S, Gill MA, García–Sastre A, Katze MG, Gale M Jr. Distinct RIG–I and MDA5 signalling by RNA viruses in innate immunity. J Virol. 2008 Jan;82(1):335–45. doi: 10.1128/JVI.01080–07. Epub 2007 Oct 17. PMID: 17942531; PMCID: PMC2224404.

Louber J, Brunel J, Uchikawa E, Cusack S, Gerlier D. Kinetic discrimination of self/non–self RNA by the ATPase activity of RIG–I and MDA5. BMC Biol. 2015 Jul 28;13:54. doi: 10.1186/s12915–015–0166–9. PMID: 26215161; PMCID: PMC4517655.

Lu R, Zhao X, Li J, Niu P, Yang B, Wu H, Wang W, Song H, Huang B, Zhu N, Bi Y, Ma X, Zhan F, Wang L, Hu T, Zhou H, Hu Z, Zhou W, Zhao L, Chen J, Meng Y, Wang J, Lin Y, Yuan J, Xie Z, Ma J, Liu WJ, Wang D, Xu W, Holmes EC, Gao GF, Wu G, Chen W, Shi W, Tan W. Genomic characterisation and epidemiology of 2019 novel coronavirus: implications for virus origins and receptor binding. Lancet. 2020 Feb 22;395(10224):565–574. doi: 10.1016/S0140–6736(20)30251–8. Epub 2020 Jan 30. PMID: 32007145; PMCID: PMC7159086.

Lutz A, Dyall J, Olivo PD, Pekosz A. Virus–inducible reporter genes as a tool for detecting and quantifying influenza A virus replication. J Virol Methods. 2005 Jun;126(1–2):13–20. doi: 10.1016/j.jviromet.2005.01.016. PMID: 15847914; PMCID: PMC1698269.

Ma C, Li Y, Zong Y, Velkov T, Wang C, Yang X, Zhang M, Jiang Z, Sun H, Tong Q, Sun H, Pu J, Iqbal M, Liu J, Dai C, Sun Y. p21 restricts influenza A virus by perturbing the viral polymerase complex and upregulating type I interferon signalling. PLoSPathog. 2022 Feb 18;18(2):e1010295. doi: 10.1371/journal.ppat.1010295. PMID: 35180274.

Ma C, Li Y, Zong Y, Velkov T, Wang C, Yang X, Zhang M, Jiang Z, Sun H, Tong Q, Sun H, Pu J, Iqbal M, Liu J, Dai C, Sun Y. p21 restricts influenza A virus by perturbing the viral polymerase complex and upregulating type I interferon signalling. PLoSPathog. 2022 Feb 18;18(2):e1010295. doi: 10.1371/journal.ppat.1010295. PMID: 35180274; PMCID: PMC8920271.

Manicassamy B, Manicassamy S, Belicha–Villanueva A, Pisanelli G, Pulendran B, García–Sastre A. Analysis of in vivo dynamics of influenza virus infection in mice using a GFP reporter virus. Proc Natl Acad Sci U S A. 2010 Jun 22;107(25):11531–6. doi: 10.1073/pnas.0914994107. Epub 2010 Jun 7. PMID: 20534532; PMCID: PMC2895123.

Mannens G, Huang ML, Meuldermans W, Hendrickx J, Woestenborghs R, Heykants J. Absorption, metabolism, and excretion of risperidone in humans. Drug MetabDispos. 1993 Nov–Dec;21(6):1134–41. PMID: 7507814.

Mariano G, Farthing RJ, Lale–Farjat SLM, Bergeron JRC. Structural Characterization of SARS–CoV–2: Where We Are, and Where We Need to Be. Front Mol Biosci. 2020 Dec 17;7:605236. doi: 10.3389/fmolb.2020.605236. PMID: 33392262; PMCID: PMC7773825.

Marié I, Durbin JE, Levy DE. Differential viral induction of distinct interferon–alpha genes by positive feedback through interferon regulatory factor–7. EMBO J. 1998 Nov 16;17(22):6660–9. doi: 10.1093/emboj/17.22.6660. PMID: 9822609; PMCID: PMC1171011.

Marques JT, Devosse T, Wang D, Zamanian–Daryoush M, Serbinowski P, Hartmann R, Fujita T, Behlke MA, Williams BR. A structural basis for discriminating between self and nonself double–

stranded RNAs in mammalian cells. Nat Biotechnol. 2006 May;24(5):559–65. doi: 10.1038/nbt1205. Epub 2006 Apr 30. PMID: 16648842.

Martín–Folgar R, Lorenzo G, Boshra H, Iglesias J, Mateos F, Borrego B, Brun A. Development and characterization of monoclonal antibodies against Rift Valley fever virus nucleocapsid protein generated by DNA immunization. MAbs. 2010 May–Jun;2(3):275–84. doi: 10.4161/mabs.2.3.11676. Epub 2010 May 2. PMID: 20400862; PMCID: PMC2881254.

Martin K, Helenius A. Transport of incoming influenza virus nucleocapsids into the nucleus. J Virol. 1991 Jan;65(1):232–44. doi: 10.1128/JVI.65.1.232–244.1991. PMID: 1985199; PMCID: PMC240510.

Matrosovich M, Matrosovich T, Garten W, Klenk HD. New low–viscosity overlay medium for viral plaque assays. Virol J. 2006 Aug 31;3:63. doi: 10.1186/1743–422X–3–63. PMID: 16945126; PMCID: PMC1564390.

Medzhitov R. Toll–like receptors and innate immunity. Nat Rev Immunol. 2001 Nov;1(2):135–45. doi: 10.1038/35100529. PMID: 11905821.

Megens AAHP, Awouters FHL. In vivo pharmacologic profile of 9– hydroxyrisperidone the major metabolite of the novel antipsychotic risperidone. Drug Dev Res 1994 33:399–412.

Michalska A, Blaszczyk K, Wesoly J, Bluyssen HAR. A Positive Feedback Amplifier Circuit That Regulates Interferon (IFN)–Stimulated Gene Expression and Controls Type I and Type II IFN Responses. Front Immunol. 2018 May 28;9:1135. doi: 10.3389/fimmu.2018.01135. PMID: 29892288; PMCID: PMC5985295.

Milián E, Julien T, Biaggio R, Venereo–Sanchez A, Montes J, Manceur AP, Ansorge S, Petiot E, Rosa–Calatrava M, Kamen A. Accelerated mass production of influenza virus seed stocks in HEK–293 suspension cell cultures by reverse genetics. Vaccine. 2017 Jun 8;35(26):3423–3430. doi: 10.1016/j.vaccine.2017.04.065. Epub 2017 May 8. PMID: 28495315.

Moeller A, Kirchdoerfer RN, Potter CS, Carragher B, Wilson IA. Organization of the influenza virus replication machinery. Science. 2012 Dec 21;338(6114):1631–4. doi: 10.1126/science.1227270. Epub 2012 Nov 22. PMID: 23180774; PMCID: PMC3578580.

Mody V, Ho J, Wills S, Mawri A, Lawson L, Ebert MCCJC, Fortin GM, Rayalam S, Taval S. Identification of 3–chymotrypsin like protease (3CLPro) inhibitors as potential anti–SARS–CoV–2 agents. Commun Biol. 2021 Jan 20;4(1):93. doi: 10.1038/s42003–020–01577–x. PMID: 33473151; PMCID: PMC7817688.

Moscona A. Neuraminidase inhibitors for influenza. N Engl J Med. 2005 Sep 29;353(13):1363–73. doi: 10.1056/NEJMra050740. PMID: 16192481.

Mousavizadeh L, Ghasemi S. Genotype and phenotype of COVID–19: Their roles in pathogenesis. J Microbiol Immunol Infect. 2021 Apr;54(2):159–163. doi: 10.1016/j.jmii.2020.03.022. Epub 2020 Mar 31. PMID: 32265180; PMCID: PMC7138183.

Müller C, Obermann W, Schulte FW, Lange–Grünweller K, Oestereich L, Elgner F, Glitscher M, Hildt E, Singh K, Wendel HG, Hartmann RK, Ziebuhr J, Grünweller A. Comparison of broad–spectrum antiviral activities of the synthetic rocaglate CR–31–B (–) and the eIF4A–inhibitor Silvestrol. Antiviral Res. 2020 Mar;175:104706. doi: 10.1016/j.antiviral.2020.104706. Epub 2020 Jan 10. PMID: 31931103; PMCID: PMC7114339.

Muller R, Saluzzo JF, Lopez N, Dreier T, Turell M, Smith J, Bouloy M. Characterization of clone 13, a naturally attenuated avirulent isolate of Rift Valley fever virus, which is altered in the small segment. Am J Trop Med Hyg. 1995 Oct;53(4):405–11. doi: 10.4269/ajtmh.1995.53.405. PMID: 7485695.

Murray JL, McDonald NJ, Sheng J, Shaw MW, Hodge TW, Rubin DH, O'Brien WA, Smee DF. Inhibition of influenza A virus replication by antagonism of a PI3K–AKT–mTOR pathway member identified by gene–trap insertional mutagenesis. Antivir Chem Chemother. 2012 May 14;22(5):205–15. doi: 10.3851/IMP2080. PMID: 22374988.

Murti KG, Webster RG, Jones IM. Localization of RNA polymerases on influenza viral ribonucleoproteins by immunogold labeling. Virology. 1988 Jun;164(2):562–6. doi: 10.1016/0042–6822(88)90574–0. PMID: 3369093.

Nemani K, Williams SZ, Olfson M, Leckman–Westin E, Finnerty M, Kammer J, Smith TE, Silverman DJ, Lindenmayer JP, Capichioni G, Clelland J, Goff DC. Association Between the Use of Psychotropic Medications and the Risk of COVID–19 Infection Among Long–term Inpatients With Serious Mental Illness in a New York State–wide Psychiatric Hospital System. JAMA Netw Open. 2022 May 2;5(5):e2210743. doi: 10.1001/jamanetworkopen.2022.10743. PMID: 35522282; PMCID: PMC9077485.

NielsenSS, AlvarezJ, BicoutDJ, CalistriP, DepnerK, DreweJA, Garin–BastujiB, RojasJLG, SchmidtCG, MichelV, ChuecaMÁM, RobertsHC, SihvonenLH, StahlK, CalvoAV, ViltropA, WincklerC, BettB, Cetre–SossahC, ChevalierV, DevosC, GubbinsS, MonacoF, Sotiria–EleniA, BrogliaA, AbrahantesJC, DhollanderS, StedeYV, ZancanaroG. RiftValleyFever – epidemiologicalupdateandriskofintroductionintoEurope. EFSAJ. 2020 Mar 6;18(3):e06041. doi: 10.2903/j.efsa.2020.6041. PMID: 33020705; PMCID: PMC7527653.

Nobusawa E, Sato K. Comparison of the mutation rates of human influenza A and B viruses. J Virol. 2006 Apr;80(7):3675–8. doi: 10.1128/JVI.80.7.3675–3678.2006. PMID: 16537638; PMCID: PMC1440390.

Onomoto K, Onoguchi K, Yoneyama M. Regulation of RIG–I–like receptor–mediated signalling: interaction between host and viral factors. Cell Mol Immunol. 2021 Mar;18(3):539–555. doi: 10.1038/s41423–020–00602–7. Epub 2021 Jan 18. PMID: 33462384; PMCID: PMC7812568.

Panne D. The enhanceosome. CurrOpin Struct Biol. 2008 Apr;18(2):236–42. doi: 10.1016/j.sbi.2007.12.002. Epub 2008 Feb 21. PMID: 18206362.

Parvin JD, Moscona A, Pan WT, Leider JM, Palese P. Measurement of the mutation rates of animal viruses: influenza A virus and poliovirus type 1. J Virol. 1986 Aug;59(2):377–83. doi: 10.1128/JVI.59.2.377–383.1986. PMID: 3016304; PMCID: PMC253087.

Patel H, Kukol A. Evolutionary conservation of influenza A PB2 sequences reveals potential target sites for small molecule inhibitors. Virology. 2017 Sep;509:112–120. doi: 10.1016/j.virol.2017.06.009. Epub 2017 Jun 17. PMID: 28628827.

Patterson KD, Pyle GF. The geography and mortality of the 1918 influenza pandemic. Bull Hist Med. 1991 Spring;65(1):4–21. PMID: 2021692.

Paules CI, Marston HD, Fauci AS. Coronavirus Infections–More Than Just the Common Cold. JAMA. 2020 Feb 25;323(8):707–708. doi: 10.1001/jama.2020.0757. PMID: 31971553.

Paz S, Sun Q, Nakhaei P, Romieu–Mourez R, Goubau D, Julkunen I, Lin R, Hiscott J. Induction of IRF–3 and IRF–7 phosphorylation following activation of the RIG–I pathway. Cell Mol Biol (Noisy–le–grand). 2006 May 15;52(1):17–28. PMID: 16914100.

Peng L, Zhang X, Cui X, Zhu D, Wu J, Sun D, Yue Q, Li Z, Liu H, Li G, Zhang J, Xu H, Liu F, Qin C, Li M, Sun J. Paliperidone protects SK–N–SH cells against glutamate toxicity via Akt1/GSK3βsignalling pathway. Schizophr Res. 2014 Aug;157(1–3):120–7. doi: 10.1016/j.schres.2014.05.037. Epub 2014 Jun 22. PMID: 24962437.

Peng L, Zhang X, Cui X, Zhu D, Wu J, Sun D, Yue Q, Li Z, Liu H, Li G, Zhang J, Xu H, Liu F, Qin C, Li M, Sun J. Paliperidone protects SK–N–SH cells against glutamate toxicity via Akt1/GSK3β signalling pathway. Schizophr Res. 2014 Aug;157(1–3):120–7. doi: 10.1016/j.schres.2014.05.037. Epub 2014 Jun 22. PMID: 24962437.

Peng L, Zhu D, Feng X, Dong H, Yue Q, Zhang J, Gao Q, Hao J, Zhang X, Liu Z, Sun J. Paliperidone protects prefrontal cortical neurons from damages caused by MK–801 via Akt1/GSK3βsignalling pathway. Schizophr Res. 2013 Jun;147(1):14–23. doi: 10.1016/j.schres.2013.03.006. Epub 2013 Apr 9. PMID: 23583326.

Pepin M, Bouloy M, Bird BH, Kemp A, Paweska J. Rift Valley fever virus(Bunyaviridae: Phlebovirus): an update on pathogenesis, molecular epidemiology, vectors, diagnostics and prevention. Vet Res. 2010 Nov–Dec;41(6):61. doi: 10.1051/vetres/2010033. PMID: 21188836; PMCID: PMC2896810.

Perrone LA, Plowden JK, García–Sastre A, Katz JM, Tumpey TM. H5N1 and 1918 pandemic influenza virus infection results in early and excessive infiltration of macrophages and neutrophils in the lungs of mice. PLoSPathog. 2008 Aug 1;4(8):e1000115. doi: 10.1371/journal.ppat.1000115. PMID: 18670648; PMCID: PMC2483250.

Peteranderl C, Herold S, Schmoldt C. Human Influenza Virus Infections. Semin Respir Crit Care Med. 2016 Aug;37(4):487–500. doi: 10.1055/s–0036–1584801. Epub 2016 Aug 3. PMID: 27486731; PMCID: PMC7174870.

Pflug A, Guilligay D, Reich S, Cusack S. Structure of influenza A polymerase bound to the viral RNA promoter. Nature. 2014 Dec 18;516(7531):355–60. doi: 10.1038/nature14008. Epub 2014 Nov 19. PMID: 25409142.

Pichlmair A, Schulz O, Tan CP, Näslund TI, Liljeström P, Weber F, Reis e Sousa C. RIG–I–mediated antiviral responses to single–stranded RNA bearing 5'–phosphates. Science. 2006 Nov 10;314(5801):997–1001. doi: 10.1126/science.1132998. Epub 2006 Oct 12. PMID: 17038589.

Pinto LH, Holsinger LJ, Lamb RA. Influenza virus M2 protein has ion channel activity. Cell. 1992 May 1;69(3):517–28. doi: 10.1016/0092–8674(92)90452–i. PMID: 1374685.

Pinto LH, Lamb RA. The M2 proton channels of influenza A and B viruses. J Biol Chem. 2006 Apr 7;281(14):8997–9000. doi: 10.1074/jbc.R500020200. Epub 2005 Dec 30. PMID: 16407184.

Poeck H, Bscheider M, Gross O, Finger K, Roth S, Rebsamen M, Hannesschläger N, Schlee M, Rothenfusser S, Barchet W, Kato H, Akira S, Inoue S, Endres S, Peschel C, Hartmann G, Hornung V, Ruland J. Recognition of RNA virus by RIG–I results in activation of CARD9 and inflammasome signalling for interleukin 1 beta production. Nat Immunol. 2010 Jan;11(1):63–9. doi: 10.1038/ni.1824. Epub 2009 Nov 15. Erratum in: Nat Immunol. 2014 Jan;15(1):109. PMID: 19915568.

Poole E, Elton D, Medcalf L, Digard P. Functional domains of the influenza A virus PB2 protein: identification of NP– and PB1–binding sites. Virology. 2004 Mar 30;321(1):120–33. doi: 10.1016/j.virol.2003.12.022. PMID: 15033571.

Portela A, Digard P. The influenza virus nucleoprotein: a multifunctional RNA–binding protein pivotal to virus replication. J Gen Virol. 2002 Apr;83(Pt 4):723–734. doi: 10.1099/0022–1317–83–4–723. PMID: 11907320.

Rajsbaum R, Albrecht RA, Wang MK, Maharaj NP, Versteeg GA, Nistal–Villán E, García–Sastre A, Gack MU. Species–specific inhibition of RIG–I ubiquitination and IFN induction by the influenza A virus NS1 protein. PLoSPathog. 2012;8(11):e1003059. doi: 10.1371/journal.ppat.1003059. Epub 2012 Nov 29. PMID: 23209422; PMCID: PMC3510253.

Rameix–Welti MA, Tomoiu A, Dos Santos Afonso E, van der Werf S, Naffakh N. Avian Influenza A virus polymerase association with nucleoprotein, but not polymerase assembly, is impaired

in human cells during the course of infection. J Virol. 2009 Feb;83(3):1320–31. doi: 10.1128/JVI.00977–08. Epub 2008 Nov 19. PMID: 19019950; PMCID: PMC2620912.

Ranjith–Kumar CT, Murali A, Dong W, Srisathiyanarayanan D, Vaughan R, Ortiz–Alacantara J, Bhardwaj K, Li X, Li P, Kao CC. Agonist and antagonist recognition by RIG–I, a cytoplasmic innate immunity receptor. J Biol Chem. 2009 Jan 9;284(2):1155–65. doi: 10.1074/jbc.M806219200. Epub 2008 Nov 19. PMID: 19019822; PMCID: PMC2613625.

Raote I, Bhattacharya A, Panicker MM. Serotonin 2A (5–HT2A) Receptor Function: Ligand–Dependent Mechanisms and Pathways. In: Chattopadhyay A, editor. Serotonin Receptors in Neurobiology. Boca Raton (FL): CRC Press/Taylor & Francis; 2007. Chapter 6. Available from: https://www.ncbi.nlm.nih.gov/books/NBK1853/

Rastogi M, Pandey N, Shukla A, Singh SK. SARS coronavirus 2: from genome to infectome. Respir Res. 2020 Dec 1;21(1):318. doi: 10.1186/s12931–020–01581–z. PMID: 33261606; PMCID: PMC7706175.

Rawling DC, Pyle AM. Parts, assembly and operation of the RIG–I family of motors. CurrOpin Struct Biol. 2014 Apr;25:25–33. doi: 10.1016/j.sbi.2013.11.011. Epub 2013 Dec 20. PMID: 24878341; PMCID: PMC4070197.

Rehwinkel J, Gack MU. RIG–I–like receptors: their regulation and roles in RNA sensing. Nat Rev Immunol. 2020 Sep;20(9):537–551. doi: 10.1038/s41577–020–0288–3. Epub 2020 Mar 13. PMID: 32203325; PMCID: PMC7094958.

Ren Y, Shu T, Wu D, Mu J, Wang C, Huang M, Han Y, Zhang XY, Zhou W, Qiu Y, Zhou X. The ORF3a protein of SARS–CoV–2 induces apoptosis in cells. Cell Mol Immunol. 2020 Aug;17(8):881–883. doi: 10.1038/s41423–020–0485–9. Epub 2020 Jun 18. PMID: 32555321; PMCID: PMC7301057.

Repetto G, del Peso A, Zurita JL. Neutral red uptake assay for the estimation of cell viability/cytotoxicity. Nat Protoc. 2008;3(7):1125–31. doi: 10.1038/nprot.2008.75. PMID: 18600217.

Resa–Infante P, Jorba N, Coloma R, Ortin J. The influenza virus RNA synthesis machine: advances in its structure and function. RNA Biol. 2011 Mar–Apr;8(2):207–15. doi: 10.4161/rna.8.2.14513. Epub 2011 Mar 1. PMID: 21358279; PMCID: PMC3127100.

Rössig L, Jadidi AS, Urbich C, Badorff C, Zeiher AM, Dimmeler S. Akt–dependent phosphorylation of p21(Cip1) regulates PCNA binding and proliferation of endothelial cells. Mol Cell Biol. 2001 Aug;21(16):5644–57. doi: 10.1128/MCB.21.16.5644–5657.2001. PMID: 11463845; PMCID: PMC87285.

Rothenfusser S, Goutagny N, DiPerna G, Gong M, Monks BG, Schoenemeyer A, Yamamoto M, Akira S, Fitzgerald KA. The RNA helicase Lgp2 inhibits TLR–independent sensing of viral

replication by retinoic acid–inducible gene–I. J Immunol. 2005 Oct 15;175(8):5260–8. doi: 10.4049/jimmunol.175.8.5260. PMID: 16210631.

Ryan–Poirier K, Suzuki Y, Bean WJ, Kobasa D, Takada A, Ito T, Kawaoka Y. Changes in H3 influenza A virus receptor specificity during replication in humans. Virus Res. 1998 Aug;56(2):169–76. doi: 10.1016/s0168–1702(98)00067–7. PMID: 9783465.

Samji T. Influenza A: understanding the viral life cycle. Yale J Biol Med. 2009 Dec;82(4):153–9. PMID: 20027280; PMCID: PMC2794490.

Sato M, Hata N, Asagiri M, Nakaya T, Taniguchi T, Tanaka N. Positive feedback regulation of type I IFN genes by the IFN–inducible transcription factor IRF–7. FEBS Lett. 1998 Dec 11;441(1):106–10. doi: 10.1016/s0014–5793(98)01514–2. PMID: 9877175.

Schaecher SR, Touchette E, Schriewer J, Buller RM, Pekosz A. Severe acute respiratory syndrome coronavirus gene 7 products contribute to virus–induced apoptosis. J Virol. 2007 Oct;81(20):11054–68. doi: 10.1128/JVI.01266–07. Epub 2007 Aug 8. PMID: 17686858; PMCID: PMC2045523.

Schilling M, Bridgeman A, Gray N, Hertzog J, Hublitz P, Kohl A, Rehwinkel J. RIG–I Plays a Dominant Role in the Induction of Transcriptional Changes in Zika Virus–Infected Cells, which Protect from Virus–Induced Cell Death. Cells. 2020 Jun 16;9(6):1476. doi: 10.3390/cells9061476. PMID: 32560274; PMCID: PMC7349056.

Schlee M, Roth A, Hornung V, Hagmann CA, Wimmenauer V, Barchet W, Coch C, Janke M, Mihailovic A, Wardle G, Juranek S, Kato H, Kawai T, Poeck H, Fitzgerald KA, Takeuchi O, Akira S, Tuschl T, Latz E, Ludwig J, Hartmann G. Recognition of 5' triphosphate by RIG–I helicase requires short blunt double–stranded RNA as contained in panhandle of negative–strand virus. Immunity. 2009 Jul 17;31(1):25–34. doi: 10.1016/j.immuni.2009.05.008. Epub 2009 Jul 2. PMID: 19576794; PMCID: PMC2824854.

Scherer KM, Mascheroni L, Carnell GW, Wunderlich LCS, Makarchuk S, Brockhoff M, Mela I, Fernandez–Villegas A, Barysevich M, Stewart H, Suau Sans M, George CL, Lamb JR, Kaminski–Schierle GS, Heeney JL, Kaminski CF. SARS–CoV–2 nucleocapsid protein adheres to replication organelles before viral assembly at the Golgi/ERGIC and lysosome–mediated egress. Sci Adv. 2022 Jan 7;8(1):eabl4895. doi: 10.1126/sciadv.abl4895. Epub 2022 Jan 7. PMID: 34995113.

Schmidt A, Schwerd T, Hamm W, Hellmuth JC, Cui S, Wenzel M, Hoffmann FS, Michallet MC, Besch R, Hopfner KP, Endres S, Rothenfusser S. 5'–triphosphate RNA requires base–paired structures to activate antiviral signalling via RIG–I. Proc Natl Acad Sci U S A. 2009 Jul 21;106(29):12067–72. doi: 10.1073/pnas.0900971106. Epub 2009 Jul 2. PMID: 19574455; PMCID: PMC2705279

Schotte A, Janssen PF, Gommeren W, Luyten WH, Van Gompel P, Lesage AS, De Loore K, Leysen JE. Risperidone compared with new and reference antipsychotic drugs: in vitro and in vivo receptor binding. Psychopharmacology (Berl). 1996 Mar;124(1–2):57–73. doi: 10.1007/BF02245606. PMID: 8935801.

Schubert K, Karousis ED, Jomaa A, Scaiola A, Echeverria B, Gurzeler LA, Leibundgut M, Thiel V, Mühlemann O, Ban N. SARS–CoV–2 Nsp1 binds the ribosomal mRNA channel to inhibit translation. Nat Struct Mol Biol. 2020 Oct;27(10):959–966. doi: 10.1038/s41594–020–0511–8. Epub 2020 Sep 9. Erratum in: Nat Struct Mol Biol. 2020 Nov;27(11):1094. PMID: 32908316.

Seitz C, Frensing T, Höper D, Kochs G, Reichl U. High yields of influenza A virus in Madin–Darby canine kidney cells are promoted by an insufficient interferon–induced antiviral state. J Gen Virol. 2010 Jul;91(Pt 7):1754–63. doi: 10.1099/vir.0.020370–0. Epub 2010 Mar 31. PMID: 20357039.

Shaw, M. L. &Palese, P. in Fields Virology 6th edn (edsKnipe, D. M. &Howley, P. M.) (Lippincott Williams & Wilkins, Philadelphia, 2013).

Shtutman M, Chang BD, Schools GP, Broude EV. Cellular Model of p21–Induced Senescence. Methods Mol Biol. 2017;1534:31–39. doi: 10.1007/978–1–4939–6670–7_3. PMID: 27812865; PMCID: PMC6764449.

Shtutman M, Chang BD, Schools GP, Broude EV. Cellular Model of p21–Induced Senescence. Methods Mol Biol. 2017;1534:31–39. doi: 10.1007/978–1–4939–6670–7_3. PMID: 27812865; PMCID: PMC6764449.

Siddiqi HK, Mehra MR. COVID–19 illness in native and immunosuppressed states: A clinical–therapeutic staging proposal. J Heart Lung Transplant. 2020 May;39(5):405–407. doi: 10.1016/j.healun.2020.03.012. Epub 2020 Mar 20. PMID: 32362390; PMCID: PMC7118652.

Sims AC, Baric RS, Yount B, Burkett SE, Collins PL, Pickles RJ. Severe acute respiratory syndrome coronavirus infection of human ciliated airway epithelia: role of ciliated cells in viral spread in the conducting airways of the lungs. J Virol. 2005 Dec;79(24):15511–24. doi: 10.1128/JVI.79.24.15511–15524.2005. PMID: 16306622; PMCID: PMC1316022.

Song P, Li W, Xie J, Hou Y, You C. Cytokine storm induced by SARS–CoV–2. Clin Chim Acta. 2020 Oct;509:280–287. doi: 10.1016/j.cca.2020.06.017. Epub 2020 Jun 10. PMID: 32531256; PMCID: PMC7283076.

Stevaert A, Naesens L. The Influenza Virus Polymerase Complex: An Update on Its Structure, Functions, and Significance for Antiviral Drug Design. Med Res Rev. 2016 Nov;36(6):1127–1173. doi: 10.1002/med.21401. Epub 2016 Aug 29. PMID: 27569399; PMCID: PMC5108440.

Subbarao EK, London W, Murphy BR. A single amino acid in the PB2 gene of influenza A virus is a determinant of host range. J Virol. 1993 Apr;67(4):1761–4. doi: 10.1128/JVI.67.4.1761–1764.1993. PMID: 8445709; PMCID: PMC240216.

Sungnak W, Huang N, Bécavin C, Berg M; HCA Lung Biological Network. SARS–CoV–2 Entry Genes Are Most Highly Expressed in Nasal Goblet and Ciliated Cells within Human Airways. ArXiv [Preprint]. 2020 Mar 13:arXiv:2003.06122v1. Update in: Nat Med. 2020 May;26(5):681–687. PMID: 32550242; PMCID: PMC7280877.

Świerczyńska M, Mirowska–Guzel DM, Pindelska E. Antiviral Drugs in Influenza. Int J Environ Res Public Health. 2022 Mar 4;19(5):3018. doi: 10.3390/ijerph19053018. PMID: 35270708; PMCID: PMC8910682.

Takahasi K, Yoneyama M, Nishihori T, Hirai R, Kumeta H, Narita R, Gale M Jr, Inagaki F, Fujita T. Nonself RNA–sensing mechanism of RIG–I helicase and activation of antiviral immune responses. Mol Cell. 2008 Feb 29;29(4):428–40. doi: 10.1016/j.molcel.2007.11.028. Epub 2008 Jan 31. PMID: 18242112.

Tan YJ. The Severe Acute Respiratory Syndrome (SARS)–coronavirus 3a protein may function as a modulator of the trafficking properties of the spike protein. Virol J. 2005 Feb 10;2:5. doi: 10.1186/1743–422X–2–5. PMID: 15703085; PMCID: PMC549520.

Tang T, Bidon M, Jaimes JA, Whittaker GR, Daniel S. Coronavirus membrane fusion mechanism offers a potential target for antiviral development. Antiviral Res. 2020 Jun;178:104792. doi: 10.1016/j.antiviral.2020.104792. Epub 2020 Apr 6. PMID: 32272173; PMCID: PMC7194977.

Taylor JK, Coleman CM, Postel S, Sisk JM, Bernbaum JG, Venkataraman T, Sundberg EJ, Frieman MB. Severe Acute Respiratory Syndrome Coronavirus ORF7a Inhibits Bone Marrow Stromal Antigen 2 Virion Tethering through a Novel Mechanism of Glycosylation Interference. J Virol. 2015 Dec;89(23):11820–33. doi: 10.1128/JVI.02274–15. Epub 2015 Sep 16. PMID: 26378163; PMCID: PMC4645327.

TeVelthuis AJ, Fodor E. Influenza virus RNA polymerase: insights into the mechanisms of viral RNA synthesis. Nat Rev Microbiol. 2016 Aug;14(8):479–93. doi: 10.1038/nrmicro.2016.87. Epub 2016 Jul 11. PMID: 27396566; PMCID: PMC4966622.

TeVelthuis AJW, Long JS, Barclay WS. Assays to Measure the Activity of Influenza Virus Polymerase. Methods Mol Biol. 2018;1836:343–374. doi: 10.1007/978–1–4939–8678–1_17. PMID: 30151582.

Thierry E, Guilligay D, Kosinski J, Bock T, Gaudon S, Round A, Pflug A, Hengrung N, El Omari K, Baudin F, Hart DJ, Beck M, Cusack S. Influenza Polymerase Can Adopt an Alternative Configuration Involving a Radical Repacking of PB2 Domains. Mol Cell. 2016 Jan 7;61(1):125–37. doi: 10.1016/j.molcel.2015.11.016. Epub 2015 Dec 17. PMID: 26711008; PMCID: PMC4712189.

Thorne LG, Reuschl AK, Zuliani–Alvarez L, Whelan MVX, Turner J, Noursadeghi M, Jolly C, Towers GJ. SARS–CoV–2 sensing by RIG–I and MDA5 links epithelial infection to macrophage inflammation. EMBO J. 2021 Aug 2;40(15):e107826. doi: 10.15252/embj.2021107826. Epub 2021 Jul 2. PMID: 34101213; PMCID: PMC8209947.

Tokimatsu I, Nasu M. [Anti–influenza A viral drug—amantadine]. Nihon Rinsho. 2000 Nov;58(11):2288–92. Japanese. PMID: 11225319.

Totura AL, Baric RS. SARS coronavirus pathogenesis: host innate immune responses and viral antagonism of interferon. CurrOpinVirol. 2012;2(3):264–275. doi:10.1016/j.coviro.2012.04.004

V'kovski P, Kratzel A, Steiner S, Stalder H, Thiel V. Coronavirus biology and replication: implications for SARS–CoV–2. Nat Rev Microbiol. 2021 Mar;19(3):155–170. doi: 10.1038/s41579–020–00468–6. Epub 2020 Oct 28. PMID: 33116300; PMCID: PMC7592455.

Wang Y, Ludwig J, Schuberth C, Goldeck M, Schlee M, Li H, Juranek S, Sheng G, Micura R, Tuschl T, Hartmann G, Patel DJ. Structural and functional insights into 5'–ppp RNA pattern recognition by the innate immune receptor RIG–I. Nat Struct Mol Biol. 2010 Jul;17(7):781–7. doi: 10.1038/nsmb.1863. Epub 2010 Jun 27. PMID: 20581823; PMCID: PMC3744876.

Wang Y, Zhang D, Du G, Du R, Zhao J, Jin Y, Fu S, Gao L, Cheng Z, Lu Q, Hu Y, Luo G, Wang K, Lu Y, Li H, Wang S, Ruan S, Yang C, Mei C, Wang Y, Ding D, Wu F, Tang X, Ye X, Ye Y, Liu B, Yang J, Yin W, Wang A, Fan G, Zhou F, Liu Z, Gu X, Xu J, Shang L, Zhang Y, Cao L, Guo T, Wan Y, Qin H, Jiang Y, Jaki T, Hayden FG, Horby PW, Cao B, Wang C. Remdesivir in adults with severe COVID–19: a randomised, double–blind, placebo–controlled, multicentre trial. Lancet. 2020 May 16;395(10236):1569–1578. doi: 10.1016/S0140–6736(20)31022–9. Epub 2020 Apr 29. Erratum in: Lancet. 2020 May 30;395(10238):1694. PMID: 32423584; PMCID: PMC7190303.

Wang W, Chen J, Yu X, Lan HY. Signalling mechanisms of SARS–CoV–2 Nucleocapsid protein in viral infection, cell death and inflammation. Int J Biol Sci. 2022 Jul 11;18(12):4704–4713. doi: 10.7150/ijbs.72663. PMID: 35874957; PMCID: PMC9305276.

Weber F. The catcher in the RIG–I. Cytokine. 2015 Nov;76(1):38–41. doi: 10.1016/j.cyto.2015.07.002. Epub 2015 Jul 10. PMID: 26168692.

Weber M, Sediri H, Felgenhauer U, Binzen I, Bänfer S, Jacob R, Brunotte L, García–Sastre A, Schmid–Burgk JL, Schmidt T, Hornung V, Kochs G, Schwemmle M, Klenk HD, Weber F. Influenza virus adaptation PB2–627K modulates nucleocapsid inhibition by the pathogen sensor RIG–I. Cell Host Microbe. 2015 Mar 11;17(3):309–319. doi: 10.1016/j.chom.2015.01.005. Epub 2015 Feb 19. PMID: 25704008; PMCID: PMC4359673.

Weber M, Weber F a. Monitoring activation of the antiviral pattern recognition receptors RIG–I and PKR by limited protease digestion and native PAGE. J Vis Exp. 2014 Jul 29;(89):e51415. doi: 10.3791/51415. PMID: 25146252; PMCID: PMC4470399.

Whittaker GR, Helenius A. Nuclear import and export of viruses and virus genomes. Virology. 1998 Jun 20;246(1):1–23. doi: 10.1006/viro.1998.9165. PMID: 9656989.

WHO Coronavirus (COVID–19) Dashboard (https://covid19.who.int/)

Willemsen J, Wicht O, Wolanski JC, Baur N, Bastian S, Haas DA, Matula P, Knapp B, Meyniel–Schicklin L, Wang C, Bartenschlager R, Lohmann V, Rohr K, Erfle H, Kaderali L, Marcotrigiano J, Pichlmair A, Binder M. Phosphorylation–Dependent Feedback Inhibition of RIG–I by DAPK1 Identified by Kinome–wide siRNA Screening. Mol Cell. 2017 Feb 2;65(3):403–415.e8. doi: 10.1016/j.molcel.2016.12.021. Epub 2017 Jan 26. PMID: 28132841.

Wu A, Peng Y, Huang B, Ding X, Wang X, Niu P, Meng J, Zhu Z, Zhang Z, Wang J, Sheng J, Quan L, Xia Z, Tan W, Cheng G, Jiang T. Genome Composition and Divergence of the Novel Coronavirus (2019–nCoV) Originating in China. Cell Host Microbe. 2020 Mar 11;27(3):325–328. doi: 10.1016/j.chom.2020.02.001. Epub 2020 Feb 7. PMID: 32035028; PMCID: PMC7154514.

Wu B, Hur S. How RIG–I like receptors activate MAVS. CurrOpinVirol. 2015 Jun;12:91–8. doi: 10.1016/j.coviro.2015.04.004. Epub 2015 May 13. PMID: 25942693; PMCID: PMC4470786.

Xu H, Zhong L, Deng J, Peng J, Dan H, Zeng X, Li T, Chen Q. High expression of ACE2 receptor of 2019–nCoV on the epithelial cells of oral mucosa. Int J Oral Sci. 2020 Feb 24;12(1):8. doi: 10.1038/s41368–020–0074–x. PMID: 32094336; PMCID: PMC7039956.

Xu T, Zheng W, Huang R. High–throughput screening assays for SARS–CoV–2 drug development: Current status and future directions. Drug Discov Today. 2021 Oct;26(10):2439–2444. doi: 10.1016/j.drudis.2021.05.012. Epub 2021 May 25. PMID: 34048893; PMCID: PMC8146264.

Hu X, Li J, Fu M, Zhao X, Wang W. The JAK/STAT signalling pathway: from bench to clinic. Signal Transduct Target Ther. 2021 Nov 26;6(1):402. doi: 10.1038/s41392–021–00791–1. PMID: 34824210; PMCID: PMC8617206.

Xu Z, Choi JH, Dai DL, Luo J, Ladak RJ, Li Q, Wang Y, Zhang C, Wiebe S, Liu ACH, Ran X, Yang J, Naeli P, Garzia A, Zhou L, Mahmood N, Deng Q, Elaish M, Lin R, Mahal LK, Hobman TC, Pelletier J, Alain T, Vidal SM, Duchaine T, Mazhab–Jafari MT, Mao X, Jafarnejad SM, Sonenberg N. SARS–CoV–2 impairs interferon production via NSP2–induced repression of mRNA translation. Proc Natl Acad Sci U S A. 2022 Aug 9;119(32):e2204539119. doi: 10.1073/pnas.2204539119. Epub 2022 Jul 25. PMID: 35878012; PMCID: PMC9371684.

Yamada S, Hatta M, Staker BL, Watanabe S, Imai M, Shinya K, Sakai–Tagawa Y, Ito M, Ozawa M, Watanabe T, Sakabe S, Li C, Kim JH, Myler PJ, Phan I, Raymond A, Smith E, Stacy R, Nidom CA, Lank SM, Wiseman RW, Bimber BN, O'Connor DH, Neumann G, Stewart LJ, Kawaoka Y. Biological and structural characterization of a host–adapting amino acid in influenza virus. PLoSPathog. 2010 Aug 5;6(8):e1001034. doi: 10.1371/journal.ppat.1001034. PMID: 20700447; PMCID: PMC2916879.

Yamada S, Shimojima M, Narita R, Tsukamoto Y, Kato H, Saijo M, Fujita T. RIG–I–Like Receptor and Toll–Like Receptor Signalling Pathways Cause Aberrant Production of Inflammatory Cytokines/Chemokines in a Severe Fever with Thrombocytopenia Syndrome Virus Infection Mouse Model. J Virol. 2018 Jun 13;92(13):e02246–17. doi: 10.1128/JVI.02246–17. PMID: 29643242; PMCID: PMC6002725.

Yamada T, Sato S, Sotoyama Y, Orba Y, Sawa H, Yamauchi H, Sasaki M, Takaoka A. RIG–I triggers a signalling–abortive anti–SARS–CoV–2 defense in human lung cells. Nat Immunol. 2021 Jul;22(7):820–828. doi: 10.1038/s41590–021–00942–0. Epub 2021 May 11. PMID: 33976430.

Yang DM, Geng TT, Harrison AG, Wang PH. Differential roles of RIG–I like receptors in SARS–CoV–2 infection. Mil Med Res. 2021 Sep 7;8(1):49. doi: 10.1186/s40779–021–00340–5. PMID: 34488908; PMCID: PMC8421188.

Yang LP, Plosker GL. Paliperidone extended release. CNS Drugs. 2007;21(5):417–25; discussion 426–7. doi: 10.2165/00023210–200721050–00005. PMID: 17447829.

Yoneyama M, Kikuchi M, Matsumoto K, Imaizumi T, Miyagishi M, Taira K, Foy E, Loo YM, Gale M Jr, Akira S, Yonehara S, Kato A, Fujita T. Shared and unique functions of the DExD/H–box helicases RIG–I, MDA5, and LGP2 in antiviral innate immunity. J Immunol. 2005 Sep 1;175(5):2851–8. doi: 10.4049/jimmunol.175.5.2851. PMID: 16116171.

Yoneyama M, Onomoto K, Jogi M, Akaboshi T, Fujita T. Viral RNA detection by RIG–I–like receptors. CurrOpin Immunol. 2015 Feb;32:48–53. doi: 10.1016/j.coi.2014.12.012. Epub 2015 Jan 14. PMID: 25594890.

Yoo JS, Kato H, Fujita T. Sensing viral invasion by RIG–I like receptors. CurrOpin Microbiol. 2014 Aug;20:131–8. doi: 10.1016/j.mib.2014.05.011. Epub 2014 Jun 23. PMID: 24968321.

Zambon MC. Epidemiology and pathogenesis of influenza. J Antimicrob Chemother. 1999 Nov;44 Suppl B:3–9. doi: 10.1093/jac/44.suppl_2.3. PMID: 10877456.

Zamoto–Niikura A, Terasaki K, Ikegami T, Peters CJ, Makino S. Rift valley fever virus L protein forms a biologically active oligomer. J Virol. 2009 Dec;83(24):12779–89. doi: 10.1128/JVI.01310–09. Epub 2009 Oct 7. PMID: 19812169; PMCID: PMC2786858.

Zebedee SL, Lamb RA. Influenza A virus M2 protein: monoclonal antibody restriction of virus growth and detection of M2 in virions. J Virol. 1988 Aug;62(8):2762–72. doi: 10.1128/JVI.62.8.2762–2772.1988. PMID: 2455818; PMCID: PMC253710.

Zeng W, Sun L, Jiang X, Chen X, Hou F, Adhikari A, Xu M, Chen ZJ. Reconstitution of the RIG–I pathway reveals a signalling role of unanchored polyubiquitin chains in innate immunity. Cell. 2010 Apr 16;141(2):315–30. doi: 10.1016/j.cell.2010.03.029. PMID: 20403326; PMCID: PMC2919214.

Zhang Y, Chen Y, Li Y, Huang F, Luo B, Yuan Y, Xia B, Ma X, Yang T, Yu F, Liu J, Liu B, Song Z, Chen J, Yan S, Wu L, Pan T, Zhang X, Li R, Huang W, He X, Xiao F, Zhang J, Zhang H. The ORF8 protein of SARS–CoV–2 mediates immune evasion through down–regulating MHC–I. Proc Natl Acad Sci U S A. 2021 Jun 8;118(23):e2024202118. doi: 10.1073/pnas.2024202118. PMID: 34021074; PMCID: PMC8201919.

Zhirnov OP. Isolation of matrix protein M1 from influenza viruses by acid–dependent extraction with nonionic detergent. Virology. 1992 Jan;186(1):324–30. doi: 10.1016/0042–6822(92)90090–c. PMID: 1727609.

Zhou P, Yang XL, Wang XG, Hu B, Zhang L, Zhang W, Si HR, Zhu Y, Li B, Huang CL, Chen HD, Chen J, Luo Y, Guo H, Jiang RD, Liu MQ, Chen Y, Shen XR, Wang X, Zheng XS, Zhao K, Chen QJ, Deng F, Liu LL, Yan B, Zhan FX, Wang YY, Xiao GF, Shi ZL. A pneumonia outbreak associated with a new coronavirus of probable bat origin. Nature. 2020 Mar;579(7798):270–273. doi: 10.1038/s41586–020–2012–7. Epub 2020 Feb 3. PMID: 32015507; PMCID: PMC7095418.

Zou J, Maeder ML, Mali P, Pruett–Miller SM, Thibodeau–Beganny S, Chou BK, Chen G, Ye Z, Park IH, Daley GQ, Porteus MH, Joung JK, Cheng L. Gene targeting of a disease–related gene in human induced pluripotent stem and embryonic stem cells. Cell Stem Cell. 2009 Jul 2;5(1):97–110. doi: 10.1016/j.stem.2009.05.023. Epub 2009 Jun 18. PMID: 19540188; PMCID: PMC2720132.

Zufferey R, Dull T, Mandel RJ, Bukovsky A, Quiroz D, Naldini L, Trono D. Self–inactivating lentivirus vector for safe and efficient in vivo gene delivery. J Virol. 1998 Dec;72(12):9873–80. doi: 10.1128/JVI.72.12.9873–9880.1998. PMID: 9811723; PMCID: PMC110499.

9 Abbreviations

Abbreviations in as found order in this study:

Influenza A virus (FLUAV), Severe Acute Respiratory Syndrome Coronavirus 2 (SARS–CoV–2), RIG–I DC (ΔCARD), Hemagglutinin (HA), Neuraminidase (NA), Nucleoprotein (NP), Polymerase basic 1 (PB1), Polymerase basic 2 (PB2), Polymerase acidic (PA), Matrix 1 (M1), Non–structural protein (NS1), Nuclear export protein (NEP), Viral RiboNucleoProtein (vRNP), Double–stranded RNA (ds RNA), Nuclear localization signals (NLSs), Viral RNA (vRNA), Viral RNA dependent RNA polymerase (RdRp), Amino acid (aa), Coronavirus disease 19 (COVID–19), World Health Organization (WHO), Acute respiratory distress syndrome (ARDS), Nucleocapsid (N), Envelope (E), Membrane (M), S (spike), Open reading frame (accessory protein) (Orf), Non–structural protein (nsp), Angiotensin–converting enzyme 2 (ACE2), Interferon (IFN), Mitochondrial antiviral–signalling protein (MAVS), European union (EU), Messenger RNA (mRNA), IFN–stimulated genes (ISGs),t Pathogen–associated molecular patterns (PAMPs), Pattern recognition receptors (PRRs), Single–stranded RNA (ssRNA), Retinoic acid–inducible gene I (RIG–I), 5′– triphosphate dsRNA (5′ppp–dsRNA), RIG–I–like–receptors (RLRs), Melanoma differentiation–associated protein 5 (MDA5), Laboratory of genetics and physiology 2 (LGP2), C–terminal domain (CTD), Caspase recruitment domain (CARD), Interferon Regulatory

Factor (IRF), Helicase (Hel), Transmembrane (TM), Interferon–α/β receptor (IFNAR), Janus kinase/signal transducer and activator of transcription (JAK–STAT), Interferon–stimulated gene factor 3 (ISGF3), IFN–induced protein with tetratricopeptide repeats (IFITs), Dopamine receptor (D2), Serotonin receptor (5–HT2A), Histamine (H1), Control (CTRL), DMEM (Dulbeccos's modified Eagle medium), FBS (Fetal Bovine Serum), Penicillin–Streptomycin–Glutamine (P/S/Q), Tris buffered saline (TBS), Deoxynucleotide (dNTP), 4′,6–diamidino–2–phenylindole (DAPI), Ammonium persulfate (APS), Dimethylsulfoxide (DMSO), Ethylenediaminetetraacetic acid (EDTA), Hydrochoric acid (HCl), L–1–tosylamido–2–phenylethyl chloromethyl ketone (TPCK)–treated trypsin, N,N,N',N'–tetramethylethylenediamine (TEMED), Plaque forming units (PFU), Immunofluorescence (IF), Sodium chloride (NaCl), Sodium dodecyl sulfate (SDS),Threshold cycle (CT), Wild type (WT), Glutathione–s–transferase (GST), Paliperidone (PP), Sodium dodecyl sulfate–polyacrylamide gel electrophoresis (SDS–PAGE), Polyvinylidene difluoride (PVDF), Bovine serum albumin (BSA), Primer Melting Temperature (Tm), Escherichia coli (E. coli), Kilo Dalton (kDA), RIG–I K270A (KA), RIG–I K270A/E373Q (KAEQ), RIG–I T409A/S411A (TASA), RIG–I ΔCARD (DC), Food and Drug Administration (FDA)

10 List of tables

11 List of figures

12 Acknowledgements

The present study was accomplished in the Institute of Virology, Faculty 10 – Veterinary Medicine of Justus Liebig University Giessen at Biomedical Research center Seltersberg. The completion of this study would be impossible without the support and help of certain people, this is why I would like, here, to thank them.

Initially, I would like to thank the supervisor of this study Prof. Dr. Friedemann Weber. I would like to thank him from my heart for his trust on giving me the opportunity to work on this project. I would also like to thank him for his scientific guidance through the study, his understanding, his help on both scientific and personal matters, his motivational spirit and for being there available every single time required.

Moreover, i would like to thank all the MBML school members for giving me the opportunity to attend the school, to provide all this knowledge and the constructive discussions we had. Thank you deeply Professor Werner Seeger, Prof Dr Rory Morty, Professor Elie El Agha, Dr Ana Ivonne Vázquez-Armendariz, Dr Ivana Mižíková and Dr Janine Koepke.

Furthermore, I would like to thank all colleagues who throughout all these years became friends, for their overall help in every day Lab and outside the lab matters making it a happy environment. Thus, I would like to thank Patrick Schmerer for being my German brother and being the person that I had the first beer with in Germany. Thank you Ulrike Felgenhauer, for the “potatoes” and Simone Lau for the “coffees”. Thank you Gleyder Roman Sosa, for being the (cloning) Gleyder, and Stephanie Devignot for the ″baguettes″. Furthermore, I would like to thank Lyudmila Shalamova who took care of the work required for S3, Andreas Schoen for all the tips, and Besim Berisha for all the technical help. I deeply thank them for being there whenever scientifically and personally assistance was required as true friends. Furthermore, i would like to thank Dr Aglaia Pappa, Ulrike Felgenhauer, Gleyder Roman Sosa, for their time and help on the stage of proofreading of this thesis.

I would also like to thank Mrs Zitzlaff and Mrs Biedenkopf for their administrative assistance all these years and Mrs Herzog for the conversations in German and cookies.

Also, i would like to thank Prof. Dr. Stephan Bauer, Benjamin Rupf, Prof. Dr. Dr. Benjamin Lamp, Carina Reuscher, Dr Christin Mueller, Dr Marco Binder and Dr. Jan Rehwinkel for their scientific assistance.

Moreover, I would like to thank the examination committee for their time.

Last but not least, I would like to thank my family. My soon to be wife for being there, pushing me to continue, understand, support me throughout these years. My mother and brother for their love, support, understanding through all these years for this big step of my career. With them, I would like to thank my Father whose effort helped me follow my dreams and from up there help me make them true.